10-3-2018 10:00 AM

Near-Earth Asteroid Resources: Review and Analogue Study of Highly Siderophile Elements in Main-Group Pallasites

Liam R. J. Innis
The University of Western Ontario

Supervisor
Osinski, Gordon R.
The University of Western Ontario

Graduate Program in Geology
A thesis submitted in partial fulfillment of the requirements for the degree in Master of Science

Abstract

The potential for Near-Earth asteroids (NEAs) as targets for space resource utilization has been explored. Water and platinum group elements (PGE)s have been identified as resources with potential profitability in existing markets. A parameterization accounting for asteroid size, resource concentration, and accessibility yields just seven and three potentially viable NEA targets for water and PGEs respectively. Improved NEA discovery campaigns, with emphasis on spectroscopy, and advancements in space transportation and autonomous robotic technology are crucial to future success of NEA resource utilization. LA-ICP-MS was used to evaluate main-group pallasites (PMG) for PGE potential. Bulk metal concentrations of most PGEs are lower than in iron meteorites, making the associated parent body(ies) of the PMG suboptimal for resource utilization. Average subsolidus partition coefficients are $1 < D_{T/K}(Ir) < D_{T/K}(Pt) \approx D_{T/K}(Os) < D_{T/K}(Rh) < D_{T/K}(Ru) < D_{T/K}(Pd)$ and appear to be applicable to all instances of taenite/kamacite, regardless of parent body conditions.

Keywords

Space resource utilization, asteroid mining, platinum group elements, highly siderophile elements, subsolidus partitioning, pallasite, taenite, kamacite.

Co-Authorship Statement

Joe Petrus, the LA-ICP-MS Laboratory Technician at the Chemical Fingerprinting Laboratory at Laurentian University, is considered a coauthor for chapter 3 of this thesis. He performed major and trace elemental analyses on the taenite and kamacite phases of all six pallasite main-group samples used in this study. The samples and the external reference material North Chile were provided by Liam Innis, as were the analysis locations and the list of elements to be detected. The details of the procedure, including spot size, dwell time, etc., were at Joe Petrus' discretion. He was also responsible for the internal standardization, PGE interference correction, and data reduction. Lastly, he provided revisions for the portion of the methods section pertaining to the LA-ICP-MS procedure and the analytical accuracy portion of the discussion.

The remainder of this thesis was written in its entirety by Liam Innis with revisions from supervisor Dr. Gordon Osinski.

Dedication

For my parents, Megan and John

Thank you for your unwavering support

&

For Bob

You were not able to see me complete this work,

but I hope it would have made you proud

Acknowledgments

Thesis writing, like child rearing, takes a village. I would like to thank, in no particular order; my supervisor, Dr. Gordon Osinski, for his guidance and feedback; Dr. Phil McCausland, for his assistance in cutting pallasite samples; Marc Beauchamp, for his assistance and expertise on the EPMA; and Joe Petrus, for his excellent LA-ICP-MS analysis and co-authorship. I would like to thank Dr. Tony Withers and Dr. Robert Linnen for helpful conversations about diffusion. I would also like to thank Dr. Kim Tait, Brendt Hyde, and the Royal Ontario Museum for the use of their meteorites. Finally, I would like to thank my fellow students – in Dr. Osinski's lab group and out – for their support, advice, and camaraderie throughout the last two years.

Table of Contents

List of Tables

List of Figures

List of Acronyms

BCC	Body Centered Cubic
BSE	Backscattered Electron
CNEOS	Center for Near-Earth Object Studies
CNSA	China National Space Administration
COPUOS	Committee on the Peaceful Uses of Outer Space
COTS	Commercial Orbital Transportation Services
CR	Cooling Rate
CRS	Commercial Resupply Services
CSA	Canadian Space Agency
CSLCA	Commercial Space Launch Competitiveness Act
CZ	Cloudy Zone
ECAS	Eight Color Asteroid Survey
EPMA	Electron Probe Micro Analyzer
ESA	European Space Agency
FCC	Face Centered Cubic
FTS	Flow Through Shares
GEO	Geostationary Orbit
GTO	Geostationary Transfer Orbit
HCP	Hexagonal Closest Packed
HSE	Highly Siderophile Element
ISAS	Institute of Space and Astronautical Science
ISRU	In Situ Resource Utilization
JAXA	Japan Aerospace Exploration Agency
JPL	Jet Propulsion Laboratory
KREEP	Potassium Rare-Earth Element and Phosphorous
LA-ICP-MS	Laser Ablation Inductively Coupled Plasma Mass Spectrometry
LEO	Low Earth Orbit
LOD	Limit of Detection
MBA	Main-Belt Asteroid
MDA	MacDonald, Dettwiler and Associates
MG	Main Group (in reference to PMG)
NASA	National Aeronautics and Space Administration
NEA	Near-Earth Asteroid
NEO	Near-Earth Object
OST	Outer Space Treaty
PGE	Platinum Group Element
PMG	Pallasite Main Group
PMG-an	Pallasite Main Group with Anomalous Characteristics
PPP	Private-Public Partnership
SMASS	Small Main-Belt Asteroid Spectroscopic Survey
SRU	Space Resource Utilization

1 Background and Outline

1.1 Introduction

The presence of natural resources beyond Earth is well known. In recent years, the prospect of utilizing these resources for the betterment of humankind has captured the imagination of academics, space professionals, industrialists, and investors alike. The act of harvesting, processing, and ultimately creating useful products from the naturally occurring resources in space can be described as space resource utilization (SRU). SRU is currently in its infancy. Laboratory tests and analogue missions have been performed but, except for solar energy, no space resource has yet been utilized (Sanders and Larson 2015).

One method in development, and with widespread support, is in situ resource utilization (ISRU). ISRU is the use of space resources to create products or services in support of robotic or manned space exploration missions. Leveraging space resources incurred along the path of exploration could potentially provide cost savings, mass reduction, reduced risk and increased mission flexibility (Sanders 2015). Resources considered for ISRU include water, solar wind implanted volatiles (e.g., H, C, N), metals and minerals in extraterrestrial soil, atmospheric gases, and solar energy (Sanders and Larson 2015). The recycling of waste and spent hardware from human crews, and even the vacuum and micro-gravity of space, are also considered part of ISRU.

Propellant is a significant and ubiquitous need in space missions and is an excellent example of the potential efficacy of ISRU. A full appreciation for the value of producing propellant outside of Earth's gravity well can be garnered through inspection of Tsiolkovsky's rocket equation. The equation,

$$\Delta V = v_e \cdot \ln(\frac{m_0}{m_f}), \qquad \text{(Eq. 1)}$$

relates the change in velocity of the rocket (ΔV) with the exhaust velocity (v_e) and mass fraction of the propellant (m_0 or wet mass, the mass of the rocket and propellant before burn, and m_f or dry mass, the mass of rocket after burn) (Forward 1995). ΔV is the change in velocity required to move from one place, or orbit, in space to another (Ross 2001). It

can be thought of the travel cost in space. The exhaust velocity depends on the fuel and oxidizer selected but is at a maximum (for chemical rockets with benign exhaust products) for the pair of liquid hydrogen and liquid oxygen. With exhaust velocity maximized, and ΔV dictated by the start and end points of travel, the only way to ensure a rocket reaches its destination is through careful engineering to manipulate the propellant mass fraction; minimizing the mass of the non-propellant portion of the rocket. For example, the Saturn S-IVB, the third stage of the Saturn V rocket, which famously delivered the Apollo astronauts to the Moon, was ~88% propellant by mass (Holt and Monk 2009). The presence of the natural logarithm, ln, in the equation dictates that increasing the mass ratio of wet to dry mass provides diminishing returns on increasing ΔV.

In the current approach to space exploration, rockets launch with all the propellant required for the entire mission. This exacerbates the effect of the exponential relationship between travel cost and propellant. The propellent needed later in a mission (e.g., to get from Low Earth Orbit [LEO] to Mars Orbit) must be carried from the onset (Earth's surface). At this stage the propellant reserved for later use is deadweight, causing the rocket to accelerate more slowly and increasing the propellant expenditure required to achieve escape velocity.

The culmination is that to transport 1 kg of mass to Mars, 11 kg must be launched from Earth (Sanders 2015). If space resources can be leveraged to provide for a cis-lunar (located between Earth and the Moon) propellant depot, rockets could be launched with only enough propellant to escape Earth's gravity well, before refueling and departing for their ultimate destination. This would reduce launch mass and cost. It would also permit the design of rockets with lower propellant mass fractions, allowing more mass to be dedicated to scientific instrumentation and engineering buffers. The result is less expensive, more capable, and safer rockets. This strategy is not limited to cis-lunar space. Propellant manufacture on the Moon or Mars to service ascent vehicles would provide similar benefits for sample return or human crewed missions to these bodies.

While usually discussed in the sphere of supporting exploration missions, the production and sale of space resources in the private sector can also be considered as ISRU. The same cis-lunar propellant depot from earlier could service spacecraft for the public and private

sectors alike. An example of this would be the development of a satellite servicing industry. Propellant from SRU could power a fleet of spacecraft designed to refuel satellites and more rapidly transfer them from their launch orbits into Geostationary Orbit (GEO), providing value to the existing satellite industry (Metzger 2016).

For ISRU to be worthwhile for public agencies, they must demonstrate at least one of a cost saving, risk mitigating, or mission enhancing benefit. The private sector, on the other hand, must demonstrate profitability in a reasonably brief time span after initial investment. Given the expense and risk associated with operating in space, and the embryonic state of the space market, meeting this constraint is not trivial. Regardless, upsides such as the near-infinite scaling potential and first to market advantage have enticed a handful of companies already (e.g., Planetary Resources 2012, Deep Space Industries 2017). For SRU and the space market to thrive, private interests must eventually account for the bulk of space resource production and consumption.

SRU discussions generally focus on the Moon, Mars and its moons, and the Near-Earth Asteroids (NEAs). These bodies are prospective for their variety and concentration of resources present, proximity to Earth, and attractiveness as exploration targets. As the sphere of human activity in space expands, bodies such as main-belt asteroids, comets, and other planetary surfaces will more frequently enter the conversation.

The Moon's appeal is not limited to its proximity to Earth (~ 6 km s^{-1} from LEO). It has sufficient resources, and surface gravity, to serve as a proving ground for modern human exploration (including ISRU) as part of a "bootstrap" approach to Martian exploration (e.g., Zuniga et al. 2015). It, of course, offers its own significant economic and scientific value as well. While no single lunar resource stands above all others, the Moon is host to a number of potentially significant resources including solar wind implanted volatiles, water (in permanently shadowed regions near the poles, in hydrated minerals at high-latitudes, and in ubiquitous pyroclastic deposits), oxygen (from water or oxide / silicate minerals in the regolith), metals (from basalt, meteoritic material, ilmenite, and regolith), silicon (silicate minerals), rare earth elements (KREEP – potassium, rare earth element, and phosphorus rich basalt), uranium and thorium (Crawford 2015).

ISRU on Mars and its two moons, Phobos and Deimos, would likely be in support of local exploration (Mazanek et al. 2015), and not as feedstock for the cis-lunar space economy. An area of active interest is oxygen production from Mars' thin but CO_2-rich atmosphere. NASA's Mars 2020 rover will include the Mars OXygen ISRU Experiment (MOXIE) instrument. MOXIE serves as proof of concept, essentially a $1/100^{th}$ scale model of an oxygen processing plant that would provide the liquid oxygen needed for a Mars Ascent Vehicle (Meyen et al. 2016). Oxygen produced from such a plant could also be used in life support systems. Other ISRU applications under investigation in the Martian system include methane production (for fuel), regolith transportation, and launch pad construction (Benaroya et al. 2013).

Perhaps the most promising source of space resources are the Near-Earth Asteroids (NEAs). Not only are they rich and diverse resource hosts, they are also some of the most accessible objects in the solar system. Approximately one fifth of NEAs have lower one-way rendezvous from LEO than the Moon (Benner 2018). NEAs vary in composition, and can be enriched in resources including water, base metals, platinum group elements, and volatiles. The existing need for propellant in space makes water especially valuable in the near-term of SRU, and NEAs especially promising. For example, C-type "carbonaceous" asteroids are estimated to contain as much as 20 wt% water, stored in about equal fractions hydrated minerals and subsurface water ice (Elvis 2014).

Up to this point, SRU has only been discussed as a source for materials in space. This is in acknowledgement of the cost effectiveness of sourcing resources near the site of demand, the rationalization for ISRU to begin with. A possible exception however, are the platinum group elements (PGEs: Ru, Rh, Pd, Os, Ir, and Pt). Their high value, due to their scarcity, catalytic applications, corrosion resistance, and high melting points, may permit their economical import. Metallic asteroids are enriched in PGEs at concentrations that exceed the richest ores on Earth (Todd et al. 1982, Wasson et al. 1998) but, given the increased risk and complexity associated with SRU, it is unclear whether primary PGE production from NEAs will be economically viable. PGE production from NEAs may only be economical as a by-product of base metal production, which in turn will only be profitable when the space market develops the appropriate demand. Ultimately their incidence,

concentration, ease of extraction, and the market response will determine whether their import to Earth is economical. To aid in the assessment of NEAs as PGE sources, the concentration and distribution of PGEs in metallic asteroids must be known as certainly and specifically as possible.

1.2 Outline of Thesis

The second chapter of this thesis discusses the SRU potential of NEAs. It takes the form of a thorough literature review, first addressing the nature and distribution of asteroids and meteorites; between them informing the incidence, abundance, and grade of asteroid resources. It then explores the logistical feasibility, legality, and economic viability of NEA SRU. It then summarizes Canadian opportunities and current ventures in the field.

The third chapter of this thesis examines the concentration, distribution, and behavior of the highly siderophile elements (HSE: PGE + Re & Au) in main group pallasites (PMG). Pallasites are meteorites composed of roughly equal parts of the silicate mineral olivine and FeNi alloy. The FeNi alloy in pallasites and iron meteorites is the destination of most HSEs during parent body differentiation. An enhanced understanding of HSE concentration, distribution, and mobility in main-group pallasites complements the existing literature on HSE behavior in magmatic iron meteorites, providing a more complete picture of the presence of HSE in the metal of differentiated asteroids. This knowledge can be used to make first order approximations of HSE content in metallic asteroids and more accurately appraise the feasibility of primary HSE production from NEAs.

1.3 References

Benaroya, H., Metzger, P., and Muscatello, A. 2013. Special issue on in situ resource utilization: Introduction. Journal of Aerospace Engineering, **26**: 1–4.

Benner, L.A.M. 2018. Near-Earth Asteroid Delta-V for Spacecraft Rendezvous. Available from https://echo.jpl.nasa.gov/~lance/delta_v/delta_v.rendezvous.html [accessed 24 January 2018].

Crawford, I.A. 2015. Lunar resources: A review. Progress in Physical Geography, **39**: 137–167.

Deep Space Industries. 2017. Prospector-1 | Deep Space Industries. Available from

http://deepspaceindustries.com/prospector-1/ [accessed 8 December 2017].

Elvis, M. 2014. How many ore-bearing asteroids? Planetary and Space Science, **91**: 20–26. Elsevier.

Forward, R.L. 1995. A transparent derivation of the relativisitic rocket equation. doi:10.2514/6.1995-3060.

Holt, J.B., and Monk, T.S. 2009. Propellant Mass Fraction Calculation Methodology for Launch Vehicles and Application to Ares Vehicles. *In* AIAA SPACE 2009 Conference & Exposition. Pasadena, California. pp. 1–7.

Mazanek, D.D., Merrill, R.G., Brophy, J.R., and Mueller, R.P. 2015. Asteroid Redirect Mission concept: A bold approach for utilizing space resources. Acta Astronautica, **117**: 163–171.

Metzger, P.T. 2016. Space development and space science together, an historic opportunity. Space Policy, **37**: 77–91. Elsevier Ltd.

Meyen, F.E., Hecht, M.H., and Hoffman, J.A. 2016. Thermodynamic model of Mars Oxygen ISRU Experiment (MOXIE). Acta Astronautica, **129**: 82–87. Elsevier.

Planetary Resources. 2012. Asteroid mining plans revealed by Planetary Resources, Inc. | Planetary Resources. Available from https://www.planetaryresources.com/2012/04/asteroid-mining-plans-revealed-by-planetary-resources-inc/ [accessed 21 May 2018].

Ross, S.D. 2001. Near-Earth Asteroid Mining. Space Industry Report, 1–24.

Sanders, G.B. 2015. Space resource utilization: near-term missions and long-term plans for human exploration. *In* 6th Annual Joint Planetary & Terrestrial Mining Sciences Symposium/Space Resources Roundtable. Montreal, QC.

Sanders, G.B., and Larson, W.E. 2015. Final review of analog field campaigns for in Situ Resource Utilization technology and capability maturation. Advances in Space Research, **55**: 2381–2404. COSPAR.

Todd, S.G., Keith, D.W., Le Roy, L.W., Schissel, D.J., Mann, E.L., and Irvine, T.N. 1982. The J-M platinum-palladium reef of the Stillwater complex, Montana: I. Stratigraphy and petrology. Economic Geology, **77**: 1454–1480.

Wasson, J.T., Choi, B.-G., and Jerde, E.A. 1998. Chemical classification of iron meteorites : XII . New members of the magmatic groups. Geochimica et

Cosmochimica Acta, **62**: 715–724.

Zuniga, A.F., Rasky, D., and Pittman, R.B. 2015. Lunar COTS: an economical and sustainable approach to reaching Mars. AIAA Space 2015 Conference and Exposition,: 1–24.

2 Near-Earth Asteroid Resources: A Review

2.1 Introduction

Through centuries of study and decades of space exploration, the presence of a range of resources across the solar system has been established. Only recently has the prospect of harnessing these resources been considered a possibility. The act of harvesting, processing, and ultimately creating useful products from resources acquired in space can be described as space resource utilization (SRU). Presently, space agencies are investigating a method of SRU called in situ resource utilization (ISRU). ISRU entails leveraging the resources incurred along the path of exploration to create products or services in support of the mission (Sanders and Larson 2015). SRU is not limited to the public sector however. It is the opinion of some investors and industry professionals that SRU, and the hypothetical accompanying expansion of the space market, is a potentially regime-changing opportunity.

For SRU to be worthwhile for public agencies, there must be at least one of a cost saving, risk mitigating, or mission enhancing benefit. Alternately, the private sector must demonstrate profitability in a reasonably brief time span after initial investment. Considering the complexity of operations in space and the inchoate nature of the space market, this amounts to a substantial challenge. Undeterred, companies with the intentions of mining asteroids have already formed, including Washington's Planetary Resources and Silicon Valley's Deep Space Industries (Planetary Resources 2012, Deep Space Industries 2017). The United States government, and that of Luxembourg, have shown their support, passing legislation legalizing the sale of space resources (McCarthy 2015, Government of Luxembourg 2017).

Due to their resource variety and enrichment, proximity to Earth, and attractiveness as exploration targets, previous work has identified the Moon, Mars and its moons, and Near-Earth Asteroids (NEAs) as prime targets for SRU (e.g., Crawford 2015). The Moon is close to Earth, has various resources, and can serve as a proving ground for modern human exploration techniques prior to a human-crewed mission to Mars (e.g., Zuniga, Rasky, and Pittman 2015). SRU in the Martian system will likely be directly in support of local

missions, and so less significant to the private sector (Mazanek et al. 2015). Lastly, NEAs, the focus of the current study, host a variety of resources and are very accessible; ~20% of NEAs have lower one-way rendezvous travel costs than the Moon (Benner 2018). Their composition varies with type, and can be enriched in water, base metals, semiconductors, platinum group elements (PGEs), and volatiles.

The goal of this study is not to argue the supremacy of NEAs as potential resource hosts; a well-developed space market would likely make use of resources from many different bodies in support of different needs. Rather, we focus on NEAs due to the importance of NEAs in the near-term of SRU. As well as being accessible, NEAs are enriched in a resource vital to the early development of SRU and the space market: water.

This review will first explore the nature and distribution of asteroids and meteorites, informing the incidence, abundance, and grade of asteroid resources. The following sections will then explore logistical feasibility, legal implications, and economic viability. Lastly it will discuss current ventures and Canadian opportunities in the field.

2.2 Asteroid Characteristics

Asteroids are typically relatively small, rocky bodies devoid of atmospheres that orbit the Sun. They range in size from almost 1000 km to 1 m in diameter (Rubin and Grossman 2010). Very broadly, they are composed of rock, metal, and volatiles in various combinations. Asteroids are divided into populations based on their orbits and reflectance spectra. The asteroids are numerous, but their combined mass is less than that of Earth's Moon. The mass distribution of the asteroids is uneven, with the largest asteroid, 1 Ceres, also classified as a dwarf planet, making up a third of the mass of the main belt asteroids alone (Hilton 2002).

2.2.1 Orbital Families

2.2.1.1 Main Belt Asteroids

The main belt asteroids (MBAs) are the largest group of asteroids. They orbit the Sun at ~2.2 to ~3.2 au (astronomical unit; one au is the average distance from the Sun to the Earth), between the orbits of Mars and Jupiter. The proximity of the MBAs to Jupiter's immense

gravitational influence forms the Kirkwood Gaps. These are gaps in the distribution of MBA semi-major axes located at mean motion resonances with Jupiter (e.g., Wisdom 1983). An asteroid in orbital resonance with Jupiter makes frequent alignments with the planet. With each pass, the body's orbit is slightly perturbed. These perturbations accumulate over time, destabilizing the orbit, and sending the body indiscriminately out of the orbital resonance. The most pronounced gaps occur at the 4:1, 3:1, 5:2, 7:3, and 2:1 resonances. Select Kirkwood gaps are used to delineate the belt into the inner main-belt, middle main-belt, and outer main-belt. The inner main-belt is inwards of 2.5 au (3:1), the middle main-belt is from 2.5 au to 2.82 au (5:2), and the outer main-belt is outwards of 2.82 au. Mars' gravity also forms mean motion resonances with MBAs. A portion of the MBAs ejected towards the Sun by Jupiter and Mars become NEAs. (Nesvorny and Roig 2017).

2.2.1.2 Near-Earth Asteroids

The NEAs are those asteroids that are no farther than 1.3 au from the Sun during their closest approach along their elliptical orbits (Shoemaker et al. 1979). The NEA population is subdivided into the Amors, Apollos, Atens, and Atiras (Fig. 1) (Shoemaker et al. 1979, Di Carlo et al. 2017). The Amors orbit the Sun outside of Earth's orbit and never cross inside it. The Apollos are on average farther away from the Sun than Earth but cross into Earth's orbit from the outside. Atens have shorter orbits than Earth but cross Earth's orbit from the inside. Atiras are by far the least populous group and have shorter orbits than Earth and never cross its path.

The NEAs are more desirable for the near-term of SRU than other asteroid populations due to their relative proximity to Earth. The travel cost in space can be measured in units of speed. This parameter is called ΔV. It is the change in velocity required to move from one location, or orbit, in space to another (Ross 2001). Because their orbits are so similar to Earth's, the ΔV for one-way rendezvous from low Earth orbit (LEO) to ~20% of NEAs is less than the ΔV from LEO to the Moon (Benner 2018). Another consequence of Earth-like orbits is long synodic periods, i.e., the more similar a body's orbit is to Earth's, the longer the time period between closest passes. After rendezvous via optimal trajectory, the launch window for a minimum ΔV return trip is often many years or a decade later.

Missions of shorter duration would have to budget for a non-optimal trip one way or another.

2.2.1.3 Jupiter's Trojans

The Jovian Trojan asteroids share the orbital path of a Jupiter, residing in stable points ~60° proceeding or trailing it. These are the L4 and L5 Lagrangian points respectively. In the context of asteroids, they are also referred to as Trojan points. Like all planets, Jupiter and the Sun orbit around each other at their common centre of mass. The gravitational force felt by small objects near Trojan points also acts through the common centre of mass of the Sun and Jupiter. This causes the asteroid's and the planet's orbital periods to be the same, making the configuration stable though time (Robutel and Souchay 2010). To date, astronomers have discovered over 6,000 Jovian Trojans, but some estimate Jupiter's Trojans to be as numerous as the asteroids of the main belt (Yoshida and Nakamura 2005). Other planets with at least one known Trojan are: Venus (1), Earth (1), Mars (4), Uranus (2), and Neptune (17) (Connors et al. 2011; de la Fuente Marcos and de la Fuente Marcos 2014, 2017).

2.2.2 Spectral Types

In addition to orbital groups, asteroids are also classified by their reflectance spectra in the visible and infrared regions of the electromagnetic spectrum. In theory, asteroids with similar reflectance are interpreted to possess similar surface mineralogies and, therefore, similar compositions. However, factors such as the difficulty of modeling mineral absorption, regolith effects, and space-weathering, may cause objects with dissimilar mineralogies to have similar spectra and be grouped together (Burbine 2016).

The colour of asteroids was first measured photographically by Bobrovnikoff (1929) but these measurements were too sparse and rudimentary to form the basis of a classification scheme. Chapman et al. (1975) put forth the first asteroid taxonomy and introduced the use of letters (C for carbonaceous, S for silicaceous), now a standard feature of all asteroid taxonomies. Next, Tholen submitted his 1984 PhD thesis entitled *Asteroid Taxonomy from Cluster Analysis of Photometry* which proved to be incredibly influential, forming the basis for modern taxonomies and still frequently referenced itself (Tholen 1984). Tholen

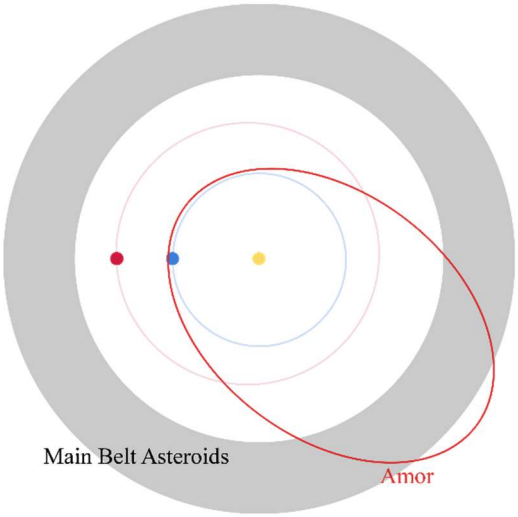

a > 1 au

1.017 au < q < 1.3 au

n = 8034

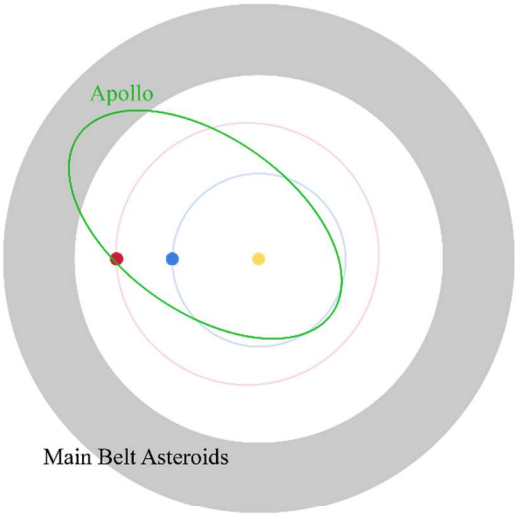

a > 1 au

q < 1.017 au

n = 9430

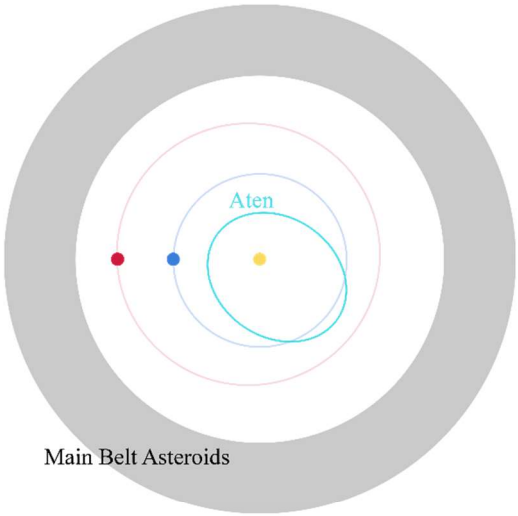

a < 1 au

Q > 0.983 au

n = 1392

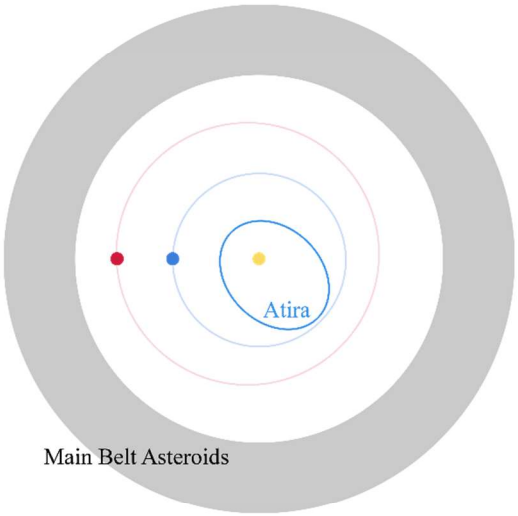

a < 1 au

Q < 0.983 au

n = 30

Figure 1. NEA orbital groups. The yellow, blue, and red circles designate the Sun, Earth, and Mars respectively. The orbital criteria for each group are listed below each image. a = semimajor axis, half the long axis of the ellipse that is traced by a body's orbit. Q = aphelion, the point of furthest distance from the Sun in a body's orbit. q = perihelion, the point nearest the Sun in a body's orbit. Data from IAU Minor Planet Center, accurate as of 10/17/2018.

delineated most of his spectral classes using data from eight broad bandpass filters (ranging from 0.34 – 1.04 μm) from the Eight-Color Asteroid Survey (ECAS) (Zellner et al. 1985).

Exceptions are the E, M, and P types, which are spectrally featureless in the observed wavelengths, and are instead differentiated by their albedos. Tholen (1984) made use of 911 observations of 589 asteroids. The taxonomy consists of 7 types in two groups and 7 more ungrouped types. They are the C-group (B-type, C-type, F-type, G-type), S-type, X-group (E-type, M-type, P-type), A-type, D-type, T-type, Q-type, R-type, and V-type. Like Chapman et al. (1975)'s taxonomy, C-group are carbonaceous, and S-type are silicaceous or stony. The new X-group contains metallic asteroids, while the remainder have anomalous or intermediate characteristics.

In the following years a number of studies made amendments or additions to Tholen's taxonomy, but not until Bus and Binzel (2002) was there an effort to overhaul the taxonomy (Burbine 2016). Their taxonomy was developed using data from the Small Main-belt Asteroid Spectroscopic Survey (SMASS), which was much higher resolution than ECAS data, and were therefore able to discern narrower spectral features. It was also developed using a larger sample of asteroids; 1447 compared to Tholen's 589 (Bus and Binzel 2002). It did however, use a smaller spectral range (0.44 – 0.92 μm) and did not account for albedo. The SMASS system was designed to agree with previous classification schemes whenever possible, given the differences in data. 13 of the 26 classes have single-letter names; 12 taken from preceding taxonomies (A, B, C, D, K, O, Q, R, S, T, V, and X) and one novel class (L). The remaining 13 classes have lowercase modifiers to denote asteroids with intermediate spectral qualities. Just over half the classes are sorted into one of three complexes, broadly consistent with Tholen's groups. The taxonomy is as follows: C-complex (B-type, C-type, Cg-type, Ch-type, Cgh-type, Cb-type), S-complex (S-type, Sa-type, Sk-type, Sl-type, Sq-type, Sr-type and endmembers A-type, K-type, L-type, Q-type, R-type), X-complex (X-type, Xc-type, Xe-type, Xk-type), T-type, D-type, Ld-type, O-type, and V-type (Bus and Binzel 2002). The C, S, and X designations have the same meaning as in Tholen (1984).

The next iteration is the Bus-DeMeo taxonomy (DeMeo et al. 2009). This study expanded the observational range into the near-infrared, using spectra from 371 asteroids in a wavelength range of 0.45 – 2.45 μm. The study presents 24 classes with a 25th Xn class being added after publication (Burbine 2017; DeMeo et al. 2009). The class designations are nearly identical to those of Bus and Binzel; only the Ld, Sl, and Sk classes were removed while the Sv and Xn classes were added. Most bodies measured in both studies retained their classification. Those that did change mostly belonged to the S-complex subclasses (DeMeo et al. 2009). This taxonomy uses a 'w' at the end of certain classes to signify that the body has experienced space weathering. The taxonomy is as follows: C-complex (B-type, C-type, Cb-type, Cg-type, Cgh-type, Ch-type), S-complex (S-type, Sa-type, Sq-type, Sr-type, Sv-type), X-complex (X-type, Xc-type, Xe-type, Xk-type, Xn-type), A-type, D-type, K-type, L-type, O-type, Q-type, R-type, T-type and V-type (DeMeo et al. 2009).

2.2.3 Spectral Class Distribution

The differences in the mean albedo of asteroid spectral classes introduces discovery bias into the population of observed asteroids. Spectral classes with high average albedo (e.g., S-complex) are more readily discovered for a given diameter than asteroids with lower albedo (e.g., C-complex) (Fig. 2). The number of NEAs with spectral types is very low compared to the number of known NEAs (Carry et al. 2016), thus, when considering the resource potential of the NEAs as a population, it is helpful to consider the debiased distribution, while bearing in mind that spectral data must be available for a specific asteroid for it to be considered as a potential mining target. Stuart and Binzel (2004) provide a bias-corrected distribution of spectral classes for NEAs by using a methodology that combines spectral and albedo data sets.

2.3 Meteorites as Analogues

Since no space agency has yet managed a sample return of more than a few milligrams of an asteroid, meteorites are the main samples of asteroid material currently available for study. The lack of spatial resolution and the aforementioned difficulties in interpreting asteroid spectra make meteorite – asteroid comparisons difficult, complicating the study of

asteroid geology. Nevertheless, in the near-term, meteorites remain the best and only physical samples of asteroids available to scientists.

2.3.1 Meteorite Taxonomy

Meteorites are classified into chemical groups, each containing rocks from a single parent body. The ultimate goal of meteorite classification is to couple each chemical group to its parent body in space. This goal has thus far proven elusive. The howardite-eucrite-diogenite (HED) clan of meteorites, thought to originate from the crust of asteroid 4 Vesta, is the only group of meteorites correlated with a specific asteroidal parent body (e.g., Consolmagno and Drake 1977). Besides a small portion derived from the Moon and Mars, the majority of meteorites are derived from asteroids (Weisberg et al. 2006).

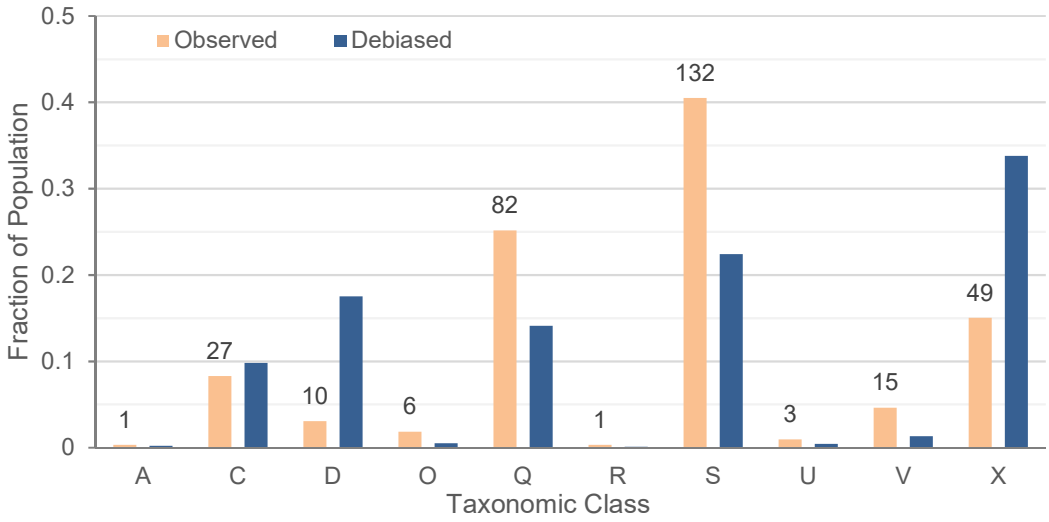

Figure 2. Observed and debiased distribution of taxonomic classes in the NEA population. Observed data (n = 326) are from JPL Small-Body Database (accessed 05/06/18). For asteroids with both Tholen and Bus & Binzel classifications the latter took precedence. Some spectral classes were combined in accordance with the debiased estimations from (Stuart and Binzel 2004). The numbers at the end of the orange columns are the total number of NEAs of that class in JPL Small Body Database.

Traditionally, meteorites were divided into three categories based on composition alone: stony, stony-iron, and iron (Weisberg et al. 2006). Modern taxonomies incorporate their chemical, isotopic, compositional, and petrological nature to group samples that are genetically related (Weisberg et al. 2006). The first distinction made is the degree of

differentiation of the parent body. Meteorites from undifferentiated bodies are called chondrites, named for the small (1 – 2 mm) silicate spheres called chondrules that they often, but do not necessarily, contain (Weisberg et al. 2006). Meteorites from differentiated bodies are called achondrites, primitive achondrites, or nonchondrites, depending on the taxonomy, and can be texturally altered but chemically primitive, partially melted, or fully differentiated. The literature contains numerous taxonomies that demonstrate no consensus on classification hierarchy, except for the final distinction of chemical group. For example, a particular specimen will belong to the same chemical group in all schemes, say a IIIAB iron, but that group could be deemed to be either a differentiated nonchondrite or an achondrite. For a thorough review of the subject the reader is referred to Weisberg et al. (2006). Provisional meteorite – asteroid associations can be made by comparing visible and near infrared meteorite and asteroid spectra (Table 1). The data in Table 1 is speculative in nature and should be regarded as such.

Table 1. Possible meteorite associations and mineralogies of asteroid classes[1].

Asteroid class	**Prototypical asteroid**	**Possible meteorite correlation(s)**	**Select minerals** (major, *minor or accessory*)
A-type (Th, B&B, B-D)	246 Asporina	pallasite:	kamacite, taenite, olivine, *troilite, schreibersite, chromite*
		R:	olivine, pyroxene, sodic plagioclase, troilite, chromite, *rare PGE-bearing sulfides*
		brachinite:	olivine, clinopyroxene, orthopyroxene
C-complex (B&B, B-D)	1 Ceres	CM[2]:	phyllosilicates (kaolinite-serpentine group minerals), olivine, pyroxene, magnetite, sulphides, calcite*, gypsum, insoluble carbon, organic compounds*
		ureilite:	Ca and Cr rich olivine, clinopyroxene, carbonaceous matrix
		CI[3]:	phyllosilicates (serpentine/saponite), magnetite, sulphides, carbonates, *organic compounds*
		CR:	olivine, pyroxene, phyllosilicates (serpentine-subgroup, saponite, chlorite-group), metallic Fe-Ni
		K[4]:	enstatite, olivine, metallic Fe-Ni, feldspathic mesostasis, troilite, *silica*
D-type (Th, B&B, B-D)	1143 Odysseus	C2-ungrouped:	phyllosilicates, olivine
E-type (Th) *Xe-type (B&B, B-D)*	44 Nysa	Aubrite[5]:	enstatite, plagioclase, olivine, diopside, *metallic Fe-Ni, troilite*
K-type (B&B, B-D)	42 Isis	CV:	olivine, pyroxene, phyllosilicates, metallic Fe-Ni, troilite, chromite, *PGE-rich metal nuggets (in Fremdlinge)*
		CO:	olivine, pyroxene, plagioclase, metallic Fe-Ni, troilite, chromite
		CK:	olivine, pyroxene, calcic plagioclase, metallic Fe-Ni, pentlandite, troilite, chromite, *magnetite, rare PGE-bearing sulfides*
		C3-ungrouped:	olivine, orthopyroxene

Table 1 cont.

M-type (Th) *X-complex (B&B, B-D)*	16 Psyche	iron:	metallic Fe-Ni (mostly kamacite and taenite), sulfides, graphite, chromite, *nitrides, phosphides, carbides*
		EH:	enstatite, plagioclase, Si-bearing metallic Fe-Ni, silica, sulfides, *olivine*, nitrides*
		EL:	enstatite, plagioclase, Si-bearing metallic Fe-Ni, silica, sulfides, *olivine*, nitrides*
		mesosiderite:	metallic Fe-Ni metal (mostly kamacite and taenite), orthopyroxene, pigeonite, plagioclase, troilite, schreibersite, tridymite, olivine, *chromite, apatite, whitlockite*
		CB[6]:	metallic Fe-Ni, sulphide*, olivine, pyroxene
		CH:	metallic Fe-Ni (kamacite, taenite, tetrataenite, and plessite), olivine, pyroxene, plagioclase, spinel, *troilite*
Q-type (Th, B&B, B-D)	1862 Apollo	L[7]:	olivine, pyroxene, plagioclase, metallic Fe-Ni, troilite, *chromite, orthoclase*
		H[7]:	olivine, pyroxene, metallic Fe-Ni, plagioclase, troilite, *chromite, apatite*
		LL[7]:	olivine, pyroxene, plagioclase, troilite, metallic Fe-Ni, *chromite, orthoclase*
S-complex (B&B, B-D) *S-type (Th)*	5 Astraea	L, H, LL, mesosiderite:	*See above*
		Acapulcoite[8]:	orthopyroxene, olivine, metallic Fe-Ni, plagioclase, troilite, limonite, clinopyroxene, *chromite*
S-complex (B&B, B-D) *S-type (Th) cont.*	5 Astraea	lodranite[8]:	orthopyroxene, olivine, metallic Fe-Ni, plagioclase, troilite, limonite, clinopyroxene, *chromite*
		angrite:	pyroxene, olivine, *anorthite**
		winonaite[9]:	low-Ca pyroxene, olivine, calcic pyroxene, plagioclase, metallic Fe-Ni, troilite, *chromite, alabandite, schreibersite, graphite, K-feldspar, apatite*
S-type (Th) *S-complex (B&B, B-D)*	3 Juno	ureilite:	*See above*
T-type (Th, B&B, B-D)	96 Aegle	C2-ungrouped:	*See above*
V-type (Th, B&B, B-D)	4 Vesta	HED:	pigeonite*, pyroxene, calcic plagioclase, free silica*, *troilite, kamacite, ilmenite*

[1]Meteorite associations are from (Burbine 2016). Prototypical asteroids are from (DeMeo et al. 2009; Tholen 1984). Unless otherwise indicated mineralogies are from (Rubin 1997). *only found in some members of class / petrographic types. [2](Howard et al. 2011); [3](King et al. 2015); [4](Weisberg et al. 1996); [5](Watters and Prinz 1979); [6](Krot et al. 2005); [7](McSween et al. 1991); [8](Rubin 2007); [9](Benedix et al. 1998).

2.4 Asteroid Resources

Through asteroid spectroscopy and the study of meteorites we know that asteroids contain a diverse array of resources including water (in hydrated minerals and ice), base metals, semiconductors, PGEs, and volatiles. For an asteroid resource to be considered for SRU, however, it must demonstrate mission enhancing or profit earning potential.

A large part of the motivation for SRU is the potential cost savings of garnering resources required in space near the site of demand. The additional expense associated with acquiring

resources in space must be offset by the cost savings of reduced launch mass. With rocket launches out of the equation, the most cost-effective means of meeting demand on Earth will remain mining the planet itself. It follows that for any resource to be considered for SRU there must be demand for it in space. Currently, the only resource with significant demand in space is water. A possible exception to this rule is the PGEs. They are sufficiently valuable that their import to Earth is potentially economical.

This section is divided into subsections for the short and long terms of NEA SRU potential. The short-term section focuses on the feasibility of leveraging resources with existing demand, water and PGEs, while the long-term section details asteroid resources for which demand may develop in the future.

2.4.1 The Short Term

Excluding the engineering cost of extracting a target resource from an individual asteroid, the viability of an asteroid as a mining target is a function of its value and accessibility. An asteroid's value can be estimated as the product of its volume, density, concentration of the desired resource, and value of that resource. Its accessibility can be quantified as the minimum ΔV required for spacecraft rendezvous from LEO. For the purpose of the following parameterization, the minimum value that an asteroid must have to be considered a viable target will be set at $1 B, about the cost of an average space exploration mission, and not far off the operating costs of large mines on Earth.

2.4.1.1 Platinum Group Elements

PGEs are highly valued due to their scarcity, usefulness as catalysts, resistance to corrosion, and high melting points (Zientek and Loferski 2014). Except for the less valuable element, Ru, each element was valued between $12,800 and $35,600 USD kg^{-1} ($400 to $1,100 USD / troy ounce) on average in 2017 (BASF 2018). These values are high enough that they may allow for economic production of asteroid-bound PGEs for the Earth market. This is an advantage over other asteroid resources as it dispels the need to wait for the space market to develop the appropriate demand.

The scarcity of PGEs is driven by their highly siderophile nature. During Earth's differentiation they partitioned strongly into the core, leaving the crust and mantle extremely depleted (McDonough and Sun 1995). What little PGEs that are found outside of the core are possibly the product of a late chondritic veneer (e.g., Schmidt 2007). Like Earth, some asteroids are also differentiated. Subsequent collisions have fragmented some of these bodies; exposing their PGE-enriched core material. These are the metallic X-complex asteroids, thought to be largely composed of FeNi alloy, and are the parent bodies of iron meteorites.

The literature contains limited data on the full suite of PGE concentration in iron meteorites. Iridium concentrations are well studied however, as they are used in iron meteorite taxonomy (Scott et al. 1973). PGE occurrence in iron meteorites can be estimated as totaling seven times Ir abundance in CI chondritic ratios (Elvis 2014). A group of 71 iron meteorites from various chemical groups complied in two papers by Wasson and his collaborators have a mean concentration of 27 $\mu g\ g^{-1}$ total PGE (Wasson et al. 1989, 1998). Meteorites enriched in the 50^{th} and 90^{th} percentiles in the distribution contain 14 $\mu g\ g^{-1}$ and 68 $\mu g\ g^{-1}$ of PGEs respectively.

Asteroids are too small to be spatially resolved by ground-based telescopes. Instead, telescopic observations provide apparent magnitude (h). This is the brightness of an object as perceived by an observer on Earth. Apparent magnitude can then be used to calculate absolute magnitude (H), the brightness of an object as seen from a standard distance. From H, and an assumed average albedo for NEAs of 0.14, asteroid diameter is calculated. Lastly, volume is determined assuming a spherical shape. While virtually all asteroids are not spherical, this assumption is made considering that the diameter calculated will be intermediate between the asteroid's long and short axes, resulting in a reasonable approximation of asteroid volume. There appears to be no correlation between absolute magnitude (H) and taxonomic class in the NEA population (Stuart and Binzel 2004), i.e., taxonomic classes are uniformly dispersed throughout the size range of NEAs.

The density of metallic asteroids remains poorly constrained. Iron meteorites have densities of ~7,900 $kg\ m^{-3}$ but asteroids, particularly those of small mass ($< \sim 10^{20}$ kg), are expected

to have significant porosity (Henderson and Perry 1954; Carry 2012). A 2012 study on asteroid density found a large spread in the densities of asteroids in the Bus-DeMeo X-complex (Carry 2012). The author suggests that limitations of the taxonomy (e.g., not considering albedo) cause asteroids of dissimilar composition to be grouped together in the X-complex. Only considering asteroid densities of reasonable accuracy, and those from X-complex subclasses with densities indicative of metallic composition (Xc and Xk, ρ_{50} from Table 3 in (Carry 2012)), yields a mean density of 4,000 kg m^{-3} from 12 asteroids.

"Average" (50^{th} percentile PGE concentration) and "good" (90^{th} percentile) metallic asteroids reach values of $1 B at diameters of 119 m and 71 m respectively. As volume, and, therefore, mass scales with the cube of the radius, asteroids of increasing size rapidly increase in value. A 240 m asteroid would be worth $8.2 B and $39 B in the average and good cases respectively (Table 2). Accordingly, asteroids lose their value with decreasing size just as rapidly. Asteroids of 100 m and 60 m are only worth ~$0.6 B in the average and good cases, insufficient to warrant a mining venture.

Table 2. Value of PGEs in metallic asteroids.

Diameter (m)	Mass (kg)	PGE Concentration (ppm)	PGE Value ($ / kg)	Value of asteroid ($M)
100	2.09×10^{9}	14.28	19,903	$595
120	3.62×10^{9}	14.28	19,903	$1,029
160	8.58×10^{9}	14.28	19,903	$2,438
240	2.90×10^{10}	14.28	19,903	$8,229
60	4.52×10^{8}	67.66	19,903	$609
75	8.84×10^{8}	67.66	19,903	$1,190
120	3.62×10^{9}	67.66	19,903	$4,874
240	2.90×10^{10}	67.66	19,903	$38,989

Of the 326 asteroids with a spectral classification (Bus & Binzel and/or Tholen) in the JPL Small-Body Database, 15% (n = 49) are X-complex. This is a small fraction of the total known NEA population and does not account for discovery bias favouring higher albedo asteroids, particularly S-complex, over the lower albedo C and X-complexes (Stuart and Binzel 2004). In a 2004 study Stuart and Binzel provide a debiased depiction of the taxonomic distribution of NEAs. They estimate 34% of NEAs belong to the X-complex.

Due to the paucity of spectral type designations among known NEAs, the debiased fraction will be used for subsequent inferences made in this section.

Neeley et al. (2014) compared infrared and visible observations of 29 X-complex asteroids to meteorite spectra. They mainly targeted Xc- and Xk-types, as they are devoid of any strong spectral features, indicative of FeNi metal. Eighteen of the asteroids also had radar data available. Of these, 22% (n = 4) were determined to be analogous to iron meteorites by both the radar data and at least one of the two the methods employing infrared / visible data (Neeley et al. 2014). In the paper that introduced their taxonomy, Bus and DeMeo classified 32 X-complex asteroids of which 66% (n = 21) were either Xc- or Xk-type (DeMeo et al. 2009).

In summary, the fraction of X-complex NEAs is 0.34, the fraction of X-complex asteroids that are Xc- or Xk-type is 0.66, and the fraction of Xc- and Xk- types that are metallic is 0.22. The product of these numbers reveals ~5% of NEAs are expected to be metallic.

As mining missions will require heavy payloads both to and from the asteroid, targets with low ΔV are prioritized. Elvis (2014) suggests a maximum ΔV of 4.5 km s^{-1} for the accessibility cut off, as this figure at least doubles the payload capacity versus a mission to a median NEA (6.65 km s^{-1}). Only 1.4% of the 17,607 NEA ΔVs calculated by Benner have $\Delta V \leq 4.5$ km s^{-1} (2018).

Adapting the approach taken by Elvis (2014), the fraction of NEAs that are expected to be prospective PGE sources is

$$P_{NEA\text{-}PGE} = P_{type} \cdot P_{cnct} \cdot P_{\Delta V}, \quad \text{(Eq. 2)}$$

$$= 0.05 \cdot 0.50 \cdot 0.014,$$

$$= 0.00035,$$

where P_{type} is the fraction of metallic asteroids, P_{cnct} is the fraction of asteroids with favourable PGE concentrations (in this case 50th percentile or better), and $P_{\Delta V}$ is the fraction of accessible asteroids. By this metric, 0.035%, or approximately 1 out of every 2,900

NEAs are prospective for PGEs. Using an assumed average albedo of 0.14, the number of known NEAs with D ≥ 119 m is 8,907 (CNEOS 2018). The product of these numbers reveals that three members of the known NEA catalogue are expected to be potentially viable PGE sources. While this may seem bleak, it is mostly limited by the stringent ΔV requirement. If propulsion technology advances enough to facilitate missions with ΔV ≤ 5.5 km s^{-1}, the number of prospective asteroids increases to 25 (~ 1 / 350).

These estimates are based on the currently known fraction of the NEA population (Fig. 3). The size distribution of the entire NEA population can be estimated by a simple power law (Stokes et al. 2003). The function is

$$N\,(>D(km)) = 942D^{-2.354}, \qquad \text{(Eq. 3)}$$

where N is the cumulative number of NEAs above a given diameter D. From the power law there are expected to be 141,323 NEAs with D ≥ 119 m. This increases the number of prospective NEAs for PGEs to 49 at ΔV ≤ 4.5 km s^{-1} and 403 at ΔV ≤ 5.5 km s^{-1}.

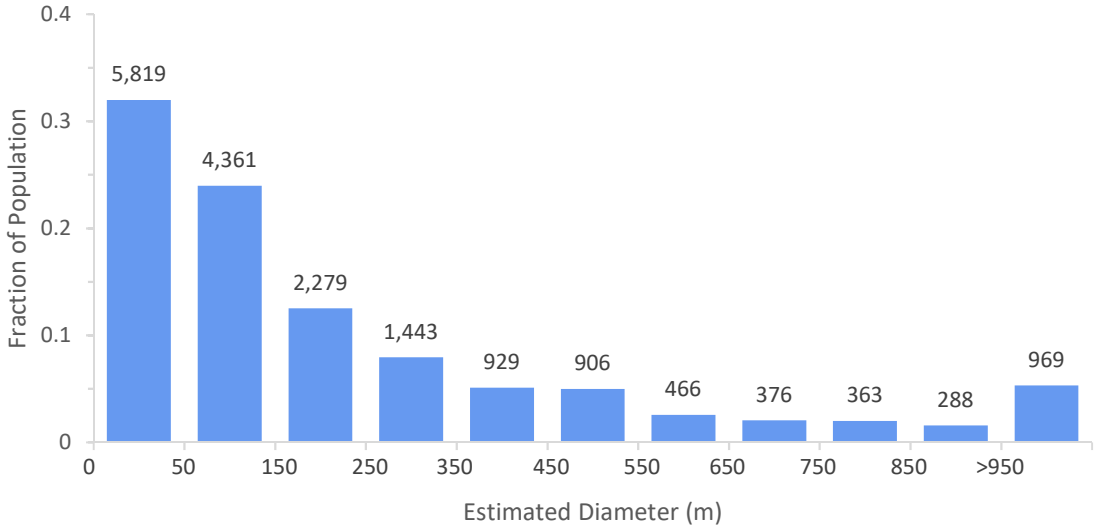

Figure 3. Size distribution of known NEAs. Diameter estimates are calculated from absolute magnitude (H) using an assumed average albedo (a) of 0.14. Absolute magnitudes are from JPL Small Body Browser, current as of 21/05/18. The number of NEAs in each bin is labeled on the end of the columns.

An important consideration is the effect of increased supply on PGE value. An estimated 560,000 kg of PGEs were produced from mined and recycled sources globally in 2016 (NRC 2018). A $1 B asteroid contains 50,200 kg. While price does not scale linearly with supply, adding 10 % to the global supply would likely depress the price to some extent. A $10 B asteroid would contain nearly the entire annual PGE production, depressing prices even further. This effect is possibly alleviated by selling asteroid derived PGEs over an extended time span.

The above estimates do not account for the engineering cost of PGE extraction. While this is hard to directly estimate, the value per tonne of asteroid material compared to ores on Earth can shed light on the potential extraction budget. Earth's highest-grade PGE ore are in the Stillwater Complex, Montana. The most enriched zone of the complex is the J-M reef. A 5.5 km long and 2.1 m thick section of this zone contains PGE value of ~$550 USD / t in Pt and Pd (Todd et al. 1982). The reserves here are small relative to South Africa's Bushveld Complex, the world's largest producer. The South African ore was worth ~$100 USD / t in Pt, Pd, Rh, Ru, Ir, and Au in 2015 (Thormann et al. 2017). 50^{th} and 90^{th} percentile metallic asteroids are worth ~$280 USD / t and ~$1,350 USD / t respectively.

Considering the relative grades and the increased complexity of space-based PGE extraction, the engineering costs may dictate that only highly concentrated metallic asteroids can be considered as mining targets, or that PGE production from asteroids will only be economical as a by-product of another process. The viability of PGE production from NEAs is further explored in section 2.5.2.

2.4.1.2 Water

Unlike PGEs, water is a strategic resource in the short term of NEA SRU due to its existing demand in space. To be economical, it must be more cost-effective to source and process it from NEAs than to launch it from Earth. The value of water in space is derived from its vast array of potential applications. Most importantly in the short term, it can be electrolyzed into its constituent hydrogen and oxygen which upon recombination create an exothermic reaction that can be harnessed for rocket propulsion. It can also be used for radiation shielding, agriculture, respiration (O_2 from electrolysis) and, of course, drinking

for humans. Presently, the market for water in space is delivery to the International Space Station and as propellant for satellite station-keeping (Sommariva 2015). In the near future, the advent of a cis-lunar propellant depot and a fleet of satellite-servicing space-tug vehicles could considerably increase demand (Metzger 2016). A cis-lunar propellant depot would decrease costs faced by public agencies and private interests, lower the barrier to entry for space operations, and stimulate activity in the space market. Space-tug vehicles, operated independently or by the asteroid mining corporations themselves, could rapidly transport satellites from LEO to geostationary orbit (GEO), saving satellite operators from lost profits accrued over the months it takes to deploy communications satellites via ion propulsion (Metzger 2016).

Moving forward, an important potential application of water in space is for radiation shielding. Of the types of radiation prevalent beyond Earth's magnetosphere, galactic cosmic rays and solar particle events pose the greatest risk to human health (Cucinotta and Durante 2006). Together, they are the source of all cosmic radiation (Sihver 2008). Unlike other forms of radiation (e.g., gamma rays) cosmic rays are not most effectively shielded by dense, high atomic mass materials (Sihver 2008). Their interaction with these materials produces secondary radiation, in some cases to the effect of increasing the total intensity. Liquid hydrogen is the most effective shield against cosmic radiation with low atomic mass hydrogen-bearing compounds, such as water, also performing well (Sihver 2008). Water is much simpler to store than liquid hydrogen, and large reservoirs would be required for hydration at any rate, making it the logical choice for radiation shielding.

As was the case for PGEs, the portion of asteroids prospective for water extraction can be estimated using the methods of Elvis (2014). Water is expected to be found in the highest concentrations on C-complex asteroids (Ross 2001), in hydrated phyllosilicates and in subsurface ice. Accounting for discovery bias, 9.8% of NEAs are estimated to be in the C-complex (Stuart and Binzel 2004).

The contribution of hydrated phyllosilicates to the water content of C-complex asteroids can be estimated by meteorite analogy. A study by Jarosewich (1990) compiled chemical analyses determining water content in 22 carbonaceous chondrite samples. Removing the

duplicate analyses (three measurements of Murchison and the pair of ALH 83100 and ALH 83102) leaves 19 chondrites with a mean water content of 3.9 wt%. Eleven of these have < 2 wt% H_2O (~58%) and six (32%) have > 6 wt% H_2O. This higher group will be considered the portion of C-complex NEAs enriched in water (0.32). Elvis (2014) used 10 wt% H_2O as the contribution of hydrated phyllosilicates to the water content of C-complex asteroids but the current study will use the more conservative of 6 wt%.

The contribution of subsurface ice to the total water content is harder to estimate. Carbonaceous chondrites have porosities of 1 – 20% while C-complex NEAs have macro-scale porosities of 28 – 60% (Carry 2012; Elvis 2014). This leaves large volumes to be potentially occupied by water ice and other volatiles, but without prospecting spacecraft it is impossible to know the contents of the voids. Elvis (2014) estimated 10 wt% H_2O as subsurface ice, a value which shall also be used in the current study.

The fraction of NEAs prospective for water is then

$$P_{NEAWater} = P_{type} \cdot P_{cnct} \cdot P_{\Delta V}, \quad \text{(Eq. 4)}$$

$$= 0.098 \cdot 0.32 \cdot 0.014,$$

$$= 0.00044,$$

when using the same accessibility cut off as before. This is equivalent to about one in 2,300 NEAs. Carry (2012) gives reasonably accurate densities for 19 C-complex asteroids with a mean density of 1,410 kg m^{-3} (ρ_{50}, Table 3 in (Carry 2012)). If water can be sold in space for \$5,000 kg^{-1}, half of the historical cost of launching a kilogram of mass into LEO, a NEA as small as 12 m is worth over \$1 B (Table 3). There are 17,371 known NEAs of D > 12 m for a total of seven NEAs prospective for water. Increasing the minimum ΔV by 1 km s^{-1} brings the total to 62 NEAs. The validity of the figure selected for the value of water in space is discussed in section 2.5.2.

Table 3. Value of water in C-complex NEAs.

Diameter (m)	Mass (kg)	Water Concentration (wt %)	Water Value ($ / kg)	Value of asteroid ($M)
8	3.78×10^5	16	5000	$302
12	1.28×10^6	16	5000	$1,021
16	3.02×10^6	16	5000	$2,419
50	9.23×10^7	16	5000	$73,827

There are expected to be vastly more NEAs of small size (< 50 m) than currently known. There are 4,991 known NEAs of 12 – 50 m. From the power law there are expected to be 3×10^7 NEAs in this size range. This brings the total number of NEAs prospective for water to 13,000 at $\Delta V \leq 4.5$ km s^{-1} (Stokes et al. 2003).

Another possible reservoir of water on asteroids is surficial water ice. It is expected to be rare on asteroids due to the rate of sublimation close to the Sun but it has been detected independently by two teams on asteroid 24 Themis (Campins et al. 2010; Rivkin and Emery 2010). Ceres, a C-complex asteroid and the solar system's largest, is one of two targets of NASA's Dawn mission. Dawn began orbiting Ceres in March 2015 and continues to do so at the time of writing. It this time it has generated global maps using its framing camera and visible and infrared mapping spectrometer as well as gathered elemental data with its Gamma Ray and Neutron Detector. From these data it has been determined that Ceres contains ~17 – 30 wt% H_2O, has rare surface water ice, and that ice has remained within a meter of the surface for the body's lifetime (Prettyman et al. 2017).

2.4.2 The Long Term

As time progresses, the maturation of SRU and the cis-lunar economy will allow for increasingly diverse ventures. The array of resources available in asteroids could potentially permit opportunities including more ambitious and frequent space exploration missions, space tourism, and possibly a permanent human presence in space. Key resources for this level of development include base metals, semiconductors, and life-sustaining volatiles (Table 4). Sourcing and manipulating base metals such as iron in space permits the fabrication of infrastructure at scales unhindered by the need to escape Earth's gravity

well. Semiconductors are ubiquitous in modern electronics and their presence in asteroids permits the fabrication of electronics in space. A promising application is to build enormous solar panel arrays in orbit (e.g., Glaser 1977; Sanchez and McInnes 2013). Here the collection of energy is independent of weather conditions and the scale of the array is not limited by the need for the structure to support its own weight. The energy collected can be used in space or perhaps even transmitted back to Earth (Glaser 1977). Asteroids also contain volatile elements like C, N, P, and S, all of which are required by human metabolism. Nitrogen is particularly important because it is needed as an inert atmospheric component as well as a source of nutrition.

2.5 Logistics

The logistical challenges of asteroid mining are varied, complex, and often without precedent. This section will illustrate the stages involved in asteroid mining from initial discovery to final product. Proven technologies and methods will be presented when possible, although many aspects of this section will be speculative in nature.

Many logistical specifics will change on a case by case basis depending on factors like mission architecture, target resource, target asteroid, etc., but the process can be broadly divided into three major categories: 1) Discovery and Characterization; 2) Harvesting and Transportation; and 3) Extraction. The first phase, Discovery and Characterization, describes the progression from asteroid discovery to target selection. Next, Harvesting and Transportation, deals with the retrieval and relocation of asteroid material. The final phase, Extraction, describes a collection of processes used to make finished products from raw asteroid material. The phases are presented as such for ease of communication but in practice the boundaries between them, particularly the final two phases, will likely not be so clear cut.

Table 4. Resources in asteroids, adapted from Sanchez and McInnes (2013).

Resource	Asteroid Class	Fraction of NEA swarm	Resource mass fraction	Space-based application	Resource mass in 120 m asteroid (t)
Fe, Ni, Co	metallic X-complex[1]	0.05	95 wt %[3]	Infrastructure material	3,438,156
PGEs	metallic X-complex[1]	0.05	68 ppm	Import to Earth, electronics	245
Semiconductors	metallic X-complex[1]	0.05	1,600 ppm[4]	Electronics (e.g., solar panels)	5,791
H_2O	water-rich C-complex	0.03	16 wt %	Propellant, radiation shielding, hydration, hygiene, respiration (O_2 - electrolysis), space resource refinement, agriculture	255,147
N_2	C-complex	0.10[2]	934 ppm[5]	Atmosphere, fertilizer	1,192
Silicates	S-complex	0.22[2]	70 wt %[6]	Agriculture, radiation shielding	1,710,030
Organics	C-complex	0.10[2]	4,000 ppm[7]	Agriculture	5,103

Resources are listed with their asteroid class of highest concentration but may be found in other classes as well. Organics refers to organic molecules only, bulk C content is expected to be considerably higher. Fraction of NEA swarm and resource mass fraction are from the text unless otherwise noted. [1]Based on iron meteorites with 90th percentile Ir enrichment [2](Stuart and Binzel 2004); [3](Wasson 1974); [4](Ross 2001; Kargel 1997); [5](Alexander et al. 2012; average of CM chondrites from the supplementary material); [6](McSween et al. 1991); [7](Botta and Bada 2002).

2.5.1 Discovery and Characterization

NEAs are continually discovered and cataloged by numerous organizations for reasons of scientific interest and as an attempt to identify potentially Earth impacting bodies. NASA's Jet Propulsion Laboratory (JPL) runs the Center for Near Earth Object Studies (CNEOS), which supports many discovery surveys at institutions throughout the United States. The five NASA-supported surveys that discovered at least a single new NEO in 2017 are the Catalina Sky Survey (991; Tucson, Arizona), Pan-STARRS1 (893; Maui, Hawaii), ATLAS (98; Hawaii), LINEAR (22; Socorro, New Mexico), and NEOWISE (26; spacecraft in polar orbit) (CNEOS 2018). CNEOS, originally called the NEO Observations program, was founded in 1998 as a response to a US Congressional mandate of the same year ordering NASA to discover 90% of NEOs with a diameter larger than 1 km (CNEOS 2017). Having accomplished this, based on estimations of the total number of NEAs > 1 km, e.g., (Stuart and Binzel 2004), in 2005 the mandate was expanded to include the discovery of 90% of

NEOs with a diameter greater than 140 m. It is estimated there are 15,000 such objects of which about half are discovered. Of the 18,000+ known NEOs of any size only 107 are comets. NEOs are discovered by taking telescopic photographs of the same area of the night sky several minutes apart (Steel 2001). Distant stars and galaxies remain in the same relative location in the photographs, but nearby objects do not. Software links moving objects into “tracklets”. Tracklets without correspondence to known NEOs are reviewed by astronomers. Those likely to be newly discovered NEOs are displayed on the Minor Planet Center’s NEO Confirmation Page to permit follow up observations by telescopes the world over (Wainscoat et al. 2016).

After ground-based observation provides a robust catalogue of NEA characteristics (size, orbital elements, spectral type) prospecting spacecraft will be deployed to the most promising asteroids to finely characterize them before the investment of a full-blown mining mission is made. There is precedence for spacecraft observation of asteroids. Including NASA’s Dawn mission there have been 10 missions visiting 14 asteroids with two more missions en route and four in the planning stage (Table 5). Current spacecraft asteroid observations total 3 NEAs and 11 main-belt asteroids. Even with NASA and JAXA’s growing interest in asteroid missions, the scale of spaceborne asteroid observations required for efficient prospecting requires an in-house solution.

The spacecraft will take measurements of size (shape), density, structure (rubble-pile or monolith), composition, and resource distribution. This can be accomplished with onboard sensors, cameras, and spectrometers. These spacecrafts may also include assay probes to directly sample the surface / shallow subsurface of promising regions. A single spacecraft will have to be deployed for each potential target, dictating lightweight and inexpensive design to enable multiple simultaneous deployments from a single launch vehicle.

Since only one in 2,900 and one in 2,300 NEAs are potential PGE and water sources respectively, and the prospect deploying thousands of space probes is clearly unfeasible, the need for enhanced ground-based characterization of NEAs with an emphasis on spectral class determination and small body discovery (for water-bearing NEAs) is very apparent.

Table 5. Asteroid exploration missions.

Mission Status	Mission Name	Agency	Launch Date	Completion Date	Asteroid Target(s)	Mission Type
Complete	Galileo[1]	NASA	18-Oct-89	21-Sep-03	Gaspra, Ida	both Flyby
	NEAR - Shoemaker[2]	NASA	17-Feb-96	28-Feb-01	Mathilde, *Eros*	Flyby, Orbit
	Cassini[3]	NASA/ESA	15-Oct-97	15-Sep-17	Masursky	Flyby
	Deep Space 1[4]	NASA	24-Oct-98	18-Dec-01	Braille	Flyby
	Stardust[5]	NASA	07-Feb-99	15-Jan-06	Annefrank	Flyby
	Hayabusa[6]	ISAS (now part of JAXA)	09-May-03	13-Jun-10	*Itokawa*	Orbit/Sample return
	Rosetta[7]	ESA	02-Mar-04	30-Sep-16	Šteins, Lutetia	both Flyby
Ongoing	New Horizons[8]	NASA	19-Jan-06	2038	APL	Flyby
	Dawn[9]	NASA	27-Sep-07	late 2018	Vesta, Ceres	both Orbit
	Chang'e 2[10]	CNSA	01-Oct-10	2029	*Toutatis*	Flyby
En route	**Hayabusa2**[11]	JAXA	03-Dec-14	01-Dec-20	*Ryugu*	Orbit/Sample return
	OSIRIS-Rex[12]	NASA	08-Sep-16	24-Sep-23	*Bennu*	Orbit/Sample return
Planned	**NEA Scout**[13]	NASA	15-Dec-19	2023	*1991 VG*	Flyby
	Lucy[14]	NASA	Oct-2021	2033+	Eurybates, Polymele, Leucus, Orus, Patroclus, Donald-johanson	all Flyby
	DESTINY+[15]	JAXA	2022	2026+	*Phaethon*	Flyby
	Psyche[16]	NASA	2022	arrive 2026	Psyche	Orbit

Missions with titles in bold have asteroids for primary targets. Asteroid names in italics are *NEAs*, main belt is in normal text, and trojans are underlined. All dates 2018 and onwards are projected and subject to change. Completion dates for Stardust and Hayabusa and the dates of sample cannister reentry. [1](JPL 2018a); [2](NASA 2018a); [3](JPL 2018b); [4](JPL 2018c); [5](JPL 2018d); [6](JPL 2018e); [7](ESA 2018a); [8](JHUAPL 2006); [9](JPL 2018f); [10](ESA 2018b); [11](JAXA 2018); [12](NASA 2018b); [13](Mahoney 2018); [14](Garner 2017); [15](Kruger 2017); [16](JPL 2018g).

2.5.2 Harvesting and Transportation

The two aspects of this phase are grouped together in acknowledgement of variable mission architectures and despite their different technological requirements. The first decision of this phase is the extent to which material will be concentrated prior to transport. Previous authors have suggested two approaches; “asteroid capture” and “in situ mining” (Probst et al. 2016). In the former, asteroids, in entirety or part, are captured and transported to a designated location for subsequent resource extraction. In the latter, asteroid resources are concentrated or extracted in the unaltered orbit of the asteroid prior to transport. In situ mining allows for more efficient transport at the cost of increased reliance on autonomy; communication delay between Earth and NEAs is often several minutes each way. Asteroid capture would enable near real-time manoeuvres and shorter delays between extraction and sale, allowing operations to respond to changes in demand. This comes at the cost of decreased transportation efficiency and increased propulsion needs.

Depending on the target resource, the degree of autonomy required to run a mining operation, including troubleshooting and mitigating unexpected events, is beyond the capabilities of current technology, leading some researchers (e.g., Mazanek et al. 2015) to suggest asteroid capture is the only viable option. While technologically feasible at small scales, asteroid capture’s efficiency is severely limited by the maximum possible mass retrieved. It is possible that the first successful asteroid mining mission will have to wait for, or build, the appropriate autonomous robotics and/or propulsion technology. It is important to note that the complexity of resource extraction depends on the target resource and asteroid. Extraction of volatiles, like water, from rocky or rubbly asteroids is presumably a simpler task than the extraction of precious metals from a monolithic asteroid of solid FeNi alloy. The former may even be within the capabilities of current autonomous robotics (TransAstra Corp. 2018). The estimates below will account for transportation only, and not the engineering cost of harvesting and/or concentrating the target resource.

A study by Brophy et al. (2012) for the Keck Institute for Space Studies investigated the feasibility of capturing a boulder from a large NEA, or an entire small NEA, and bringing it to cis-lunar space. They found that current propulsion technology can transport a 7 m diameter asteroid of ~500 t from a favourable orbit to cis-lunar space in ~10 years. The

study estimates the cost of such a venture to be ~$2.6 B. Their estimate is based on the orbit of asteroid 2008 HU4, the eighth most accessible of all known NEAs with a ΔV of 3.91 km s^{-1} (Benner 2018). Operations at asteroids with ΔV's of up to 4.5 km s^{-1} will be more expensive. It should also be noted that the Brophy et al. study includes a 30% ($611 B) buffer for reserves.

Transporting 500 t of material from a NEA in a favourable orbit to cis-lunar space for $2.6 B is equivalent to $5,294 kg^{-1} (Brophy et al. 2012). This figure includes research, development, spacecraft testing, and the price of the launch vehicle. Removing all but the recurring costs from the Brophy et al. estimate yields an expense of $2,634 kg^{-1} to transport asteroid material into cis-lunar space.

At this cost, an in situ water mine capable of 90% purity could deliver water to cis-lunar space for $2,927 kg^{-1}. An equivalent asteroid capture mission returning unprocessed asteroid material at 16 wt% water does so for $16,463 kg^{-1}.

If the value of water in space is assumed to be $5,000 kg^{-1}, a 90% pure concentrate is worth $4,500 kg^{-1} and unprocessed asteroid material is worth $800 kg^{-1}. Accounting for the cost of transport, the concentrate provides net gains of $1,866 kg^{-1} and the raw material incurs losses of $1,834 kg^{-1}. The case for in situ concentration is therefore strong, unless advances in propulsion technology can reduce transport costs by a factor of ~4.

The value of water in space is estimated to be half of $10,000 kg^{-1}, the canonical cost of launching mass from Earth's surface to LEO. The validity of this figure could soon be contested due to recent innovations in the commercial space launch sector. SpaceX's Falcon 9 can bring payloads to LEO for $2,719 kg^{-1} (fully expendable build at max capacity) and their Falcon Heavy is purported to do the same for $1,411 kg^{-1}, although the latter has only a single test flight to date (SpaceX 2017). The rockets are advertised to deliver mass to geosynchronous transfer orbit (GTO) for $7,470 kg^{-1} and $3,371 kg^{-1} respectively. If SpaceX's Falcon Heavy matures into a reliable technology, it represents a significant decrease in the value of resources in space. Similar degrees of innovation will have to be made in the production of asteroid resources to ensure a competitive advantage.

At this transport cost, the need for in situ concentration of PGE production is even more apparent. Raw material from 50th and 90th percentile enriched metallic asteroids is worth just \$0.28 kg^{-1} and \$1.35 kg^{-1} respectively while a 90% pure concentrate is worth ~\$18,000 kg^{-1}. Significant in situ concentration is therefore a requirement for PGE production from NEAs; the cost of which is largely unknown. Further, the complexity of autonomous operations required for in situ PGE concentration is similarly unknown. These difficulties make PGE production from NEAs a daunting engineering challenge.

2.5.3 Extraction

In this, the final phase, resources are (further) concentrated and processed into final products. The following methods are conceptual in nature but draw on proven technology when possible.

Water can be extracted from asteroids by thermal dehydration of phyllosilicate minerals (e.g., King et al. 2015). TransAstra Corp. is a Los Angeles based company developing its own method of thermal dehydration called optical mining (TransAstra Corp. 2018). TransAstra's concept is to use concentrated sunlight and a containment bag to simultaneously extract volatiles and excavate the asteroid. In a full-scale test using a synthetic CI-like asteroid and a 10 m diameter solar collector they successfully demonstrated their technology. As predicted, the escaping volatiles caused the host rock to fracture, continually exposing fresh surfaces. Once liberated, the volatiles can be separated and purified by fractional distillation.

Most NEAs are understood to be "rubble-piles" or unconsolidated rock fragments held together by electrostatic, Van der Waal, and gravitational forces (Daniels 2013, Mazanek et al. 2015). A popular suggestion is to concentrate metallic phases by combing their surfaces with an electromagnetic rake (Kargel 1994).

Biomining techniques use microbes to extract metal from ores. Globally, ~20% of copper and ~5% of gold are extracted via biomining (Johnson et al. 2013). A paper by Klas et al. (2015) explores the feasibility of utilizing biomining on asteroids. The authors suggest extremophiles – microorganisms resistant to extremes in temperature, pressure, pH and

radiation – may be of potential use for space-biomining applications. All are dependent on the presence of liquid water however, so construction of an enclosed volume in which an appropriate temperature and atmosphere can be maintained is required. In addition to metal extraction, some microbes are also capable of methanogenesis (Klas et al. 2015). These microorganisms consume compounds like acetate, hydrogen, and carbon dioxide, materials found in carbonaceous asteroids, and produce methane. This simple hydrocarbon is a viable alternative to liquid hydrogen for rocket propellant as it is nearly as efficient, less hazardous, and allows for denser and warmer storage. The authors suggest that the high surface area to volume ratio of rubble-pile asteroids is advantageous for biomining, because of both increased exposure and the unconsolidated nature that provides natural radiation shielding for deeply penetrating microbes. There is cause for concern, however, legally and scientifically, regarding contamination of the asteroid. If the body is of significant scientific interest less obtrusive resource extraction methods should be employed, if any. Legal implications are further discussed below.

The Mond process is a method of obtaining pure nickel from nickel oxides. First described in 1890, the process uses carbon monoxide to form nickel carbonyl ($NiCO_4$) which is then decomposed to form pure nickel, impure residue, and carbon monoxide (Mond et al. 1890). The resultant nickel can be deposited onto a substrate or as a powder. Other metals like iron and chromium also form carbonyls and can be similarly extracted. Iron and nickel can be used for structural fabrication and 3-D printing (from their powders) while the residues will be PGE-enriched.

When considering the logistics of space-based resource production it is also prudent to consider the environmental impact. On one hand, moving a portion of resource production into space reduces the quantity of waste and pollutants that must be accommodated by the Earth (Hlimi 2014). Further, if production is fully automated then the risk to human health associated with the use of chemicals like nickel carbonyl can be negated. In the long-term, minerals important to renewable energy production could be sourced from NEAs, reducing the cost of renewable energy technologies (Metzger 2016). At some point it may even be possible to generate carbon-free solar power in space for use on Earth (Metzger 2016).

On the other hand, there are legal and ethical concerns regarding the contamination of asteroid material. Pristine asteroid material has high scientific value (e.g., NASA 2018b); processing large quantities of asteroid material for economical benefit could potentially destroy clues regarding the nature and evolution of our solar system that lay previously unspoiled for more than four billion years. The legal implications of contaminating extra-terrestrial material is discussed below. A resource production scheme that removes a large portion of an asteroid's mass also has the potential to alter its orbit, necessitating great care as to not inadvertently send an asteroid on a collision course with Earth. There is also concern that any form of increased activity in space will contribute to the growing problem of space debris, fragments of anthropogenic material, particularly those that orbit the Earth, that can cause destructive impacts with satellites and spacecraft (Hlimi 2014). As with resource production on Earth, asteroid mining missions must predict and minimize any deleterious effects on the surrounding environment.

2.6 Asteroid Mining and the Law

In addition to the logistical challenges of asteroid mining, one must also consider the legal implications. Early space legislation was drafted at a time when space was the exclusive domain of governmental bodies, and so little thought was given to the potential commercialization of space and the material in it. More recently, some governments have made efforts to encourage private sector involvement in space resources, but complications persist.

2.6.1 International Space Law

The history of space policy begins with the creation of the Committee on the Peaceful Uses of Outer Space (COPUOS) by the United Nations General Assembly in 1958. Made permanent the next year, the Committee was formed to "govern the exploration and use of space for the benefit of all humanity: for peace, security and development" (COPUOS 2017a). Originally consisting of 18 members, COPUOS now has 84, including all major spacefaring nations. COPUOS was pivotal to the creation of the five treaties and the five principles that govern the exploration of outer space (COPUOS 2017a). The first and most

influential of the treaties is the "Outer Space Treaty" of 1967. Of the remaining treaties and principles, the "Moon Agreement" of 1984 is most pertinent to SRU.

2.6.1.1 The Outer Space Treaty

The Outer Space Treaty (OST) is the most fundamental piece of space legislation produced to date. Officially named the *Treaty on Principles Governing the Activities of States in the Exploration and Use of Outer Space, Including the Moon and Other Celestial Bodies*, the treaty entered into force on October 10, 1967 after it was ratified by the three depository governments of the United States, the Soviet Union, and the United Kingdom (COPUOS 2017b). The Treaty contains 27 articles. The first 12 directly govern the exploration and use of space while the last 15 are administrative. Of the 12 that deal with space directly, I, II, VI, IX, and XII have potential ramifications on SRU including asteroid mining. The OST is well endorsed, having been ratified by 107 nations with 23 more signatories at the time of writing.

Article I sets the tone for the document by stating that "[t]he exploration and use of outer space […] shall be carried out for the benefit and in the interests of all countries […] and shall be the province of all mankind (United Nations 1966)." This passage illustrates the overarching intent of the Treaty; that outer space should be made, and remain, available to all parties equally.

Article II states that "[o]uter space, including the Moon and other celestial bodies, is not subject to national appropriation by claim of sovereignty, by means of use or occupation, or by any other means (United Nations 1966)." The word national would suggest that appropriation of celestial bodies is only forbidden for State governments but as seen in Article VI, States are responsible for all national activities in space, be they governmental or not. This article forms the basis of the argument against the legality of the acquisition and sale of space resources.

Article VI places international responsibility on States for national activities in space, be they governmental or non-governmental. States must authorize and continually supervise the activities of non-governmental entities in their jurisdiction (United Nations 1966).

Article IX forbids cross-contamination of Earth and celestial bodies. While the introduction of processed asteroid materials to Earth are unlikely to cause the "adverse changes in the environment" that the article prohibits, certain extraction techniques (e.g., biomining) could be deemed to contaminate the asteroid, and therefore be impermissible according to this Article (United Nations 1966).

Article XII states that stations, installations, vehicles, and equipment in space are to be made available on a reciprocal basis for visits from representatives of other States Parties to the Treaty. A possible implication to the space mining industry is the inability to preserve the exclusive knowledge of novel technologies and methods (United Nations 1966).

2.6.1.2 The Moon Agreement

The *Agreement Governing the Activities of States on the Moon and Other Celestial Bodies* (Moon Agreement) entered into force on July 11, 1984 (COPUOS 2017b). The Moon Agreement directly addresses the exploitation of space resources, a unique feature among the five UN space treaties. Note that for the purposes of this Agreement the term Moon refers to not only the Moon but also any celestial body within the solar system.

Article 6, paragraph 2 of the Agreement asserts that States Parties may collect and distribute samples of the moon for scientific study (United Nations 1979). States Parties may also use appropriate quantities of space resources in support of their missions (ISRU).

Article 11, paragraph 3, reaffirms the prohibition of sovereign claims laid out in Article II of the OST by stating that "[n]either the surface nor the subsurface of the moon, nor any part thereof or natural resources in place, shall become property of any State, international intergovernmental or non-governmental organization, national organization or non-governmental entity or of any natural person (United Nations 1979)." Paragraph 5 goes on to say that States Parties to the Agreement agree to form "an international regime […] to govern the exploitation of the natural resources of the Moon as such exploitation is about to become feasible (United Nations 1979)." Paragraph 7(d) establishes "[a]n equitable sharing by all States Parties in the benefits derived from those resources" with special consideration for those directly or indirectly involved and to developing nations.

These paragraphs prohibit the commercialization of space resources except by an international regime designed for the mutual benefit of all States Parties. Fortunately for private asteroid mining firms, the Agreement has only 17 members, none of which are major factors in space exploration.

2.6.2 National Legislation

To date, two nations – the United States and Luxembourg – have passed legislation encouraging private sector involvement in space resource development by explicitly granting their citizens the legal right to own and sell space resources.

2.6.2.1 The United States

The United States Commercial Space Launch Competitiveness Act (CSLCA) came into force on November 25, 2015 (McCarthy 2015). Title IV sec. 51303 states that it is legal for U.S. citizens to engage in the commercial exploration and recovery of space resources. U.S. citizens are granted the right to "possess, own, transport, use, and sell" any obtained space resource in accordance with applicable law, including U.S. international obligations. By its citizens exercising this right the bill claims that U.S. is not asserting sovereignty or claiming ownership of any celestial object.

2.6.2.2 Luxembourg

In July 2017 the small country of Luxembourg became to first European nation to pass space resource legislation with the Loi du 20 juillet 2017 sur l'exploration et l'utilisation des ressources de l'espace (Law of 20 July 2017 on the exploration and use of space resources) (Government of Luxembourg 2017a). Effective August 1, 2017, the bill grants similar rights as the United States' CSLCA (ownership rights to extracted material but not the object from which the material was extracted) but with the modification that these rights are available not only to citizens, but also to any corporation with an office in the country of Luxembourg. This is not the first pro-space move to come from the small nation; Luxembourg was instrumental to the creation of SES, Europe's first private satellite company, now the world's largest, which remains headquartered in the country

(Government of Luxembourg 2017b). US firms Planetary Resources and Deep Space Industries both have offices in the country.

There is a lack of consensus in the space law community as to whether these Acts are in accordance with the OST. Under international law, property rights can only be attributed by a superior power (Tronchetti 2015). This power, the State, can only attribute property rights if the State itself has rights to the property first. In this sense, for State governments to grant space resource property rights to their citizens they are in effect appropriating the property rights for themselves first. This is in violation of Article II of the OST. Others argue that the OST does not expressly prohibit the commercialization of space resources and national legislation such as these are valid interpretations of the rights afforded to each State in accordance with Article VI of the same treaty.

2.7 State of the Asteroid Mining Industry

Thus far, Planetary Resources has launched and tested two versions of their Arkyd spacecraft; Arkyd-3 Reflight in 2015 and Arkyd-6 in 2018 (Planetary Resources 2017). Their first spacecraft to collect data from asteroids, Arkyd-301, is in development. The Arkyd-301 will be designed to be small and inexpensive enough to permit the simultaneous deployment of multiple reproductions by a single launch vehicle, each destined for its own target asteroid. (Planetary Resources 2018). Spacecraft miniaturization, a trend also evidenced by the recent popularity of CubeSats, is the key to deploying enough spacecrafts to explore numerous NEAs in a timely and cost-effective manner. The Arkyd-301 will perform compositional surface mapping and will also include four on-board probes to directly sample the asteroid (Planetary Resources 2018). Data from the Arkyd-301 fleet will be used to select Planetary Resources' first mining target and inform the development of their mining architecture. Planetary Resources missed funding goals throughout 2018 and has been forced to downsize. While its long-term goals remain, it has pivoted to satellite Earth observation in an effort to secure a consistent revenue stream.

Deep Space Industries has placed an emphasis on developing propulsion technology. It has two thrusters currently available for purchase; Comet and Meteor. Comet uses molecular water as propellant and is flight ready while Meteor uses hydrogen peroxide and will ship

in late 2018 (Deep Space Industries 2018a, 2018b). It is also iterating towards a low-mass, low-cost prospecting spacecraft. This craft will be built on its Xplorer spacecraft platform (Deep Space Industries 2018c). Expected to be ready by 2020, this platform will be capable of transporting a 10 kg payload from LEO to interplanetary space, a feat not yet accomplished by any spacecraft (typically spacecraft require thrust from a rocket to escape Earth's gravitational influence) (Deep Space Industries 2018c).

Planetary Resources, Deep Space Industries, and TransAstra are not the only companies working towards making asteroid mining a reality. Luxembourg based Kleos Space S.à.rl., a subsidiary of UK based Magna Parva Limited, is collaborating with the Luxembourg Institute of Science and Technology and has received funds from the Luxembourg government to develop in-space manufacturing technology (LIST 2018). Aten Engineering, headquartered out of Portland, Oregon, is working towards making efficiencies in the domain of asteroid detection and characterization (Aten Engineering 2018). OffWorld is a robotics company with branches in Pasadena, California and Luxembourg. Its long-term goal is to create autonomous industrial robots for use on Earth, the Moon, Mars, and asteroids (OFFWORLD 2018).

2.8 Private-Public Partnerships

In 2004, President George W. Bush announced his new U.S. Space Exploration Policy. This Policy ordered a return to the Moon in 2020 and the retirement of the Space Shuttle program in late 2010, upon completion of the International Space Station (Hackler 2014). The next year, newly appointed NASA administrator Mike Griffin established the Commercial Crew and Cargo Program Office. The office spawned the Commercial Orbital Transportation Services (COTS) and Commercial Resupply Services (CRS) programs. These were not the first attempts at privatizing Space Shuttle and Space Station activities, but they were the first programs to clearly illustrate the effectiveness of Private-Public Partnerships (PPPs) in the space sector (Hackler 2014). PPPs are designed to split the cost, risk, and effort between government and industry. The private partner accepts more risk and responsibility versus a traditional arrangement, incentivizing increased efficiency. COTS and CRS culminated in the development and deployment of SpaceX's Dragon and

Orbital Sciences Corp.'s (now Orbital ATK) Cygnus, the first two private spacecraft to dock with and resupply the International Space Station (Hackler 2014).

The success of COTS has been described as a "new era in spaceflight" (Hackler 2014). Eager to capitalize on the success of their earlier program, the same team has developed Lunar Commercial Orbital Transfer Services (Zuniga et al. 2015). This program would seek industry partnership for developing services in cis-lunar space like transportation, lunar ISRU, and propellant depots. This infrastructure would serve as a base for future Mars exploration.

A paper by Entrena Utrilla (2017) proposes the simultaneous and synergistic development of an asteroid resource utilization PPP dubbed Asteroid COTS. Given the recent success of PPPs enjoyed by NASA, and the potential gains the agency would see from advancement of commercial spacecraft and the installation of cis-lunar propellant depots, an asteroid resource PPP seems a likely possibility. NASA has awarded contracts to asteroid mining companies before; Deep Space Industries and Planetary Resources each received two contracts as part of the Asteroid Redirect Mission (Mahoney 2014).

2.9 Opportunities for Canada

Canada is a world leader in mining. In 2016, Canada produced $111 B worth of minerals (including mineral fuels), the sixth most of any nation (Reichl et al. 2018). Mining is Canada's third largest industry, worth 8.5% of its GDP in February 2018 (Statistics Canada 2018). Canada also has a distinguished and celebrated history of space robotics, most famously the Canadarm and Canadarm2, both created by MacDonald, Dettwiler and Associates (MDA), now part of Maxar Technologies Ltd (MDA 2018). MDA is not the only Canadian robotics company developing space platforms. Sudbury, Ontario, based Deltion Innovations Ltd was awarded a ~$1 million contract from the Canadian Space Agency (CSA) in December 2016 to build a rotary multi-purpose tool (CSA 2016). While developed for use on the moon and Mars, the tool is potentially suitable for asteroid use. The CSA funding is shared by two other Ontario firms: Kanata's Neptec Design Group and North Bay's Atlas Copco.

A potential advantage held by Canada is an innovation in federal mining law called flow through shares (FTS). The FTS program allows resource corporations to transfer exploration and development expenses to investors (Government of Canada 2008a). Investors can then use these expenses to lower their taxable income. This allows a space mining start up with massive exploration costs and no immediate income to transfer its tax incentive to its high-income investors. The program allows for transfer of 100% and 30% of exploration and development expenses respectively (Government of Canada 2008b). The program has been instrumental in stimulating Canada's mineral and oil industries. With the magnified expense associated with extraterrestrial exploration, the law may prove even more effective in this arena.

Considering the above, asteroid mining might seem like a natural fit for Canada, but there are yet to be any tangible steps in that direction. Despite the present expertise, the private sector is so far devoid of any companies working directly on any aspect of asteroid mining. The government is also yet to make a move, with no space mining legislation passed and no indication on where it stands on the legality of SRU. The time for Canadian investment in space resources is now if Canada is to remain a leader in the global mining economy.

2.10 Future Work

Economic utilization of asteroid resources is not an impossible goal, but before the wealth of the solar system can be realized there are significant hurdles to overcome. Advances in spacecraft propulsion technology and/or robotic resource extraction autonomy will be required to transport and process material at a sufficient scale to be economical. Before this stage however, the catalogue of NEAs, with particular pertinence to spectral data, must be expanded. The paucity of prospective asteroid mining targets (1 / 2,300 for water) dictates that extensive ground-based observations must be made prior to the selection of asteroids to which prospecting spacecraft will be sent. New NEA discoveries should have their spectra immediately characterized by follow up observations and efforts should be made to make spectral observations for as many known NEAs as possible. Since asteroid resources are likely to be acquired via appropriation of the resource only, and not of the host asteroid, the exclusive knowledge of prospective asteroids is extremely valuable, even before spacecraft visitation or the commencement of a mining operation.

2.11 References

Alexander, C.M.O.D., Bowden, R., Fogel, M.L., Howard, K.T., Herd, C.D.K., and Nittler, L.R. 2012. The provenances of asteroids, and their contributions to the volatile inventories of the terrestrial planets. Science, **337**: 721–723.

Aten Engineering. 2018. Aten Engineering Home. Available from https://www.atenengineering.com/ [accessed 21 May 2018].

BASF. 2018. BASF Catalysts. Available from https://apps.catalysts.basf.com/apps/eibprices/mp/ [accessed 21 May 2018].

Benedix, G.K., McCoy, T.J., Keil, K., Bogard, D.D., and Garrison, D.H. 1998. A petrologic and isotopic study of winonaites: Evidence for early partial melting, brecciation, and metamorphism. Geochimica et Cosmochimica Acta, **62**: 2535–2553.

Benner, L.A.M. 2018. Near-Earth Asteroid Delta-V for Spacecraft Rendezvous. Available from https://echo.jpl.nasa.gov/~lance/delta_v/delta_v.rendezvous.html [accessed 24 January 2018].

Bobrovnikoff, N.T. 1929. The Spectra of Minor Planets. Lick Observatory Bulletin, **407**: 18–27.

Botta, O., and Bada, J.L. 2002. Extraterrestrial organic compounds in meteorites. Surveys in Geophysics, **23**: 411–467.

Brophy, J.R., Friedman, L., and Culick, F. 2012. Asteroid retrieval feasibility. *In* IEEE Aerospace Conference Proceedings. pp. 1–51.

Burbine, T.H. 2016. Asteroids. Cambridge University Press.

Bus, S.J., and Binzel, R.P. 2002. Phase II of the small main-belt asteroid spectroscopic survey. A feature-based taxonomy. Icarus, **158**: 146–177.

Campins, H., Hargrove, K., Pinilla-Alonso, N., Howell, E.S., Kelley, M.S., Licandro, J., Mothé-Diniz, T., Fernández, Y., and Ziffer, J. 2010. Water ice and organics on the surface of the asteroid 24 Themis. Nature, **464**: 1320–1321.

Di Carlo, M., Romero Martin, J.M., Ortiz Gomez, N., and Vasile, M. 2017. Optimised low-thrust mission to the Atira asteroids. Advances in Space Research, **59**: 1724–1739. COSPAR.

Carry, B. 2012. Density of asteroids. Planetary and Space Science, **73**: 98–118. Elsevier.

Carry, B., Solano, E., Eggl, S., and DeMeo, F.E. 2016. Spectral properties of near-Earth and Mars-crossing asteroids using Sloan photometry. Icarus, **268**: 340–354.

Chapman, C.R., Morrison, D., and Zellner, B. 1975. Surface properties of asteroids: A synthesis of polarimetry, radiometry, and spectrophotometry. Icarus, **25**: 104–130.

CNEOS. 2017. NEO Search Program. Available from https://cneos.jpl.nasa.gov/about/search_program.html [accessed 4 December 2017].

CNEOS. 2018. Discovery Statistics. Available from https://cneos.jpl.nasa.gov/stats/site_all.html [accessed 1 May 2018].

Connors, M., Wiegert, P., and Veillet, C. 2011. Earth's Trojan asteroid. Nature, **475**: 481–483.

Consolmagno, G.J., and Drake, M.J. 1977. Composition and evolution of the eucrite parent body: evidence from rare earth elements. Geochimica et Cosmochimica Acta, **41**: 1271–1282.

COPUOS. 2017a. COPUOS United Nations Office for Outer Space Affairs. Available from http://www.unoosa.org/oosa/en/ourwork/copuos/index.html [accessed 8 December 2017].

COPUOS. 2017b. Space Law Treaties and Principles. Available from http://www.unoosa.org/oosa/en/ourwork/spacelaw/treaties.html [accessed 8 December 2017].

Crawford, I.A. 2015. Lunar resources: A review. Progress in Physical Geography, **39**: 137–167.

CSA. 2016. Proactive disclosure of contracts over $10,000 - Canadian Space Agency. Available from http://www.asc-csa.gc.ca/eng/publications/contracts-details.asp?trimestre=&id=11237 [accessed 4 December 2017].

Cucinotta, F.A., and Durante, M. 2006. Cancer risk from exposure to galactic cosmic rays: implications for space exploration by human beings. Lancet Oncol, **7**: 431–435.

Daniels, K.E. 2013. Rubble-pile near earth objects: Insights from granular physics. *In* Asteroids: Prospective Energy and Material Resources. *Edited by* V. Badescu. Springer Berlin Heidelberg, Berlin, Heidelberg. pp. 271–286.

Deep Space Industries. 2017. Prospector-1 | Deep Space Industries. Available from

http://deepspaceindustries.com/prospector-1/ [accessed 8 December 2017].

Deep Space Industries. 2018a. Comet SmallSat Propulsion | Deep Space Industries. Available from http://deepspaceindustries.com/comet/ [accessed 21 May 2018].

Deep Space Industries. 2018b. Meteor | Deep Space Industries. Available from http://deepspaceindustries.com/meteor/ [accessed 21 May 2018].

Deep Space Industries. 2018c. Xplorer | Deep Space Industries. Available from http://deepspaceindustries.com/xplorer/ [accessed 21 May 2018].

DeMeo, F.E., Binzel, R.P., Slivan, S.M., and Bus, S.J. 2009. An extension of the Bus asteroid taxonomy into the near-infrared. Icarus, **202**: 160–180. Elsevier Inc.

Elvis, M. 2014. How many ore-bearing asteroids? Planetary and Space Science, **91**: 20–26. Elsevier.

Entrena Utrilla, C.M. 2017. Asteroid-COTS: Developing the cislunar economy with private-public partnerships. Space Policy, **39**–**40**: 14–19. Elsevier Ltd.

ESA. 2018a. Rosetta. European Space Agency. Available from http://sci.esa.int/rosetta/ [accessed 4 June 2018].

ESA. 2018b. Chang'e-2 - Satellite Missions - eoPortal Directory. Available from https://earth.esa.int/web/eoportal/satellite-missions/c-missions/chang-e-2 [accessed 4 June 2018].

Garner, R. 2017. Lucy: The First Mission to Jupiter's Trojans. Available from https://www.nasa.gov/content/goddard/lucy-the-first-mission-to-jupiter-s-trojans [accessed 4 June 2018].

Glaser, P.E. 1977. The potential of satellite solar power. *In* Proceedings of the IEEE. pp. 1162–1176.

Government of Canada. 2008a. Flow-through shares (FTSs). Available from https://www.canada.ca/en/revenue-agency/services/tax/businesses/topics/flow-through-shares-ftss.html [accessed 30 November 2017].

Government of Canada. 2008b. How the flow-through share (FTS) program works. Available from https://www.canada.ca/en/revenue-agency/services/tax/businesses/topics/flow-through-shares-ftss/investors/flow-through-share-program-works.html [accessed 30 November 2017].

Government of Luxembourg. 2017a. Loi du 20 juillet 2017 sur l'exploration et

l'utilisation des ressources de l'espace. - Legilux. Available from http://legilux.public.lu/eli/etat/leg/loi/2017/07/20/a674/jo [accessed 4 December 2017].

Government of Luxembourg. 2017b. Space resources in Luxembourg. Available from http://www.spaceresources.public.lu/en/space-resources-luxembourg.html [accessed 4 December 2017].

Hackler, R. 2014. Commercial Orbital Transportation Services A New Era in Spaceflight. Available from https://www.nasa.gov/sites/default/files/files/SP-2014-617.pdf.

Henderson, E.P., and Perry, S.H. 1954. A discussion of the densities of iron meteorites. Geochimica et Cosmochimica Acta, **6**: 221–240.

Hilton, J.L. 2002. Asteroid masses and densities. *In* Asteroids III. *Edited by* W.F. Bottke, A. Cellino, P. Paolicchi, and R.P. Binzel. The University of Arizona Press. pp. 103–112.

Hlimi, T. 2014. The Next Frontier: An Overview of the Legal and Environmental Implications of Near-Earth Asteroid Mining. Annals of Air and Space Law, **39**: 409–453.

Howard, K.T., Benedix, G.K., Bland, P.A., and Cressey, G. 2011. Modal mineralogy of CM chondrites by X-ray diffraction (PSD-XRD): Part 2. Degree, nature and settings of aqueous alteration. Geochimica et Cosmochimica Acta, **75**: 2735–2751. Elsevier Ltd.

Jarosewich, E. 1990. Chemical analyses of meteorites: A compilation of stony and iron meteorite analyses. Meteoritics, **25**: 323–337.

JAXA. 2018. JAXA | Asteroid Explorer "Hayabusa." Available from http://global.jaxa.jp/projects/sat/hayabusa2/ [accessed 4 June 2018].

JHUAPL. 2006. New Horizons Tracks an Asteroid. Available from http://pluto.jhuapl.edu/News-Center/News-Article.php?page=061506 [accessed 4 June 2018].

Johnson, D., Grail, B., and Hallberg, K. 2013. A new direction for biomining: extraction of metals by reductive dissolution of oxidized ores. Minerals, **3**: 49–58.

JPL. 2018a. Missions | Galileo. Available from https://www.jpl.nasa.gov/missions/galileo/ [accessed 4 June 2018].

JPL. 2018b. New Cassini Images of Asteroid Available – Cassini Legacy: 1997-2017.

Available from https://saturn.jpl.nasa.gov/news/2194/new-cassini-images-of-asteroid-available/ [accessed 4 June 2018].

JPL. 2018c. Missions | Deep Space 1. Available from https://www.jpl.nasa.gov/missions/deep-space-1-ds1/ [accessed 4 June 2018].

JPL. 2018d. Stardust - NASA's Comet Sample Return Mission. Available from https://stardust.jpl.nasa.gov/home/index.html [accessed 4 June 2018].

JPL. 2018e. Missions | Hayabusa. Available from https://www.jpl.nasa.gov/missions/hayabusa/ [accessed 4 June 2018].

JPL. 2018f. Dawn Mission | Mission. Available from https://dawn.jpl.nasa.gov/mission/ [accessed 4 June 2018].

JPL. 2018g. Missions | Psyche. Available from https://www.jpl.nasa.gov/missions/psyche/ [accessed 4 June 2018].

Kargel, J.S. 1994. Metalliferous asteroids as potential sources of precious metals. Journal of Geophysical Research, **99**: 21,129-21,141.

King, A.J., Solomon, J.R., Schofield, P.F., and Russell, S.S. 2015. Characterising the CI and CI-like carbonaceous chondrites using thermogravimetric analysis and infrared spectroscopy. Earth, Planets and Space, **67**: 198. Earth, Planets and Space.

Klas, M., Tsafnat, N., Dennerley, J., Beckmann, S., Osborne, B., Dempster, A.G., and Manefield, M. 2015. Biomining and methanogenesis for resource extraction from asteroids. Space Policy, **34**: 18–22.

Krot, A.N., Amelin, Y., Cassen, P., and Meibom, A. 2005. Young chondrules in CB chondrites from a giant impact in the early Solar System. Nature, **436**: 989–992.

Kruger, H. 2017. Dust analysis on board the Destiny+ mission to 3200 Phaethon. EPSC Abstracts, **11**.

de la Fuente Marcos, C., and de la Fuente Marcos, R. 2014. Asteroid 2013 ND15: Trojan companion to venus, PHA to the Earth. Monthly Notices of the Royal Astronomical Society, **439**: 2970–2977.

de la Fuente Marcos, C., and de la Fuente Marcos, R. 2017. Asteroid 2014 YX49: A large transient Trojan of Uranus. Monthly Notices of the Royal Astronomical Society, **467**: 1561–1568.

LIST. 2018. A new cooperation within spaceresources.lu initiative. Available from

https://www.list.lu/fr/news/a-new-cooperation-within-spaceresourceslu-initiative/ [accessed 21 May 2018].

Mahoney, E. 2014. NASA Selects Studies for the Asteroid Redirect Mission. Available from https://www.nasa.gov/content/nasa-selects-studies-for-the-asteroid-redirect-mission [accessed 4 December 2017].

Mahoney, E. 2018. NEA Scout | NASA. doi:10.2514/6.2014-4435.

Mazanek, D.D., Merrill, R.G., Brophy, J.R., and Mueller, R.P. 2015. Asteroid Redirect Mission concept: A bold approach for utilizing space resources. Acta Astronautica, **117**: 163–171.

McDonough, W.F., and Sun, S. s. 1995. The composition of the Earth. Chemical Geology, **120**: 223–253.

McCarthy, K. 2015. H.R.2262 - 114th Congress (2015-2016): U.S. Commercial Space Launch Competitiveness Act. Available from https://www.congress.gov/bill/114th-congress/house-bill/2262 [accessed 28 November 2017].

McSween, H.Y., Bennett, M.E., and Jarosewich, E. 1991. The mineralogy of ordinary chondrites and implications for asteroid spectrophotometry. Icarus, **90**: 107–116.

MDA. 2018. Space-Based Robotics Solutions. Available from https://mdacorporation.com/isg/robotics-automation/space-based-robotics-solutions [accessed 21 May 2018].

Metzger, P.T. 2016. Space development and space science together, an historic opportunity. Space Policy, **37**: 77–91. Elsevier Ltd.

Mond, L., Langer, C., and Quincke, F. 1890. Action of carbon monoxide on nickel. Journal of the Chemical Society, Transactions, **57**: 749–753.

NASA. 2018a. In Depth | NEAR Shoemaker – Solar System Exploration: NASA Science. Available from https://solarsystem.nasa.gov/missions/near-shoemaker/in-depth/ [accessed 4 June 2018].

NASA. 2018b. OSIRIS-REx Overview. Available from https://www.nasa.gov/content/osiris-rex-overview [accessed 4 June 2018].

Neeley, J.R., Clark, B.E., Ockert-Bell, M.E., Shepard, M.K., Conklin, J., Cloutis, E.A., Fornasier, S., and Bus, S.J. 2014. The composition of M-type asteroids II: Synthesis of spectroscopic and radar observations. Icarus, **238**: 37–50.

Nesvorny, D., and Roig, F. 2017. Dynamical Origin and Terrestrial Impact Flux of Large Near-Earth Asteroids. In Press,: 1–18.

NRC. 2018. Platinum facts | Natural Resources Canada. Available from http://www.nrcan.gc.ca/mining-materials/facts/platinum/20520#L2 [accessed 6 June 2018].

OFFWORLD. 2018. OFFWORLD Home. Available from https://www.offworld.ai/ [accessed 21 May 2018].

Planetary Resources. 2012. Asteroid mining plans revealed by Planetary Resources, Inc. | Planetary Resources. Available from https://www.planetaryresources.com/2012/04/asteroid-mining-plans-revealed-by-planetary-resources-inc/ [accessed 21 May 2018].

Planetary Resources. 2017. Timeline | Planetary Resources. Available from https://www.planetaryresources.com/company/timeline/ [accessed 21 May 2018].

Planetary Resources. 2018. Arkyd-301 | Planetary Resources. Available from https://www.planetaryresources.com/missions/arkyd-301/ [accessed 21 May 2018].

Prettyman, T.H., Yamashita, N., Toplis, M.J., McSween, H.Y., Schörghofer, N., Marchi, S., Feldman, W.C., Castillo-Rogez, J., Forni, O., Lawrence, D.J., Ammannito, E., Ehlmann, B.L., Sizemore, H.G., Joy, S.P., Polanskey, C.A., Rayman, M.D., Raymond, C.A., and Russell, C.T. 2017. Extensive water ice within Ceres' aqueously altered regolith: Evidence from nuclear spectroscopy. Science, **355**: 55–59.

Probst, A., González Peytaví, G., Eissfeller, B., and Förstner, R. 2016. Mission concept selection for an asteroid mining mission. Aircraft Engineering and Aerospace Technology, **88**: 458–470.

Reichl, C., Schatz, M., and Zsak, G. 2018. World Mining Data 2018. *In* Federal Ministry of Science, Research and Economy, Austria.

Rivkin, A.S., and Emery, J.P. 2010. Detection of ice and organics on an asteroidal surface. Nature, **464**: 1322–1323. Nature Publishing Group.

Robutel, P., and Souchay, J. 2010. An introduction to the dynamics of trojan asteroids. *In* Lecture Notes in Physics. Springer. doi:10.1007/978-3-642-04458-8_4.

Ross, S.D. 2001. Near-Earth Asteroid Mining. Space Industry Report,: 1–24.

Rubin, A.E. 1997. Mineralogy of meteorite groups. Meteoritics & Planetary Science, **32**: 231–247.

Rubin, A.E. 2007. Petrogenesis of acapulcoites and lodranites: A shock-melting model. Geochimica et Cosmochimica Acta, **71**: 2383–2401.

Rubin, A.E., and Grossman, J.N. 2010. Meteorite and meteoroid: New comprehensive definitions. Meteoritics and Planetary Science, **45**: 117–125.

Sanchez, J.P., and McInnes, C.R. 2013. Available asteroid resources in the earth's neighbourhood. *In* Asteroids: Prospective Energy and Material Resources, 1st edition. *Edited by* V. Badescu. Springer-Verlag Berlin Heidelberg. pp. 439–458.

Sanders, G.B., and Larson, W.E. 2015. Final review of analog field campaigns for in Situ Resource Utilization technology and capability maturation. Advances in Space Research, **55**: 2381–2404. COSPAR.

Schmidt, G. 2004. Are high-temperature fractionations in the solar nebula preserved in highly siderophile element systematics of the Earth's mantle? Meteoritics and Planetary Science, **39**: 1995–2007.

Scott, E.R.D., Wasson, J.T., and Buchwald, V.F. 1973. The chemical classification of iron meteorites-VII. A reinvestigation of irons with Ge concentrations between 25 and 80 ppm. Geochimica et Cosmochimica Acta, **37**: 1957–1976.

Shoemaker, E.M., Williams, J.G., Helin, E.F., and Wolfe, R.F. 1979. Earth-crossing asteroids: Orbital classes, collision rates with Earth, and origin. *In* Asteroids. pp. 253–282.

Sihver, L. 2008. Transport calculations and accelerator experiments needed for radiation risk assessment in space. Zeitschrift fur Medizinische Physik, **18**: 253–264.

Sommariva, A. 2015. Rationale, strategies, and economics for exploration and mining of asteroids. Astropolitics, **13**: 25–42.

SpaceX. 2017. Capabilities & Services | SpaceX. Available from http://www.spacex.com/about/capabilities [accessed 8 December 2017].

Statistics Canada. 2018. Gross domestic product at basic prices, by industry (monthly). Available from http://www.statcan.gc.ca/tables-tableaux/sum-som/l01/cst01/gdps04a-eng.htm [accessed 21 May 2018].

Steel, D. 2001. Searching for NEOs using wide-field telescopes. *In* The New Era of Wide

Field Astronomy, ASP Conference Series, Vol. 232.

Stokes, G.H., Yeomans, D.K., Bottke, W.F., Jewitt, D., Chesley, S.R., Kelso, T.S., Evans, J.B., McMillan, R.S., Gold, R.E., Spahr, T.B., Harris, A.W., and Worden, S.P. 2003. Study to determine the feasibility of extending the search for near-Earth objects to smaller limiting diameters. *In* NASA Office of Space Science Solar System Exploration Division.

Stuart, J.S., and Binzel, R.P. 2004. Bias-corrected population, size distribution, and impact hazard for the near-Earth objects. Icarus, **170**: 295–311.

Tholen, D.J. 1984. Asteroid taxonomy from cluster analysis of photometry. The University of Arizona.

Thormann, L., Buchspies, B., Mbohwa, C., and Kaltschmitt, M. 2017. PGE production in southern Africa, part 1: Production and market trends. Minerals, **7**. doi:10.3390/min7110224.

Todd, S.G., Keith, D.W., Le Roy, L.W., Schissel, D.J., Mann, E.L., and Irvine, T.N. 1982. The J-M platinum-palladium reef of the Stillwater complex, Montana: I. Stratigraphy and petrology. Economic Geology, **77**: 1454–1480.

TransAstra Corp. 2018. TransAstra Corp. Home. Available from http://www.transastracorp.com/ [accessed 28 February 2018].

Tronchetti, F. 2015. The Space Resource Exploration and Utilization Act: A move forward or a step back? Space Policy, **34**: 6–10. Elsevier Ltd.

United Nations. 1966. Treaty on Principles Governing the Activities of States in the Exploration and Use of Outer Space, including the Moon and Other Celestial Bodies. Available from http://www.unoosa.org/oosa/en/ourwork/spacelaw/treaties/outerspacetreaty.html [accessed 4 December 2017].

United Nations. 1979. Agreement Governing the Activities of States on the Moon and Other Celestial Bodies. Available from http://www.unoosa.org/oosa/en/ourwork/spacelaw/treaties/moon-agreement.html [accessed 4 December 2017].

Wainscoat, R., Chambers, K., Lilly, E., Weryk, R., Chastel, S., Denneau, L., and Micheli, M. 2016. The Pan-STARRS search for Near Earth Objects. Proceedings of the

International Astronomical Union, **10**: 293–298.

Wasson, J.T. 1974. Meteorites: Classification and properties. *In* Minerals and Rocks. Volume 10, Springer-New York. 327 p. doi:10.1007/978-3-642-65863-1.

Wasson, J.T., Choi, B.-G., Jerde, E.A., and Ulff-Møller, F. 1998. Chemical classification of iron meteorites: XII. New members of the magmatic groups. Geochimica et Cosmochimica Acta, **62**: 715–724.

Wasson, J.T., Ouyang, X., Wang, J., and Eric, J. 1989. Chemical classification of iron meteorites: XI. Multi-element studies of 38 new irons and the high abundance of ungrouped irons from Antarctica. Geochimica et Cosmochimica Acta, **53**: 735–744.

Watters, T.R., and Prinz, M. 1979. Aubrites: Their origin and relationship to enstatite chondrites. Proc. Lunar Planet Sci. Conf. 10th,: 1073–1093.

Weisberg, M.K., McCoy, T.J., and Krot, A.N. 2006. Systematics and evaluation of meteorite classification. *In* Meteorites and the early solar system II. University of Arizona Press.

Weisberg, M.K., Prinz, M., Clayton, R.N., Mayeda, T.K., Grady, M.M., Franchi, I.A., Pillinger, C.T., and Kallemeyn, G.W. 1996. The K (Kakangari) chondrite grouplet. Geochimica et Cosmochimica Acta, **60**: 4253–4263.

Wisdom, J. 1983. Chaotic behavior and the origin of the 3/1 Kirkwood gap. Icarus, **56**: 51–74.

Yoshida, F., and Nakamura, T. 2005. Size distribution of faint Jovian L4 trojan asteroids. The Astronomical Journal, **130**: 2900–2911.

Zellner, B., Tholen, D.J., and Tedesco, E.F. 1985. The eight-color asteroid survey: Results for 589 minor planets. Icarus, **61**: 355–416.

Zientek, M.L., and Loferski, P.J. 2014. Platinum-Group Elements — So Many Excellent Properties. *In* USGS Mineral Resources Program.

Zuniga, A.F., Rasky, D., and Pittman, R.B. 2015. Lunar COTS: an economical and sustainable approach to reaching Mars. AIAA Space 2015 Conference and Exposition,: 1–24.

3 Abundance and Subsolidus Diffusion of Highly Siderophile Elements in Main Group Pallasites: Application to Asteroid Resource Prospecting

3.1 Introduction

The platinum group elements (PGE: Ru, Rh, Pd, Os, Ir, and Pt) are valued for their corrosion resistance, catalytic qualities, and high melting temperatures. They are used in the production of autocatalysts, jewelry, and various chemical, electrical, glass, medical, and petroleum products (Zientek and Loferski 2014). Together with Re and Au, they form a group of geochemically similar elements called the highly siderophile elements (HSEs). These elements demonstrate a strong affinity for metallic phases and were extensively fractionated into Earth's core during planetary differentiation (McDonough and Sun 1995). Consequentially, HSEs are extremely scarce in the crust.

In recent years, the prospect of leveraging resources found in space has gained momentum (e.g., Sanders and Larson 2015). While most space resources will only be economically utilized for meeting demand in space, the high value of PGEs potentially permits their economical import and sale on Earth. Having existing demand at a large scale is a unique position among space resources and is especially advantageous in the current embryonic state of the space market. Together with water, for which there is current demand in space, PGEs may be the first resources (excluding sunlight) to be harnessed from space. This process of leveraging natural resources found in space to create useful products or services, called space resource utilization (SRU), has the potential to drastically increase the significance of the space market and expand the sphere of human activity in the solar system.

Like Earth, some asteroids also experienced differentiation, concentrating HSEs into cores of their own. Some of these asteroids were subsequently fragmented by collisions in the evolving solar system; exposing core material. These fragments are metallic asteroids; the parent bodies of iron meteorites. The HSE behavior in iron meteorites is generally well characterized in the literature (e.g., Campbell and Humayun 1999; Ash et al. 2007). The same cannot be said for the main group pallasites, another type of meteorite from

differentiated asteroids. Pallasites consist predominantly of olivine and FeNi alloy with lesser quantities of chromite, sulfides, and phosphides. Like iron meteorites, they are derived from differentiated asteroidal parent bodies. Pallasites were formerly separated into two chemical groups, each representing a distinct parent body, the pallasite main group (PMG) and the Eagle Station trio. There are now at least five recognized parent bodies, with some researchers believing the number to be as high as ten (Danielson et al. 2009; Boesenberg et al. 2012). Some research on oxygen isotopes in PMG olivine also suggests that the PMG itself may contain two subgroups with distinct parent bodies (Ali et al. 2018), although for the purposes of this research the PMG will be considered as a single population. This number of recognized pallasite parent bodies, while fewer than the 50 or more proposed for iron meteorites (Burbine et al. 2002), suggests that pallasitic asteroids are not uncommon.

This study characterizes the concentration, distribution, and subsolidus mobility of a suite of elements, including the HSEs, in six PMG samples. These data complement the existing literature on iron meteorites to create a more complete picture of HSE occurrence in asteroid metal. Until the completion of asteroid sample return missions Hayabusa 2 and OSIRIS-REx in 2020 and 2023, respectively, meteorites will remain the only substantial quantity of asteroid material available for study (JAXA 2018; NASA 2018b). The following sections detail HSE mobility during subsolidus taenite-kamacite partitioning and the bulk metal composition in the PMG. This information is then used to evaluate pallasitic parent bodies as potential targets for SRU.

3.1.1 Pallasite Main Group Mineralogy

The mineralogy of pallasites is fundamental to their resource potential. Pallasites contain olivine ($[Fe,Mg]_2SiO_4$), kamacite (α-[Fe,Ni]), and taenite (γ-[Fe,Ni]), with smaller quantities of troilite (FeS), schreibersite ($[Fe,Ni]_3P$), and chromite ($FeCr_2O_4$) (Buseck 1977). They may also contain the phosphates farringtonite ($Mg_3[PO_4]_2$), stanfieldite ($Ca_4[Mg,Fe,Mn]_5[PO_4]_6$), and merrillite ($Ca_9[Mg,Fe]Na[PO_4]_7$) as minor phases (Buseck and Holdsworth 1977; Wasson and Choi 2003). Some PMG samples also include low-Ca pyroxene and phosphoran olivine (Buseck 1977).

In pallasites, the olivine grains form an interconnected framework surrounded by a metal interstitial matrix. The mean olivine abundance of the PMG is 65 vol% (Buseck 1977). This is intermediate between primitive cubic packing (52 vol%) and cubic closest packing (74 vol%) and emulates the texture of terrestrial cumulates. Some pallasites contain olivine in excess of cubic closest packing (e.g., 85 vol% in Pavlodar), evidence that continued olivine growth is possible after grain settling (Buseck 1977).

The metal in pallasites is generally composed of two phases, kamacite and taenite. They are both FeNi alloys, distinguished by their Ni content and crystal structure. Kamacite, α-(Fe,Ni), is low in Ni (~7%) and has a body-centered cubic (BCC) crystal structure. Taenite, γ-(Fe,Ni), is high in Ni (>20%) and has a face-centered cubic (FCC) crystal structure. A fine macroscopic intergrowth of the two is called plessite. Acid etching dissolves kamacite more readily than taenite and is used to easily distinguish the taenite and kamacite in hand sample and reflected microscopy (Vander Voort 2001). Acid etching also reveals a third metal phase called tetrataenite. Tetrataenite is ordered FeNi (~50 ± 5% Ni) and is present at the taenite-kamacite interface (Goldstein et al. 2014). It occurs as a solid band immediately adjacent to kamacite and as particles in the "cloudy zone" microstructure, a mix of nm-scale tetrataenite particles in a kamacite matrix, located further away from the kamacite interface (Yang et al. 2010).

Pallasite metal is initially crystallized entirely as taenite, but as the metal cools to ~700 °C it begins to exsolve kamacite (Mullane et al. 2004). The HSEs partition between the two phases for as long as diffusion endures, and kamacite continues to grow. The degree to which a given element prefers to fractionate into one phase over the other can be expressed quantitatively as a taenite-kamacite partition coefficient ($D_{T/K}$). There is some disagreement in the literature but prior studies on iron meteorites and pallasites generally determine that most HSEs prefer taenite over kamacite (e.g., Campbell and Humayun 1999; Mullane et al. 2004). Tetrataenite begins to form at lower temperatures, approximately 350 °C (Goldstein et al. 2014).

3.1.2 Pallasite Formation

While the formation conditions of pallasites are still debated, the olivine framework texture of pallasites lends itself to an interpretation that liquid metal was mixed with a solid olivine cumulate prior to complete solidification. The HSEs contained in the liquid metal melt and, therefore, the bulk of the HSEs in the PMG, are distributed by two processes (Mullane et al. 2004). The first process is fractional crystallization. Early crystallized solids are enriched in the compatible elements Os, Ir, and Re and depleted in Ni while later crystallized solids are enriched in Pd, Au and Ni (Mullane et al. 2004). The second process, and the focus of the current chapter, is subsolidus diffusion wherein the HSEs are distributed between taenite and kamacite as the latter exsolves from the former. After crystallization is complete, the HSEs are predominantly concentrated in the solid metal.

The unique mineralogy of pallasites leads to the interpretation that they are material from the core-mantle boundary of differentiated asteroids. Some formation models feature molten metal replacing silicate melt under equilibrium conditions (e.g., Boesenberg et al. 2012) while others invoke impacting to mix core and mantle material (e.g., Yang et al. 2010). Trace metal concentrations in PMG metal are very similar those in IIIAB iron meteorites, indicative of a possible common origin. Scott (1977) first proposed this, suggesting that PMG metal formed from an evolved liquid after 80% fractional crystallization formed the IIIAB core. Metallographic cooling rates show that MG pallasites cooled at 2.5 – 18 K / Myr while IIIAB irons cooled at ~50 – 350 K / Myr in the same temperature range (Yang et al. 2010; Goldstein et al. 2014). Yang et al. (2010) plotted their cooling rates against bulk Ni and found no discernable trend. Boesenberg et al. (2012) replotted the cooing rate data from Yang et al. (2010) against bulk Ir. Due to a taenite-kamacite partition coefficient near unity, Ir concentration is less prone to error than Ni, as smaller differences in concentration between the taenite and kamacite phases make the bulk concentration less dependent on the estimated taenite-kamacite ratio. Their plot shows slightly less spread in the data and a correlation between cooling rate and Ir content. This suggests that primitive MG pallasites cooled more quickly and that the PMG parent body cooled inward. Such an interpretation precludes the notion that the IIIAB irons formed deeper within the same parent body as the MG pallasites, leaving the chemical similarity

of PMG and IIIAB irons unexplained. Yang et al. (2010) maintain that MG pallasites could be the product of an impact on a differentiated asteroid that mixed olivine mantle with the Ir-poor molten metal that remained after the IIIAB-like core was ~80% crystallized.

Boesenberg et al. (2012) argue that impact models are subject to too many assumptions and lack critical details such as the properties of the initial parent body, and the formation of the minor phases. Furthermore, the abundance of pallasite parent bodies suggests that the pallasite formation mechanism is common and not the product of sheer coincidence (Boesenberg et al. 2012). The formation mechanism of Boesenberg et al. (2012) begins with heat, driven by the radioactive decay of ^{26}Al and ^{60}Fe, partially melting a ~100 km diameter chondritic asteroid. The first melt produced is sulfide-rich and denser than bulk chondrite. It travels downwards through cracks and becomes the beginning of a sulfide-rich core. As temperature continues to increase less dense silicate melts form and rise towards the surface (Boesenberg et al. 2012). These silicate melts are basaltic at first but become pyroxenitic as the bulk chemistry of the residue changes. At intermediate depths a residue of olivine, metal, and chromite will eventually form after the sulfide and silicate melts are removed (Boesenberg et al. 2012). The body then reaches peak temperature, completely melting the metal. This allows most olivine to buoyantly rise towards the basaltic-pyroxenitic crust and form a dunite layer beneath it. The remaining olivine, likely those in smaller clusters, are entrained by convection in the metallic melt driven by the heat of the sulfide-rich core (Boesenberg et al. 2012). Metal crystallization begins at the base of the dunite layer and continues downward, trapping olivine grains that float towards the liquid metal – solid metal interface. As crystallization continues the solid metal provides an insulating effect, slowing the cooling rate of later crystallized metal.

Boesenberg et al. (2012) do not invoke an evolved liquid for the onset of PMG metal crystallization. They cite the near chondritic Ir concentration and Ir/Ni ratios of pallasites such as Pavlodar and Argonia (Yang et al. 2010) as evidence against the need for a high degree of prior fractional crystallization. They argue against the assumption that the abundance of PMG with highly fractionated metal (~50% of 33 PMG in (Wasson and Choi 2003)) necessitates the same abundance on the PMG parent body. While this logic is sound, the absence of any MG pallasite with significantly higher Ir concentration than chondritic

(> 1 ppm), as would be expected for the earliest solids, is most easily explained by prior fraction crystallization from the melt. While it is possible that this material exists and is simply not represented in the meteorite catalogue, it is perhaps more likely that Ir is depleted in the PMG as a whole. The similar volatility and behavior under varying redox conditions of the HSEs makes it difficult to explain fractionation between them prior to differentiation (Walker et al. 2008), leaving fractional crystallization as the likeliest cause.

3.2 Methods

Major and trace element concentrations were determined in the taenite and kamacite phases of six PMG samples. Samples of Brahin, Brenham (PMG-an), and Springwater (PMG-an) were obtained on loan from the Royal Ontario Museum, while Esquel, Fukang, and Seymchan were newly acquired for the Western Meteorite Collection. Samples were dry cut with a wire saw at the Western Paleomagnetic & Petrophysical Laboratory and placed in one-inch diameter epoxy grain mounts. They were then progressively polished up to a one-micron diamond solution finish using an automated sample polisher.

3.2.1 EPMA

After carbon coating to ensure adequate surface conductivity, major elements were measured with a JEOL JXA-8530F field-emission electron microprobe in the Earth and Planetary Materials Analysis lab at the University of Western Ontario. All measurements used a 15 kV accelerating voltage, 20 nA sample current, and 1 um spot size. Fe, Ni, Co, and P concentrations were measured in the kamacite and taenite phases of all samples. Iron, Ni and Co were standardized using their pure metal forms and P was standardized using apatite. Count times were 20 s on peak and 10 s background for Fe, 30 s on peak and 15 s background for Ni, and 40 s on peak with 20 s background for Co and P.

3.2.2 LA-ICP-MS

Major and trace elements were measured via LA-ICP-MS in the Chemical Fingerprinting Laboratory at Laurentian University, Canada. The measurements were made with a Resonetics Resolution M-50 193 nm, 20 ns pulse duration ArF excimer laser ablation system paired to a Thermo Scientific X Series II quadrupole ICP-MS. Ablation took place

in an ultra-pure helium environment in a two-volume Laurin Technic cell (Müller et al. 2009). The ablated aerosol and helium (650 ml min^{-1}) was combined with argon (780 ml min^{-1}) and nitrogen (6 ml min^{-1}; for added sensitivity, Hu et al. 2008) immediately outside the ablation cell and was transferred to the plasma via approximately 3 m of nylon-6 tubing. Prior to data acquisition, the instruments were tuned while ablating NIST 612 to maximize sensitivity while maintaining low oxide production rates (< 0.5 % ThO^+/Th^+) and Th/U ~ 1. Backscattered electron (BSE) maps produced by the EPMA at Western were used to identify the kamacite and taenite phases and select analysis locations for LA-ICP-MS. Each sample had 12 spots taken in kamacite, all near the center of grains, and 18 spots in taenite, nine near kamacite interfaces and nine in grain centers. The Brahin sample had only 10 taenite spots due to small sample size and the low abundance of taenite. Four line scans were also taken on each sample to estimate bulk metal composition. The spot analyses were conducted with a 75 µm spot diameter, 4 J cm^{-2} fluence, and 10 Hz repetition rate. The line scans used the same conditions and a scan speed of 25 µm/s. Each analysis typically consisted of 30 s of gas blank followed by 30 s (or more for lines) of ablation. The following isotopes were analyzed: ^{51}V, ^{55}Mn, ^{57}Fe, ^{59}Co, ^{61}Ni, ^{65}Cu, ^{66}Zn, ^{69}Ga, ^{72}Ge, ^{73}Ge, ^{75}As, ^{95}Mo, ^{99}Ru, ^{101}Ru, ^{103}Rh, ^{105}Pd, ^{106}Pd, ^{182}W, ^{185}Re, ^{190}Os, ^{193}Ir, ^{195}Pt, and ^{197}Au. Dwell times were 30 ms for Ru, Pd, and Pt, 60 ms for Rh, Re, Os, Ir, and Au, and 5 ms for all remaining elements.

Analyzed reference materials included GSD, GSE, FeS1, Po725, MASS1, and four PGE blanks (PGE-free sulfides of various major element compositions to account primarily for metal-argide interferences on the light PGEs), but due to apparent fractionation differences between the standards and the sample, only the matrix matched North Chile iron meteorite was used as an external standard in the end. North Chile's chemistry is well established in the literature and it has been shown to be homogeneous on a fine scale (e.g., Wasson et al. 1989). North Chile is an officially recognized meteorite name, but it is usually used in conjunction with reference to a specific specimen (e.g., Hsu et al. 2000; Danielson et al. 2009). It is not known which specimen the North Chile sample in this study is derived from but based on Ir concentration it appears to belong to one of Rio Loa, Tocopilla, Puripica, Filomena, San Martin, or Coya Norte (Wasson and Goldstein 1968). The North Chile composition used in this study is the mean of concentrations reported by six prior studies

(Table 6) (Buchwald 1975; Ryan et al. 1990; Wasson et al. 1998; Campbell et al. 2002; Petaev and Jacobsen 2004; Bridgestock et al. 2014). These reference materials were analyzed approximately every 20 minutes including before and after each session to compensate for instrument drift. Internal standardization was done via 100% normalization with Ni concentration from the prior EPMA analysis used as verification when possible. Data reduction was done using iolite v3.5 (Paton et al. 2011) with a custom trace elements data reduction scheme to perform 100% elemental normalization (similar to Liu et al. 2008). Metal-argide interferences were found to only be a significant for $^{59}Co + ^{40}Ar$ and $^{61}Ni + ^{40}Ar$ on ^{99}Ru and ^{101}Ru, respectively. The PGE blanks were used to determine the interference production rates and subtract a concomitant amount from the kamacite and taenite signals. After this correction, the resulting concentrations determined by the two isotopes of Ru are generally within uncertainty of one another, indicative of an accurate measurement. Using this approach, the PGE concentrations obtained for the various pallasite metals are comparable to data found in the literature.

Table 6. North Chile elemental concentrations used for external standardization. Values are the mean from 6 prior studies (listed above). Uncertainty is 1σ standard deviation. Fe and Ni are in wt%, all others are in ppm.

	conc.	±		conc.	±
V	-	-	**Mo**	7.65	0.64
Mn	-	-	**Ru**	16.45	1.77
Fe	93.6	-	**Rh**	2.90	0.18
Co	4427	140	**Pd**	1.93	0.03
Ni	5.64	0.11	**W**	2.51	0.01
Cu	139.83	9.39	**Re**	0.22	0.02
Zn	0.24	-	**Os**	0.79	0.51
Ga	58.35	0.80	**Ir**	3.32	0.46
Ge	167.50	12.02	**Pt**	23.04	1.97
As	4.27	0.78	**Au**	0.59	0.02

3.2.3 Taenite-Kamacite Partition Coefficients

Taenite-kamacite partition coefficients were calculated from spot analyses in the center of kamacite bands and on the edge of taenite bands, as close to the kamacite interface as possible. The taenite measurements are taken at the edge because taenite bands often have steep compositional gradients, usually described as “M”-shaped profiles (Hsu et al. 2000).

As an increasing proportion of the FeNi metal exsolves into Fe-rich kamacite, the Ni content of both phases increases. Compositional gradients form in taenite because Ni diffusion in taenite is slow, causing Ni concentration to increase at taenite edges (Haack and McCoy 2007). Ni diffusion in kamacite is faster, so Ni can equilibrate throughout entire kamacite bands, at least until very low temperature (< 400°C) (Haack and McCoy 2007). The slow diffusion of Ni in taenite means the body cools below blocking temperature before equilibrium can be reached. This behavior is ubiquitous in meteoritic metal, but the magnitude of its effect varies with cooling rate (i.e., faster cooled meteorites have steeper compositional gradients). The result is that the partition coefficients calculated from these concentrations do not describe equilibrium conditions, but instead the distribution of elements under realistic conditions. Because the partition coefficients depend on cooling rate, they are expected to be similar, but not identical for all samples.

Since the cloudy zone and tetrataenite band are adjacent to kamacite, and the particle size and tetrataenite bandwidth are smaller than any conceivable spot size for LA-ICP-MS, the "taenite" composition used to calculate $D_{T/K}$ is actually an average value between tetrataenite and kamacite, and not a measurement of taenite at all. Diffusion acts on a small enough scale at the low temperatures at which tetrataenite forms that measurements here still produce representative values for what the concentration of taenite would be if it were still present (Goldstein et al. 2014).

3.2.4 Bulk Metal Composition

Bulk metal composition was determined by two distinct methods. The first used average values from spot analyses in the center of taenite and kamacite bands, and their respective modal abundances, to calculate bulk metal composition. This method does not account for the ~ 10 – 20 μm thick compositional gradient observed in taenite adjacent to kamacite interfaces. This causes a slight underestimation of taenite preferring elements, but the effect is minimal due to the relatively thin width of the compositional gradient compared to average taenite crystal size. Modal abundance was obtained by simplifying the BSE maps (from EPMA) in Adobe Photoshop before using ImageJ for pixel counting. The second method used the average composition of four line scans placed strategically on each sample to approximate the modal abundance of the phases.

3.2.5 Cooling Rate

In the PMG, various methods are available to constrain cooling rates over different temperature intervals. Zoning in olivine can be used to infer high-temperature cooling rates (Hsu 2003), while metallographic methods determine the low-temperature cooling rates applicable to the current study (Yang et al. 2010). There are several methods to determine metallographic cooling rates in meteoritic metal.

The Wood method (1964) is the most popular means of determining metallographic cooling rates in meteoritic metal. It involves plotting Ni content of the centre of taenite bands vs taenite band half-width. In pallasites, olivine grains are surrounded kamacite; known in this setting as swathing kamacite. In small (< 1 cm) regions of metal between olivine grains swathing kamacite is thicker than the kamacite plates detached from olivine (Yang et al. 2010). This is interpreted to mean swathing kamacite nucleated first. Being more iron-rich, kamacite preferentially removes Fe from taenite, creating local enrichments in Ni. In these areas, the nucleation temperature of kamacite is depressed in contrast to larger metal areas where the Ni enrichment effect of swathing kamacite growth is less pronounced (Yang et al. 2010). Consequentially, the Wood method, which assumes compositional homogeneity in the taenite, cannot be used (Yang et al. 2010).

The Ni profile matching method of Goldstein and Ogilvie (1965) is more applicable to pallasites. In this method, line scans are taken through kamacite-taenite bands to reveal the classic “M”-shaped Ni profile. Local bulk Ni content of the bands is then used to calculate theoretical profiles produced at varying cooling rates until a match with the measured profile is found. This method produces a unique cooling rate for each set of kamacite and taenite bands. A number of these are averaged to give a meaningful cooling rate for the entire sample. The paucity of taenite bands in the samples used by the current study prohibits the use of this technique. Cooling rates have been previously determined for Brenham, Seymchan, and Springwater by Yang et al. (2010) by using this technique however (Table 7).

An alternative method is to determine the cooling rate from the cloudy zone particle size or tetrataenite bandwidth (Yang et al. 2010). There is a negative correlation between

cooling rate and tetrataenite bandwidth or cloudy zone particle size. The cooling rate can be estimated from tetrataenite bandwidth according to

$$CR = q / d_{Tt}^{2.3}, \quad \text{(Eq. 5)}$$

where CR is the cooling rate in K / Myr, d is the tetrataenite bandwidth in nm, and q is an empirical constant equal to 14,540,000 (Yang et al. 2010). The cooling rate from cloudy zone particle size is estimated according to

$$CR = h / d_{CZ}^{2.9}, \quad \text{(Eq. 6)}$$

where CR is the cooling rate in K / Myr, d is the average diameter of the particles in the cloudy zone, and h is an empirical constant equal to 7,620,000 (Yang et al. 2010). Both equations were developed to fit IVA, IIIAB, and IVB iron and PMG data and were developed to agree with profile matching cooling rates determined in the same study.

3.3 Results

3.3.1 Mineralogy

Energy-dispersive spectroscopy analyses, wavelength-dispersive spectroscopy analyses, and BSE mosaics from the EPMA were made to map the mineralogy of each sample. All six samples have abundant kamacite with major but lesser quantities of taenite and olivine. Only for Brahin, because of its small sample size and low taenite abundance, was there insufficient taenite to warrant all 18 spot analyses. Each sample also contains minor sulfides (major for Brahin) and phosphides. The sulfides analyzed were nearly all troilite (FeS) except for one grain of pentlandite ($[Fe,Ni]_9S_8$) in Seymchan. The phosphides are mostly schreibersite ($[Fe,Ni]_3P$) with rare nickelphosphide ($[Ni,Fe]_3P$). Esquel and Brahin have minor chromite and all but Esquel and Brenham have minor quantities of phosphate minerals (major in Springwater).

3.3.2 Major and Trace Element Concentration

Major elements detected by the EPMA were almost always above detection limit. Iron, Ni and Co were above detection limits for all points while P concentration was very rarely

below detection; zero spots in Esquel and just one in each remaining sample. Major and trace element concentrations acquired by LA-ICP-MS were generally above the limit of detection (LOD). Vanadium and Mn could not be quantified because of a lack of concentration data in North Chile. Zinc, As, W, Re, Os, and Ir were sometimes below the calculated LOD with varying frequency in some samples (Table 7). Iron, Co, Ni, Cu, Ga, Ge, Mo, Ru, Rh, Pd, Pt, and Au were above LOD for all spots on every sample. Data below LOD was not considered when calculating $D_{T/K}$ or bulk metal chemistry. While all remaining data is presented in subsequent graphs, the tenuous nature of the data for some elements should be kept in mind. Zinc, for example, has partition coefficients plotted for Esquel and Springwater (Fig. 4a), but each was calculated from just a single point above LOD in the taenite and kamacite phases in each sample. Their coefficients are similar however, indicating some likelihood of their accuracy.

Table 7. Fraction of LA-ICP-MS measurements above LOD.

		Zn	As	W	Re	Os	Ir
Esquel	K	0.08	1	0.67	0	0.75	1
	T	0.11	0.44	0.67	0.11	0.33	1
Fukang	K	0.17	0.92	0.50	0.25	0.92	1
	T	0	0.44	0.67	0.11	1	1
Seymchan	K	0.08	0.08	0.75	1	1	1
	T	0	0.00	0.33	1	1	1
Brahin	K	0	0.92	0.67	0.17	1	0.92
	T	0	0.17	0.83	0.33	1	1
Springwater	K	0.08	1	0.92	0.25	1	1
	T	0.11	0.22	0.78	0.44	1	1
Brenham	K	0	0.75	0.92	0.25	1	1
	T	0	0.22	0.67	0	0.89	1
mean	**K**	**0.07**	**0.78**	**0.74**	**0.32**	**0.94**	**0.99**
	T	**0.04**	**0.25**	**0.65**	**0.33**	**0.86**	**1**

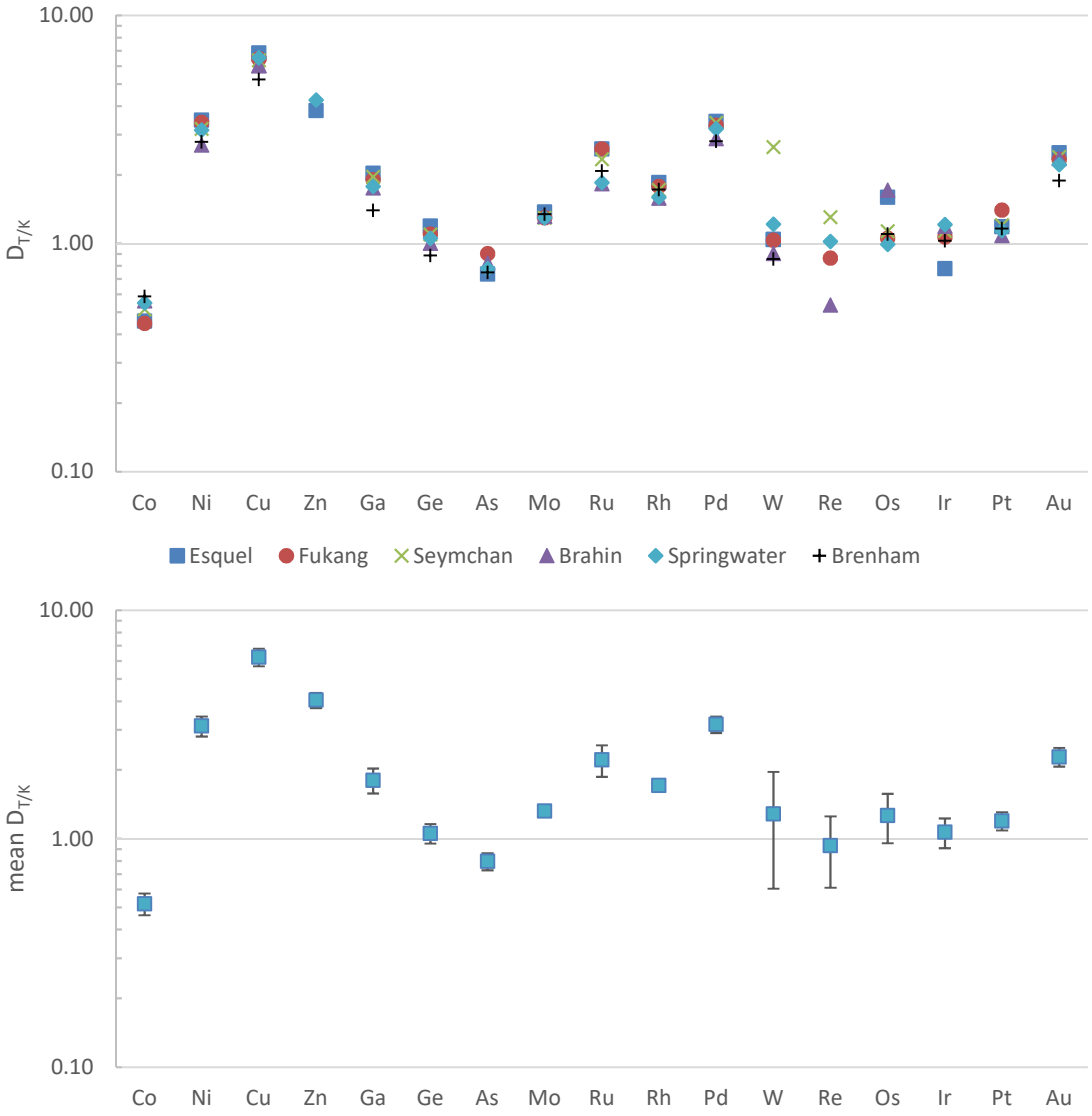

Figure 4. Taenite-kamacite subsolidus partition coefficients. (a, above) Taenite-kamacite partition coefficients for each sample. (b, below) Mean taenite-kamacite partition coefficients with 1σ standard deviation uncertainties.

The taenite-kamacite partition coefficients ($D_{T/K}$) for each sample can be seen in Figure 4a. The average $D_{T/K}$ by element with 1σ standard deviation uncertainty can be seen in Figure 4b. A tabulated version of the data in Figure 4 is also available in the appendix (Tables A1 and A2).

3.3.3 Bulk Metal Composition

The bulk metal concentrations determined by the spot and line methods can be seen in Table 8. The difference is calculated as follows:

$$\%\ diff. = \frac{Sx - Lx}{Sx}, \qquad \text{(Eq. 7)}$$

where *Sx* is the spot concentration of element x and *Lx* is the line concentration of x.

Table 8. Bulk metal composition from the spot and line methods with % difference between the two. Fe and Ni are wt%, all others are ppm. nd – no detection, all values were below LOD.

	Esquel			Fukang			Seymchan		
	Spot	**Line**	**% diff.**	**Spot**	**Line**	**% diff.**	**Spot**	**Line**	**% diff.**
Fe	91.54	88.42	3.4%	91	90.53	0.9%	90.71	89.18	1.7%
Co	5686	5320	6.4%	5898	5320	9.8%	5555	5143	7.4%
Ni	7.88	11.02	-39.9%	8.06	8.93	-10.8%	8.73	10.27	-17.7%
Cu	80.54	132.40	-64.4%	132.99	168.00	-26.3%	124.77	148.08	-18.7%
Zn	348.78	0.16	100.0%	97.71	nd	-	nd	nd	-
Ga	21.97	25.31	-15.2%	19.68	20.68	-5.1%	23.74	24.87	-4.7%
Ge	50.65	50.88	-0.5%	40.16	39.01	2.9%	62.26	60.59	2.7%
As	17.80	5.83	67.3%	18.92	6.63	65.0%	nd	8.15	-
Mo	9.90	9.53	3.8%	7.84	6.65	15.2%	8.18	9.15	-11.9%
Ru	0.93	1.07	-14.9%	0.94	1.13	-20.0%	2.12	2.16	-2.1%
Rh	1.13	1.15	-2.4%	0.93	0.91	2.2%	1.34	1.27	4.6%
Pd	4.68	7.05	-50.7%	4.94	6.11	-23.7%	4.95	5.73	-15.8%
W	0.17	0.29	-70.6%	0.16	0.13	16.8%	0.42	0.25	39.9%
Re	nd	nd	-	0.009	nd	-	0.064	0.065	-1.5%
Os	0.009	0.009	5.2%	0.021	0.032	-49.9%	0.561	0.577	-3.0%
Ir	0.029	0.048	-64.6%	0.045	0.047	-3.2%	0.677	0.667	1.5%
Pt	1.23	1.30	-6.2%	1.63	1.67	-2.3%	3.78	3.76	0.6%
Au	1.83	2.32	-26.5%	2.24	2.52	-12.7%	2.02	2.17	-7.6%

3.3.4 Cooling Rate

Cooling rates for all six samples in this study have been calculated from Eq. 2 and cloudy zone particle size data from Yang et al. 2010 (Table 9). The two agree within uncertainty and are no more than 6% different.

Table 8. Cont.

	Brahin			Springwater			Brenham		
	Spot	**Line**	**% diff.**	**Spot**	**Line**	**% diff.**	**Spot**	**Line**	**% diff.**
Fe	92.17	91.61	0.6%	87.57	84.47	3.5%	89.88	89.45	0.5%
Co	6488	5941	8.4%	5902	5220	11.6%	6130	5734	6.5%
Ni	7.17	7.78	-8.6%	11.82	14.98	-26.7%	9.50	9.96	-4.9%
Cu	88.60	96.43	-8.8%	153.44	202.00	-31.6%	121.51	149.73	-23.2%
Zn	nd	0.18	-	nd	2.73	-	nd	1.78	-
Ga	21.65	19.72	8.9%	14.98	17.85	-19.2%	24.08	27.38	-13.7%
Ge	59.46	56.55	4.9%	30.98	31.06	-0.3%	67.21	68.75	-2.3%
As	nd	7.40	-	25.89	19.30	25.4%	24.03	46.68	-94.2%
Mo	6.62	5.73	13.6%	6.74	6.95	-3.0%	7.72	7.50	2.9%
Ru	1.23	1.12	9.2%	1.00	0.96	4.0%	1.80	1.81	-0.1%
Rh	0.99	0.92	7.8%	0.78	0.75	4.1%	1.38	1.33	3.4%
Pd	4.73	4.92	-4.2%	6.68	8.48	-26.9%	5.88	6.32	-7.4%
W	0.25	0.20	20.1%	0.24	0.22	11.1%	0.37	0.41	-10.2%
Re	0.012	0.005	54.9%	nd	0.007	-	0.006	nd	-
Os	0.038	0.032	14.8%	0.055	0.056	-1.9%	0.019	0.015	21.1%
Ir	0.109	0.093	15.1%	0.074	0.062	16.3%	0.040	0.035	11.9%
Pt	2.12	2.12	0.4%	1.28	1.30	-1.5%	3.29	3.17	3.8%
Au	2.31	2.29	1.0%	2.43	2.40	1.2%	2.28	2.11	7.5%

Table 9. M-profile and cloudy zone particle size cooling rates as per Yang et al. (2010).

	Mean CZ particle size (nm)	**no. of particles**	**CZ cooling rate (K / Myr)**	**M-Profile cooling rate (K / Myr)**
Brahin	106 ± 9	8	10.20	-
Brenham	123 ± 3	203	6.63	6.2 ± 0.9
Esquel	157 ± 11	23	3.26	-
Fukang	129 ± 10	15	5.77	-
Seymchan	122 ± 5	77	6.78	7.1 ± 1.2
Springwater	132 ± 3	121	5.40	5.1 ± 0.7

3.4 Discussion

3.4.1 Analytical Accuracy

Fundamentally, LA-ICP-MS operates by focusing a laser onto the surface of a sample to ablate and aerosolize sample material. This material is transported from the ablation cell via an inert carrier gas into the ICP for ionization after which it is introduced to the mass spectrometer where the ions are separated according to their mass-charge ratio before striking the detector. Laser sampling of solid material is prone to fractionation, i.e., non-stoichiometric sampling (Russo et al. 2000). Inappropriate reference material selection and instrument drift also contribute to reduced analytical accuracy. Accuracy is improved by using lasers of shorter wavelength, optimizing instrument tuning, and using appropriate external standards and data reduction techniques (Liu et al. 2013). Multiple isotopes for single elements were also measured to reduce uncertainty where possible. Isotope concentrations were averaged to give elemental concentration.

Shorter wavelength lasers, such as the 193 nm ArF lasers used in this study, have been found to create aerosols with smaller particle sizes, reducing fractionation effects (Liu et al. 2013). Spot size, laser fluence, dwell times, and laser repetition rate were selected to find compromise between sensitivity and adverse effects such as sample heating. The standard reference material, North Chile, and 100% normalization internal standardization were used to correct for sensitivity drift of the mass spectrometer and any remaining fractionation.

The use of North Chile as a matrix-matched standard is critical to the accuracy of the measurements made in this study. The accuracy of LA-ICP-MS analyses suffer according to the relative degree of fractionation between the standard and sample (Liu et al. 2013). Using a standard with the same matrix as the sample ensures that they both exhibit the same degree of fractionation, permitting an accurate analysis even with residual fractionation unalleviated by other means.

Limits of detection were calculated as per Pettke et al. (2012). Measurements below the calculated LOD were not considered when calculating taenite-kamacite partition coefficients or bulk metal concentration. The significance of PGE interferences was also

evaluated (e.g., Cu^{65} + Ar^{40} -> Pd^{105}) and was found to be a factor for Ru only. A correctional procedure using PGE blanks yielded the same result within uncertainty for both isotopes of Ru, indicating a high likelihood of successful correction. The accuracy of the trace elements measurements made in this study can be verified by comparison with previous studies also concerning Brenham (Table 10). Osmium, Ir, Pt, Au, and Re are similar to the concentrations found by the four previous studies included in Table 10. Rhodium is in higher concentration in the current study than in Mullane et al. (2004) by a factor of ~3 and Ru is lower by a factor of ~2. The kamacite and taenite values for Pd are higher than Mullane et al. but the bulk values are near those of Chen et al. (2002). The bulk values from Wasson and Choi (2003), Chen et al. (2002), and Scott (1977) agree well with the data from this study and are often outside the range of the kamacite and taenite values reported by Mullane et al. (2004). Except for Re, which has very low concentration, the values from the current study are between those of Mullane et al. (2004) and one of the three remaining studies. On average they are within ~20% of the values reported by Wasson and Choi (2003), Chen et al. (2002), and Scott (1977).

Table 10. HSE concentrations in Brenham from the literature and the current study. Values are in ppm unless otherwise specified. B_S and B_L designate spot and line methods of bulk metal concentration calculation.

		Ru	Rh	Pd	Re (ng / g)	Os	Ir	Pt	Au
Mullane et al. 2004	K	3.35	0.41	2.77	<.006	0.019	0.014	1.99	1.11
	T	4.13	0.62	7.4	<.009	0.023	0.019	2.81	1.95
Wasson & Choi 2003	Bulk metal	-	-	-	<40	-	0.039	4.9	2.76
Chen et al. 2002	Bulk metal	-	-	5.91	2.663	0.021	-	-	-
Scott 1977	Bulk metal	-	-	-	-	-	0.038	-	2.85
this study	K	1.69	1.29	5.08	6.6	0.018	0.040	3.28	2.12
	T	2.23	1.73	8.90	5.5	0.019	0.039	3.33	2.88
	B_S	1.80	1.38	5.88	6.4	0.019	0.040	3.29	2.28
	B_L	1.81	1.33	6.32	-	0.015	0.035	3.17	2.11

3.4.2 Taenite-Kamacite Partition Coefficients

The concentrations of HSEs in taenite and kamacite can be divided to determine the subsolidus partitioning coefficient, $D(HSE)_{T/K}$. Previous studies have determined $D(HSE)_{K/T}$ in iron meteorites and a handful of pallasites. Comparison of previous studies to the current study can be seen in Table 11.

Hirata and Nesbitt (1997), Meftah et al. (2016), and Danielson et al. (2009) were the only studies to report many HSEs with $D_{T/K}$ values below 1. Hirata and Nesbitt (1997) found a positive correlation of taenite/plessite-kamacite partition coefficient and ionic radii for their two samples. The authors argue that the Fe-dominated matrix will affect the valency of the trace element atoms as they will be surrounded by a "sea of electrons", leading the elements to behave as ions. Meftah et al. (2016) also report a positive correlation between $D_{T/K}$ and ionic radius.

In contrast, Hsu et al. (2000) interpret the controlling factor of the partitioning behavior to be the atomic size and electron configuration of the HSEs and the crystal structures of taenite and kamacite. All HSEs have larger atomic radii than Fe or Ni. The slightly larger lattice sites of FCC taenite can better accommodate the larger atoms than the BCC structure of kamacite. The authors reason that atoms with filled d-orbitals prefer the FCC structure of taenite since the spherical symmetry is better suited to closest packing (Hsu et al. 2000). This suggestion is seemingly at odds with the fact that Ni diffusion is much faster through kamacite than taenite (Haack and McCoy 2007). A possible explanation is that the smaller interstitial spaces of FCC taenite impede the diffusion of Ni relative to BCC kamacite. Mullane et al. (2004) reported that each HSE preferred taenite in all their samples. The authors compare their results with previous studies and reveal that $D_{T/K}$ for each HSE is relatively constant across meteorite groups. They conclude that this consistency, combined with the fact that each chemical group likely had different parent body conditions, is evidence that $D_{T/K}(HSE)$ is independent of prevailing parent body conditions, including bulk chemistry, trace element concentration, thermal history, and light element content (S, P, and C). As per Hsu et al. (2000), they suggest that $D_{T/K}(HSE)$ is a function of each element's atomic size and symmetry.

McDonough et al. (1999), Campbell and Humayun (1999), Hsu et al. (2000), Mullane et al. (2004), and Ash et al. (2007), determined $D_{T/K}$ values for IAB, IID, IIE, IIIAB, IVA, and ungrouped irons and three main-group pallasites. Each study reported relatively consistent taenite-kamacite partition coefficients between samples, regardless of chemical group, strengthening the argument that subsolidus HSE diffusion behavior is independent of parent body conditions.

Table 11. Partitioning coefficients from previous work and the current study.

	$D_{T/K}$							
Study	**Ru**	**Rh**	**Pd**	**Re**	**Os**	**Ir**	**Pt**	**Au**
Rasmussen et al. (1988)	-	-	-	> 1	-	> 1	-	> 1
Hirata and Nesbitt (1997)	± 1	< 1	> 1	< 1	< 1	< 1	< 1	-
McDonough et al. (1999)	> 1	> 1	> 1	± 1	± 1	± 1	± 1	> 1
Campbell and Humayun (1999)	> 1	> 1	> 1	> 1	> 1	> 1	> 1	> 1
Hsu et al. (2000)	-	-	-	-	> 1	> 1	> 1	> 1
Mullane et al. (2004)	> 1	> 1	> 1	> 1	> 1	> 1	> 1	> 1
Ash et al. (2007)	> 1	> 1	> 1	± 1	± 1	> 1	> 1	> 1
Watson et al. (2008)	> 1	> 1	> 1	± 1	± 1	± 1	> 1	> 1
Danielson et al. (2009)	> 1	> 1	> 1	< 1	< 1	< 1	< 1	< 1
Meftah et al. (2016)	-	< 1	-	-	-	< 1	< 1	-
this study	> 1	> 1	> 1	± 1	± 1	± 1	> 1	> 1

± 1 designates inconsistent results with the element preferring taenite in some samples and kamacite in others. This was not possible for Rasmussen et al. (1988), Campbell and Humayun (1999), Danielson et al. (2009), and Meftah et al. (2016) where only mean values were reported or there was only one sample studied. Rasmussen et al. (1988) used instrumental neutron activation analysis, Hsu et al. (2000) and Meftah et al. (2016) used secondary ion mass spectrometry, all others used LA-ICP-MS.

Other observations of note are Ash et al. (2007) reporting that period 5 PGEs (Ru, Rh, Pd) having a stronger preference for taenite than period 6 PGEs. They also found that within samples there is a positive correlation between Ni and trace element content. This is likely due to Ni and the HSEs similar diffusive behavior during kamacite exsolution.

Watson et al. (2008) note a negative correlation of $D_{T/K}$ with atomic number for the period 4 elements [$D_{T/K}(Cu) > D_{T/K}(Ga) > D_{T/K}(Ge)$] and less well-developed positive correlations

with atomic number for periods 5 ($D_{T/K}$ generally increases from Mo – Pd) and 6 ($D_{T/K}$ generally increases from Re – Au).

In their study, Danielson et al. (2009) quantified HSE, Cr, Fe, Co, Ni, Cu, Ga, Ge, As, Mo, and W in the taenite, kamacite, sulfide, olivine, chromite, and phosphide phases in pallasite CMS 04071. Relative to CI chondrites and Fe, CMS 04071 metal is strongly depleted in Os, Re, and Ir, slightly depleted in Pt, and slightly enriched in Ru, Rh, Au, and Pd. Upon comparison with previous studies, they find a positive correlation of $D_{T/K}$(Cu, Au) with wt% Ni in taenite. They report that $D_{T/K}$(Pt) is nearly correlated with wt% Ni in taenite as well, except for a single outlier (Hirata and Nesbitt 1997). The suggestion that $D_{T/K}$ depends on a physical parameter of the parent body, like taenite Ni content, is contrary to the findings of the studies listed above. The relationship between taenite Ni content and $D_{T/K}$ is explored in the next section (Fig. 7).

Metal-sulfide partitioning coefficients ($D_{M/S}$) from Danielson et al. (2009) are reported as $10 < D_{M/S}$(Os, Ir, Pt, Au) < 100, $D_{M/S}$(Re) < 1, with no data for $D_{M/S}$(Ru, Rh, Pd). These results agree with the experimental results of Chabot (2004), except for Re, Os, and Ir, which are orders of magnitude lower than the experimental results. The authors suggest this is due to the extremely depleted values of Os and Ir in the metal phases. $D_{M/S}$(Re) is anomalous as Re is coincidentally above the detection limit in sulfide but near the detection limit in metal.

Danielson et al. (2009) also determined metal-olivine partition coefficients ($D_{M/O}$) for Re, Pt, and Au. They reported $D_{M/O}$(Pt, Au) > 10,000, in agreement with experimental work (e.g., Righter et al. 2004). $D_{M/O}$(Re) is much lower at ~10, once again skewed by the extreme depletion in CMS 04071 metal. They do not report partitioning coefficients between metal and chromite or phosphide, although Re is more concentrated in chromite than in any other phase, a result in accordance with previous studies. The authors report that phosphides have similar trace element concentrations as taenite and kamacite (Danielson et al. 2009).

In this study, Ni, Cu, Zn, Ga, Mo, Ru, Rh, Pd, Pt, and Au prefer taenite in all samples, Co and As prefer kamacite in all samples, while Ge, W, Re, Os, and Ir do not demonstrate a

consistent preference for either phase. These results can be graphically compared with previous studies that have made their data available in the appropriate form (i.e., numerical values) (Fig. 5).

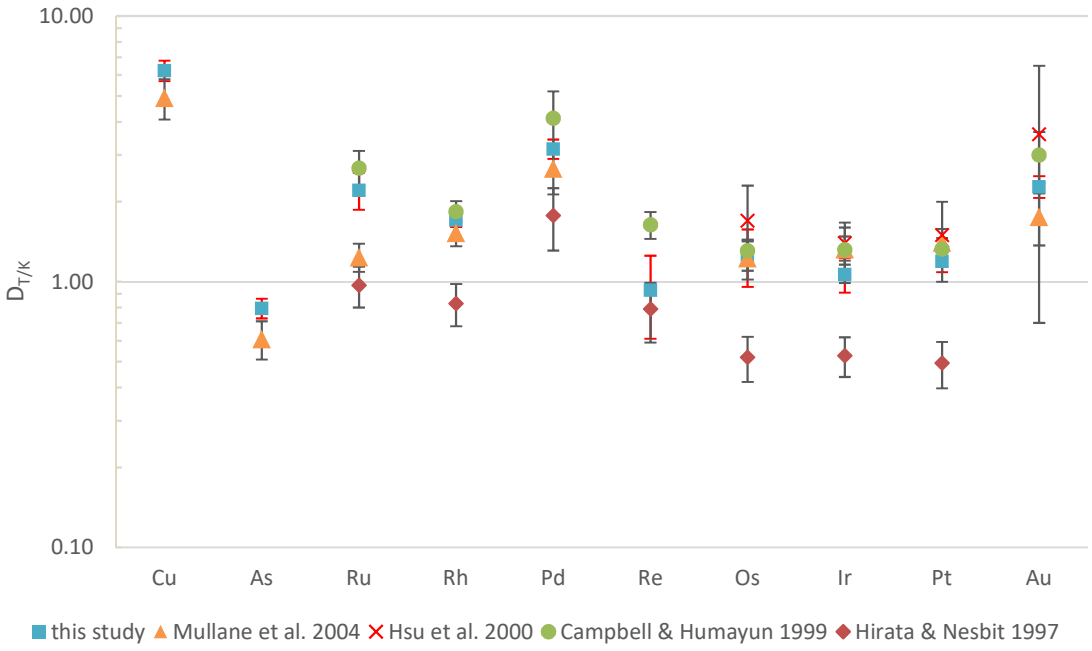

Figure 5. Taenite-kamacite partition coefficients from the current study and the literature. Error bars for the current study are displayed in red.

The partition coefficients from this study plot systematically below the values of Campbell and Humayun (1999), but often within uncertainty. The most notable exception is Re, for which the current study plots below $D_{T/K} = 1$, closer to the values of Hirata & Nesbitt (1997). In the current study, Re concentration is quite often near or below the LOD, expect for Seymchan, for which all points are above LOD and $D_{T/K}$(Re) is equal to 1.31 ± 0.36; agreeing within uncertainty with 1.64 ± 0.19, the value from Campbell and Humayun (1999).

The subsolidus taenite-kamacite partition coefficients are broadly similar for each pallasite in this study. This is an expected result whether the partitioning of HSEs is dependent on parent body conditions or not, as all samples are members of the same chemical group and are thus expected to have experienced similar parent body conditions. The $D_{T/K}$(W) is considerably higher for Seymchan than any other sample. This is the result of a single spot

in Seymchan taenite having significantly higher W concentration than either of the other two spots in taenite above the LOD or any of the spots in kamacite. If this potentially anomalous spot is removed, the $D_{T/K}$(W) becomes 0.67; considerably lower than any other sample. Upon inspection of the time resolved line data (which cannot be considered when determining partition coefficients as they are unconstrained by LOD) it seems that the lower of the two results is more likely representative of the behavior of W.

Like W, the $D_{T/K}$ for Ge, Re, Os, and Ir straddle the line at 1, with the elements preferring taenite in some samples and kamacite in others. Germanium has $D_{T/K} \geq 1$ for all samples except for Brenham. None of the samples show a strong preference for either phase and all but Esquel reach $D_{T/K}$(Ge) = 1 within uncertainty. It is possible that Ge partitions nearly equally between the two phases with uncertainty causing it to fall on either side of the line of equality. Rhenium concentration, as previously noted, was usually below LOD. The paucity of data increases the spread of $D_{T/K}$ between samples. Osmium has a $D_{T/K}$ below one only for Springwater, but the value is nearly at unity (0.99) and agrees with the mean value within uncertainty. Iridium prefers taenite in all but Esquel, but has a large uncertainty, both as a fraction of the value and in comparison with the other samples.

Brenham has lower taenite-kamacite partition coefficients than the other samples on average. This can be partially explained by the negative correlation between $D_{T/K}$ and cooling rate (Fig. 6). Since most elements in the study prefer taenite, and slower cooling rates allow for more thorough diffusion, it is intuitive that slower cooling samples would have higher $D_{T/K}$ on average.

There is a well-developed negative correlation between atomic number and $D_{T/K}$ for 4th period elements from Cu to As. The same negative correlation was noted for Cu, Ga, and Ge in Watson et al. (2008). The weaker positive correlations with atomic number noted in the same study are apparent for the 5th period elements (complete with a dip at Rh) and 6th period elements as well (Fig. 4). The apparent correlations with atomic number are probably more to do with another property that varies with atomic number, like ionic radius or atomic radius and electron configuration, than they are with atomic number itself.

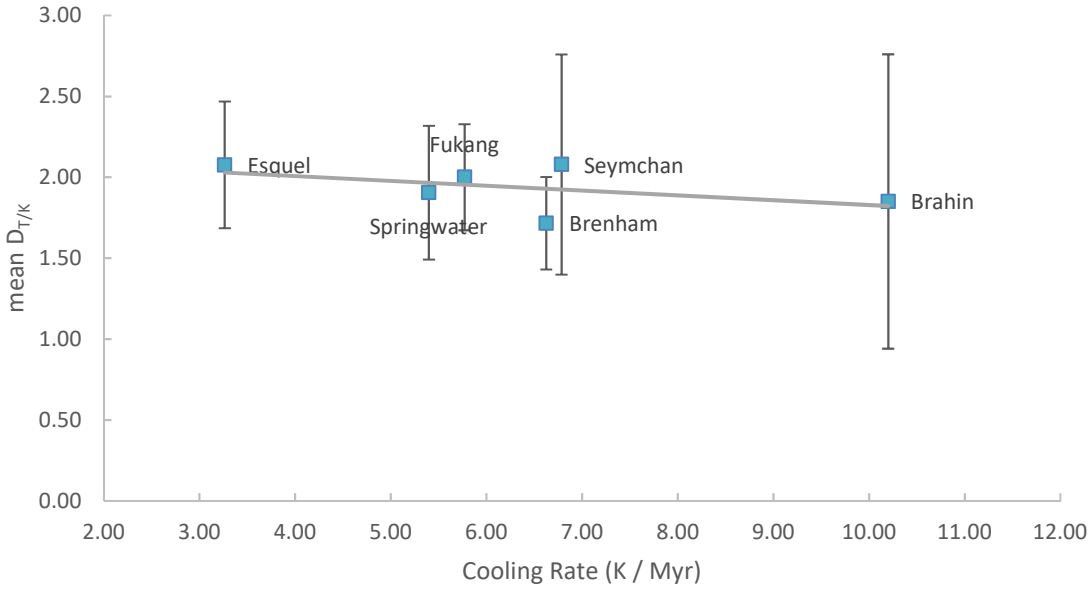

Figure 6. Cooling rate with mean taenite-kamacite partition coefficients. Uncertainties are 1σ standard deviations. Cooling rates were calculated using the data and CZ particle size method from Yang et al. (2010).

3.4.3 Control of Subsolidus Taenite-Kamacite HSE Partitioning

Trace elements can be incorporated into alloys in two ways. Atoms of the trace element (solute atoms) can reside in a lattice sites in place of host (solvent) atoms, forming substitutional alloys, or they can reside in the vacant space between host atoms, forming interstitial alloys. Given the similar size of HSE atoms, Fe, and Ni (Table 13), the HSEs are present in kamacite and taenite as substitutional alloys (e.g., Meftah et al. 2016).

3.4.3.1 Nickel Content

While the similarity of taenite-kamacite partition coefficients of meteorites spanning several chemical groups have led many to the interpretation that the partitioning behavior of HSEs between these two phases is independent of parent body conditions, some still suggest a link based on correlations in their data. Based on $D_{T/K}$ values calculated from their own sample, and those calculated by Mullane et al. (2004), Hsu et al. (2000), McDonough et al. (1999), and Hirata and Nesbitt (1997), Danielson et al. (2009) suggest a link between taenite Ni content and Cu and Au partitioning coefficients. The authors also mention that a correlation with Pt would be present as well, if it were not for the outlying data from Hirata and Nesbitt (1997). No such correlations are replicated within samples

from the current study (Fig. 7). The partitioning coefficients are consistent between samples, regardless of Ni concentration in taenite. In addition to the elements plotted in Figure 4, the $D_{T/K}$ for Ga, Ge, Mo, Ru, Rh, W, Re, Os, and Ir were also compared with taenite Ni content. No systematic variation was observed for any element. The same elements were also plotted against kamacite Ni content with a similarly null result.

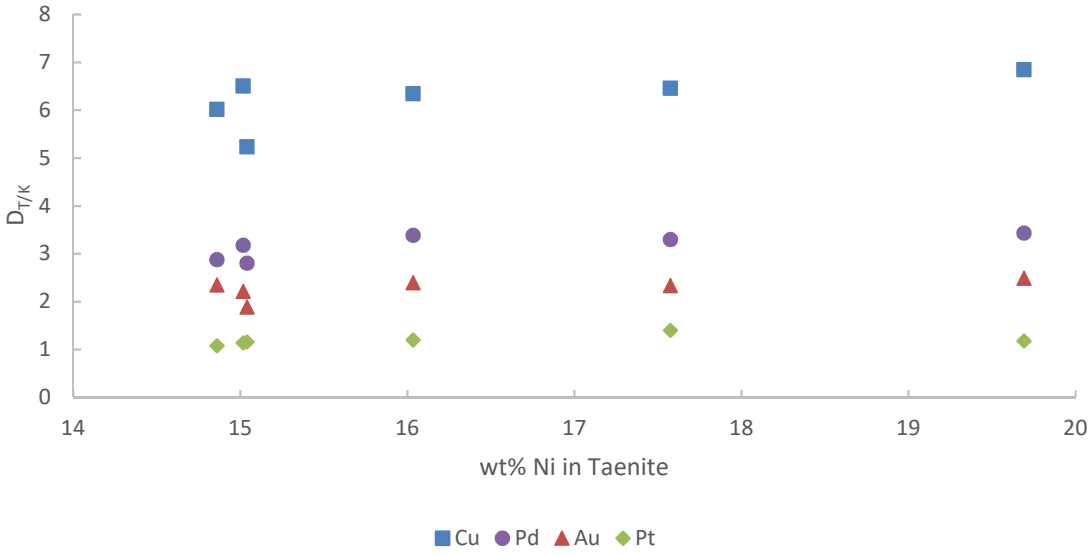

Figure 7. Taenite Ni content against taenite-kamacite partition coefficients.

3.4.3.2 Ionic Radius

As it appears that partitioning behavior is independent of the prevailing parent body conditions at the time of diffusion, the partitioning must be a function of how some intrinsic property(ies) of the elements themselves interact with the disparate crystal structures of taenite and kamacite. There is disagreement in the literature as to what these properties might be. Some argue that the ionic radii of the elements determine their subsolidus partitioning behavior (e.g., Hirata and Nesbitt 1997; Meftah et al. 2016) while others argue that the controlling factor is a combination of atomic radii and electron configuration (e.g., Hsu et al. 2000; Mullane et al. 2004). In either case, the size of the atom/ion is suspected to play a role, with larger atoms/ions preferring the slightly larger lattice sites of FCC taenite versus BCC kamacite (Pauling 1970).

The prevailing chemical bond in metal alloys is the metallic bond (Meftah et al. 2016). Metallic bonding can be thought of as an array of positively charged nuclei surrounded by a sea of electrons. The valence elections of the atoms in metallic bonds are not lost; they flow freely between atoms as a delocalized cloud. As such, elements involved in metallic bonds are not truly cations. Despite this, it is the attraction between the positively charged "cations" and the surrounding electron cloud that holds metals together and is responsible for many of their qualities including their excellent conduction of heat and electricity and their ductile deformation. Some workers (e.g., Hirata and Nesbitt 1997; Meftah et al. 2016) have proposed that the metallically bonded character of taenite and kamacite dictates that elements with diffusive mobility in the taenite-kamacite system will preferentially substitute as a function of ionic radius. Testing this proposal is complicated by the fact that elements usually do not have one unique ionic radius; they often have many as a function of oxidation state. Oxidation state, the number of protons less the number of electrons an ion has, changes the balance of electrostatic attraction between the nucleus and the electron orbitals, influencing the ionic size (Table 12). To compare against partitioning data, one must select an oxidation state for each ion. Since the mineral assemblage of pallasites is generally reducing, the lowest of the main oxidation states for each atom is plotted (Fig. 8a). A positive correlation is generally apparent, but the data is slightly scattered. The trend is improved by plotting Co, Ge, Ir, and Pt at their higher common oxidation state (Fig. 8b). It could be speculated that these elements may have, for some reason, substituted at their higher oxidation states. Previous work has found a similar correlation using fewer elements in metal grains from a chondrite (Meftah et al. 2016). These workers also found a stronger correlation by substituting Co^{3+} instead of Co^{2+}.

As in Hirata and Nesbitt (1997) and Meftah et al. (2016), the current study demonstrates a generally well-developed correlation between ionic radii and $D_{T/K}$ (Fig. 8a and b). Except for outliers Au, and Pd, the data plots along a path of increasing $D_{T/K}$ and ionic radii from Co to Cu and Zn. Germanium remains a poor fit regardless of which main oxidation state it takes. Palladium and Au are the largest ions by a wide margin, both more than 10% larger than the next largest ion. If they followed the trend of increasing $D_{T/K}$ with increasing ionic radii they would be expected to favour taenite by a factor of 10 or more. Despite this, they favour taenite relatively modestly, with $D_{T/K}(Pd) = 3.17 \pm 0.26$ and $D_{T/K}(Au) = 2.28 \pm 0.21$.

We speculate that the large size of Pd and Au make them a relatively poor fit for either phase, decreasing the preference for one over the other while still preferring taenite.

Table 12. Ionic radii as a function of oxidation state. Radii are in pm and are effective ionic radii from (Shannon 1976). IR_{bf} are the best fitting of the main oxidation states. Adapted from (Meftah et al. 2016).

At. No.	Element	1+	2+	3+	4+	5+	6+	7+	Main ox. states	Best Fit	IR_{bf}
27	Co		65	54.5					2,3	3	54.5
28	Ni		69	56	48				2	2	69
29	Cu	77	73	54					2	2	73
30	Zn		74						2	2	74
31	Ga			62					3	3	62
32	Ge		73		53				2,4	4	53
33	As			58		46			3,5	3	58
42	Mo			69	65	61	59		4,6	4	65
44	Ru			68	62	56.5			3,4	3	68
45	Rh			66.5	60	55			3	3	66.5
46	Pd		86	76	61.5				2,4	2	86
74	W				66	62	60		4,6	4	66
75	Re				63	58	55	53	4	4	63
76	Os				63	57.5	54.5	52.5	4	4	63
77	Ir			68	62.5	57			3,4	4	62.5
78	Pt		80		62.5	57			2,4	4	62.5
79	Au	137		85		57			3	3	85

Unfortunately, there are more serious problems for the interpretation that elements substitute as ions in the taenite-kamacite system. In substitutional diffusion, the solute and solvent atoms both occupy lattice sites in the crystal structure (Kikuchi and Sato 1969). For an atom to move from one lattice site to another it must be adjacent to a vacant lattice site and it must have enough energy to break the bonds between it and its closest neighbors (Kikuchi and Sato 1969). The energy required to break the bonds and the presence of vacant sites are both a function of temperature. Once free, the atom can transfer to the unoccupied lattice site. Since the space between lattice sites is smaller than the sites themselves, the transferring atom and the lattice structure both deform to facilitate the movement (Kikuchi and Sato 1969). It is not expected for the elements to behave as ions at any point during this process.

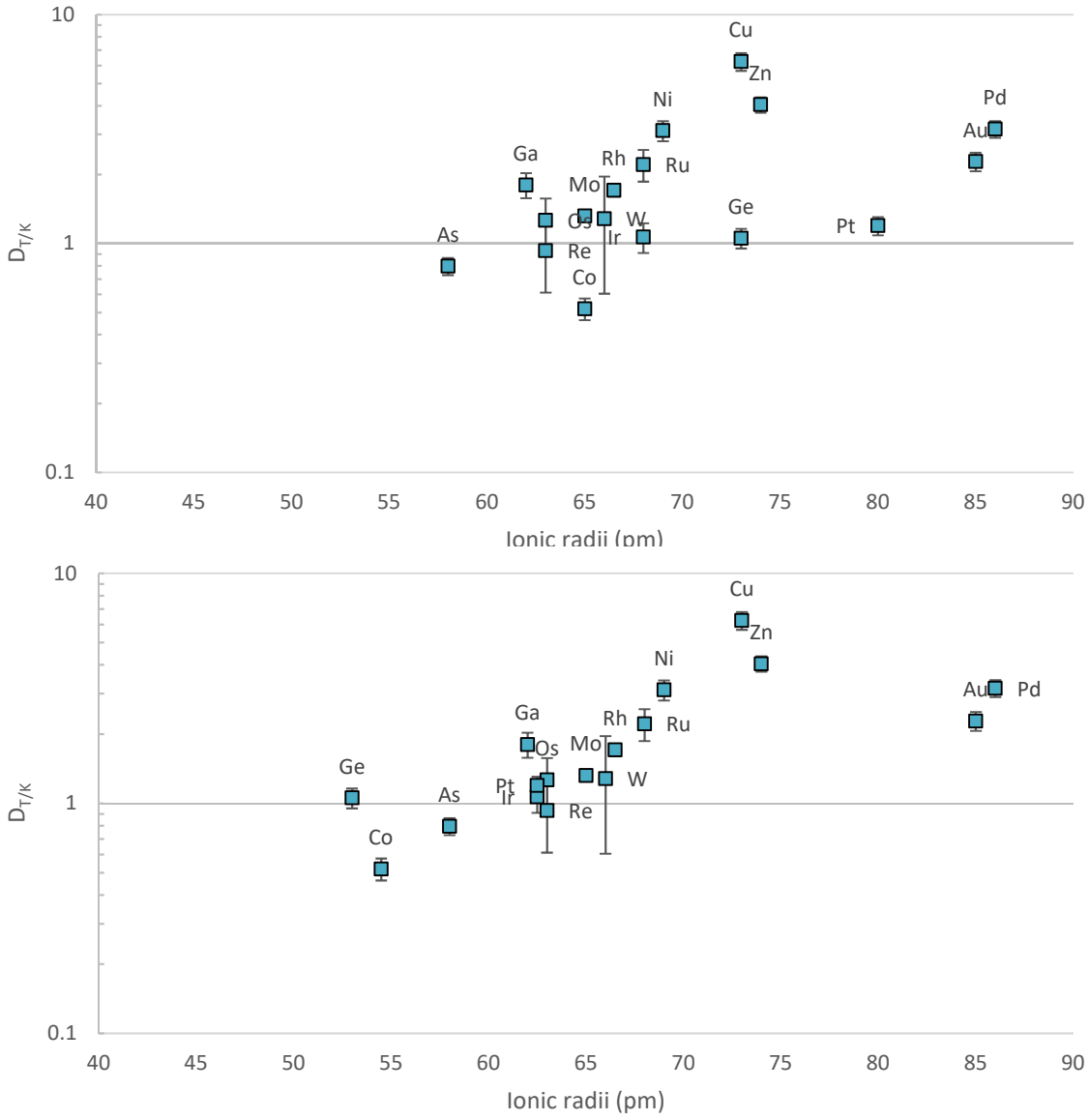

Figure 8. Ionic radii with taenite-kamacite partitioning coefficients. (a, above) Ionic radii are the most reducing of the main oxidation states. (b, below) Cobalt, Ge, Ir, and Pt are plotted at the higher of their two main oxidation states.

3.4.3.3 Atomic Radius and Electron Configuration

While the discussion above suggests that ionic radius is the primary factor in taenite-kamacite partitioning, other researchers have argued that a combination of atomic radius and electron configuration determine which phase a given element prefers (e.g., Hsu et al. 2000; Mullane et al. 2004). Based on the apparent correlation of atomic size and the number

of d-orbital electrons with the degree of preferential partitioning into taenite found in their data, Hsu et al. (2000) predict that Ag, Zn, and Cd, which have filled d-orbitals, will favour partitioning into taenite while Mn, Cr, Mo, W, V, Nb, and Ta will favour kamacite. Data from subsequent studies is inconclusive. In support of this prediction, Ash et al. (2007) report $D_{T/K}(V) < 1$, Danielson et al. (2009) report $D_{T/K}(W) < 1$, and the current study reports $D_{T/K}(Zn) > 1$. Opposed to the prediction, Ash et al. (2007) report $D_{T/K}(Mn, Mo) > 1$, Watson et al. (2008) report $D_{T/K}(Mo) > 1$, Danielson et al. (2009) report $D_{T/K}(Cr, Mo) > 1$, and the current study reports $D_{T/K}(Mo) > 1$. Like the current study, Ash et al. (2007) also report varying results for $D_{T/K}(W)$, with W preferring kamacite in some samples and taenite in others.

As is the case for ionic radius, elements do not have one unique atomic radius; they have varying atom radii depending on what type of chemical bond they are involved in. Since taenite and kamacite are dominated by metallic bonds, those will be the atomic radii considered (Table 13).

The atomic radii for elements with coordination numbers less than 12 have a Goldschmidt correction applied (Atkins 2010). As atomic radius increases with coordination number, a correction is required to increase the atomic radii quoted at lower coordination numbers, allowing for meaningful comparison between the two.

When presented graphically, and without the combined effect of electron configuration, atomic radius appears to have no correlation with $D_{T/K}$ (Fig. 9). The negative correlation between atomic number and $D_{T/K}$ for the 4th period elements of Cu to As is apparently not a manifestation of atomic radii. Rhodium, Ru, and Zn have identical atomic radii but different partitioning coefficients. An increase in d-orbital symmetry fails to explain the discrepancy; Ru has 7 d-electrons, Rh has 8, while Zn has a full outermost d-shell (10) yet the $D_{T/K}$ values increase in the order Rh < Ru < Zn.

Table 13. Select properties of atoms. BCC = body-centered cubic, FCC = face-centered cubic, HCP = hexagonal closest packed, Anom. = anomalous, DC = diamond cubic, HC = hexagonal scalenohedral. Radii from (Greenwood and Earnshaw 1997). Adapted from Hsu et al. (2000). G.C. refers to the Goldschmidt correction.

Element	At. no.	Crystal structure in pure form	Coor. no.	Electron configuration	Atomic radius (pm)	Atomic radius G. C. (pm)
Fe	26	BCC or FCC	8 or 12	$[Ar]3d^6 4s^2$	126	126
Co	27	HCP, FCC	12	$[Ar]3d^7 4s^2$	125	125
Ni	28	FCC	12	$[Ar]3d^8 4s^2$	124	124
Cu	29	FCC	12	$[Ar]3d^{10} 4s^1$	128	128
Zn	30	HCP	12	$[Ar]3d^{10} 4s^2$	134	134
Ga	31	Anom.	-	$[Ar]3d^{10} 4s^2 4p^1$	135	-
Ge	32	DC	-	$[Ar]3d^{10} 4s^2 4p^2$	-	-
As	33	HC	-	$[Ar]3d^{10} 4s^2 4p^3$	-	-
Mo	42	BCC	8	$[Kr]4d^5 5s^1$	139	143
Ru	44	HCP	12	$[Kr]4d^7 5s^1$	134	134
Rh	45	FCC	12	$[Kr]4d^8 5s^1$	134	134
Pd	46	FCC	12	$[Kr]4d^{10}$	137	137
W	74	BCC	8	$[Xe]4f^{14} 5ds^4 6s^2$	139	143
Re	75	HCP	12	$[Xe]4f^{14} 5ds^5 6s^2$	137	137
Os	76	HCP	12	$[Xe]4f^{14} 5ds^6 6s^2$	135	135
Ir	77	FCC	12	$[Xe]4f^{14} 5ds^7 6s^2$	135.5	135.5
Pt	78	FCC	12	$[Xe]4f^{14} 5ds^9 6s^1$	138.5	138.5
Au	79	FCC	12	$[Xe]4f^{14} 5ds^{10} 6s^1$	144	144

A set of rules known as the Hume-Rothery Rules describe the solubility of an element in metal (Hume-Rothery 1969). For substitutional alloys, they are that the difference in atomic radii between the solvent and the solute atoms must be no more than 15%, the solvent and solute atoms must have similar crystal structures in their pure forms, the solvent and solute atoms must have similar electronegativity (otherwise they are more likely to form compounds instead of solid-solution), and the solvent and solute atoms must have similar valency (Hume-Rothery 1969). The first rule is met by all elements in the study; Au has the largest atomic radius among them and is 14.3% larger than Fe. Further, these elements are mostly transition metals with similar electronegativities and valences (a similar concept to oxidation state). The rule pertaining to crystal structure seems to suggest

that solute atoms will prefer a phase with the same crystal structure. From Table 13 we would expect Mo and W to partition into BCC kamacite (coordination number 8) while the rest partition into taenite. Despite this, Mo partitions into taenite and HCP/FCC Co partitions into kamacite.

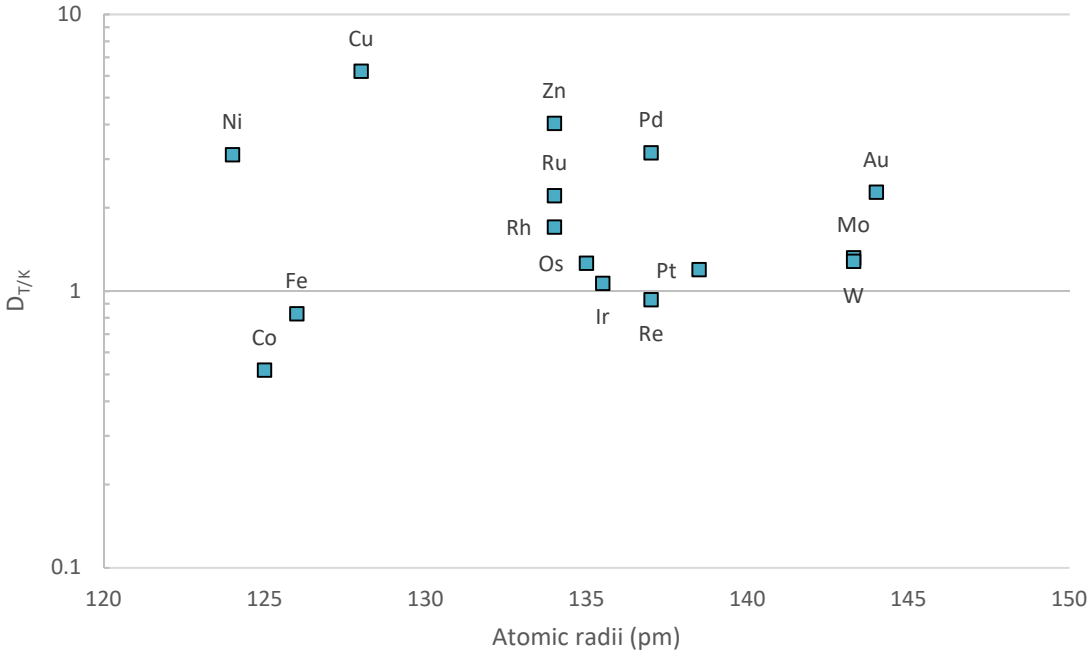

Figure 9. Atomic radius vs taenite-kamacite partition coefficient.

The comparatively well-developed correlation of $D_{T/K}$ with ionic radii is interesting, but diffusion in alloys as a function on ionic radius seems unlikely. A combination of atomic radius and electron configuration does not satisfactorily explain the observations either. As such, there must be some other unconsidered factor at play.

One possibility is atomic compressibility; with more easily compressed atoms perhaps better able to squeeze through the tighter interstices of FCC taenite (Fig. 10) (Bowen and Leak 1970; Kittel 2005). Except for Co, there appears to be a positive correlation between $D_{T/K}$ and compressibility relatively incompressible elements (< 0.01 GPa^{-1}), however; when considering Co, along with the more compressible elements, there appears to be no

systematic variation between $D_{T/K}$ and compressibility. We speculate that a satisfactory explanation could possibly be found by inquiry into crystal field theory.

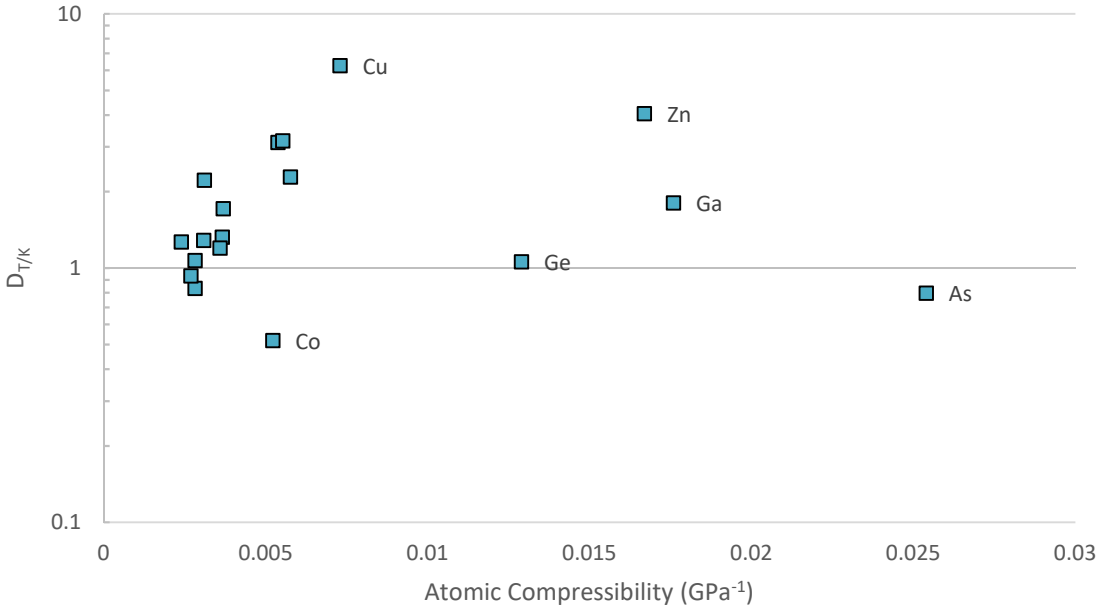

Figure 10. Atomic compressibility vs taenite-kamacite partition coefficient.

3.4.4 Bulk Metal Composition

Each of the methods of calculating bulk metal composition employed by this study has its benefits and drawbacks. The spot counting technique used image processing software to carefully compute the relative modal abundances of taenite and kamacite while the line method relied on placings approximated by eye. In either case, the calculated composition depends on the modal abundance of a single sample, which does not necessarily reflect the true modal distribution of the entire meteorite. The line scans, integrated over their length, sample a larger volume of material than the spots. As in any analysis for bulk concentration, a larger sample size is advantageous as it is more likely to be representative of the whole. The two methods produce bulk concentrations with agreement varying by element and sample (Table 8). Of all the elements, Pt has the least variation between the two methods. This is likely due to its relatively even distribution between taenite and kamacite, making it less sensitive to different effective modal abundances. Inversely, elements with larger partition coefficients, such as Cu and Pd, have a larger disparity between the two methods.

The accuracy of the line positioning in terms of capturing a representative quantity of taenite can be estimated by the difference in Ni concentration between the phases. The Ni content is higher in the line method for every sample. The closest approximation was for Brenham, with a 4.9% difference. The largest disparity was for Esquel, which has 39.9% higher Ni concentration in the line method. As expected, Esquel also has highest disparity in the concentrations of taenite-preferring elements as well. When compared to literature values, the spot method for Brenham seems to provide more accurate results (Table 10). Iridium and Au from the spot method also compare more favourably with data from Wasson and Choi (2003) for Brahin, Springwater, Brenham, and Esquel, and with data from van Niekerk et al. (2007) for Seymchan.

3.5 Conclusions

LA-ICP-MS was used to measure a suite of elements, including the HSEs, in the taenite and kamacite phases of six PMG samples. This data was used to determine the bulk concentration and constrain subsolidus partitioning behavior. Rhenium, Os, and Ir concentrations are generally low (< ~0.1 ppm, much lower for Re), followed by Ru, Rh, and Pt (~1 – 2 ppm), while Pd and Au are ~2 ppm or greater. The reported concentrations broadly agree with data from previous studies, when available. The taenite-kamacite partitioning coefficients are similar (agreeing within uncertainty or near) between samples. All HSE but Re prefer taenite on average. The coefficients increase in the order $D_{T/K}(Re) < 1 < D_{T/K}(Ir) < D_{T/K}(Pt) \approx D_{T/K}(Os) < D_{T/K}(Rh) < D_{T/K}(Ru) \approx D_{T/K}(Au) < D_{T/K}(Pd)$. The partition coefficients are similar to those reported for a variety of iron meteorite chemical groups. Additionally, no correlation was found with taenite or kamacite Ni content. Highly siderophile element partitioning is thus likely independent of parent body conditions.

A well-developed correlation between ionic radii and $D_{T/K}$ is observed. Why the elements would behave as ions, even given the delocalized nature of valence electrons in metal alloys, is unclear. No correlation was found between metallically bonded atomic radii and $D_{T/K}$. The partitioning behavior of the elements is not easily explained by electron configuration or preferred crystal structure either. Further study considering crystal field theory may reveal the mechanism for preferential diffusion between taenite and kamacite.

The general depletion of the HSEs in main-group pallasites compared to iron meteorites (e.g., Wasson et al. 1989, 1998) makes them a suboptimal source for PGEs. However; the similarity of taenite-kamacite partitioning coefficients between PMG and various iron meteorite chemical groups suggests that this behavior is independent of parent body conditions. The partition coefficients calculated in the study, and those from previous studies, are likely applicable to metallic asteroids in general.

3.6 References

Ali, A., Jabeen, I., Banerjee, N.R., Osinski, G.R., Nicklin, I., Gregory, D., and Herrmann, P. 2018. The oxygen isotope compositions of olivine in main group (MG) pallasites: New measurements by adopting an improved laser fluorination approach. Meteoritics and Planetary Science, 53: 1223–1237.

Ash, R.D., Luong, M. V., Walker, R.J., McDonough, W.F., and McCoy, T.J. 2007. Trace Element Fractionation in Kamacite and Taenite in IVA Irons. *In* Lunar and Planetary Science XXXVIII.

Atkins, P.W. 2010. Shriver & Atkins' inorganic chemistry. *In* Shriver and Atkin's inorganic chemistry, 5th ed. Oxford University Press, New York. doi:978-0-19-926463-6.

Boesenberg, J.S., Delaney, J.S., and Hewins, R.H. 2012. A petrological and chemical reexamination of Main Group pallasite formation. Geochimica et Cosmochimica Acta, **89**: 134–158. Elsevier Ltd.

Bowen, A.W., and Leak, G.M. 1970. Solute diffusion in alpha- and gamma-iron. Metallurgical Transactions, **1**: 1695–1700.

Bridgestock, L.J., Williams, H., Rehkämper, M., Larner, F., Giscard, M.D., Hammond, S., Coles, B., Andreasen, R., Wood, B.J., Theis, K.J., Smith, C.L., Benedix, G.K., and Schönbächler, M. 2014. Unlocking the zinc isotope systematics of iron meteorites. Earth and Planetary Science Letters, **400**: 153–164. Elsevier B.V.

Buchwald, V.F. 1975. Handbook of Iron Meteorites Vol 3. University of California Press, Berkeley and Los Angeles, California.

Burbine, T.H., Mccoy, T.J., Meibom, A., Gladman, B., and Keil, K. 2002. Meteoritic Parent Bodies: Their Number and Identification. *In* Asteroids III. *Edited by* W.F.

Bottke, A. Cellino, P. Paolicchi, and R.P. Binzel. The University of Arizona Press. pp. 653–667.

Buseck, P.R. 1977. Pallasite meteorites-mineralogy, petrology and geochemistry. Geochimica et Cosmochimica Acta, **41**. doi:10.1016/0016-7037(77)90044-8.

Buseck, P.R., and Holdsworth, E. 1977. Phosphate Minerals in Pallasite Meteorites. Mineralogical Magazine, **41**: 91–102.

Campbell, A.J., and Humayun, M. 1999. Microanalysis of platinum group elements in iron meteorites using laser ablation ICP-MS. 30th Lunar and Planetary Science Conference, **60637**: 1974.

Campbell, A.J., Humayun, M., and Weisberg, M.K. 2002. Siderophile element constraints on the formation of metal in the metal-rich chondrites Bencubbin, Weatherford, and Gujba. Geochimica et Cosmochimica Acta, **66**: 647–660.

Chabot, N.L. 2004. Sulfur contents of the parental metallic cores of magmatic iron meteorites. Geochimica et Cosmochimica Acta, **68**: 3607–3618.

Chen, J.H., Papanastassiou, D.A., and Wasserburg, G.J. 2002. Re-Os and Pd-Ag systematics in Group IIIAB irons and in pallasites. Geochimica et Cosmochimica Acta, **66**: 3793–3810.

Danielson, L.R., Righter, K., and Humayun, M. 2009. Trace element chemistry of Cumulus Ridge 04071 pallasite with implications for main group pallasites. Meteoritics and Planetary Science, **44**: 1019–1032.

Goldstein, J.I., and Ogilvie, R.E. 1965. The growth of the Widmanstatten pattern in metallic meteorites. Geochimica et Cosmochimica Acta, **29**: 893–920.

Goldstein, J.I., Yang, J., and Scott, E.R.D. 2014. Determining cooling rates of iron and stony-iron meteorites from measurements of Ni and Co at kamacite-taenite interfaces. Geochimica et Cosmochimica Acta, **140**: 297–320. Elsevier Ltd.

Greenwood, N.N., and Earnshaw, A. 1997. Chemistry of the elements. *In* 2nd ed. Butterworth-Heinemann, Oxford, Boston. doi:https://doi.org/10.1016/C2009-0-30414-6.

Haack, H., and McCoy, T.J. 2007. 1.12 - Iron and Stony-Iron Meteorites. *In* Treatise on Geochemistry. *Edited by* H.D. Holland and K.K.B.T.-T. on G. Turekian. Pergamon, Oxford. pp. 1–22.

Hirata, T., and Nesbitt, R.W. 1997. Distribution of platinum group elements and rhenium

between metallic phases of iron meteorites. Earth and Planetary Science Letters, **147**: 11–24.

Hsu, W.B. 2003. Minor element zoning and trace element geochemistry of pallasites. Meteoritics & Planetary Science, **38**: 1217–1241.

Hsu, W.B., Huss, G.R., and Wasserburg, G.J. 2000. Ion probe measurements of Os, Ir, Pt, and Au in individual phases of iron meteorites. Geochimica et Cosmochimica Acta, **64**: 1133–1147.

Hu, Z., Gao, S., Liu, Y., Hu, S., Chen, H., and Yuan, H. 2008. Signal enhancement in laser ablation ICP-MS by addition of nitrogen in the central channel gas. Journal of Analytical Atomic Spectrometry, **23**: 1093–1101.

Hume-Rothery, W. 1969. The structure of metals and alloys. *In* 5th ed. *Edited By*R.E. (Raymond E. Smallman and C.W. Haworth. Metals & Metallurgy Trust, London.

JAXA. 2018. JAXA | Asteroid Explorer "Hayabusa." Available from http://global.jaxa.jp/projects/sat/hayabusa2/ [accessed 4 June 2018].

Kikuchi, R., and Sato, H. 1969. Substitutional Diffusion in an Ordered System. The Journal of Chemical Physics, **51**: 161–181.

Kittel, C. 2005. Introduction to Solid State Physics. 8th ed. John Wiley & Sons, Inc., Hoboken, NJ.

Liu, Y., Hu, Z., Gao, S., Günther, D., Xu, J., Gao, C., and Chen, H. 2008. In situ analysis of major and trace elements of anhydrous minerals by LA-ICP-MS without applying an internal standard. Chemical Geology, **257**: 34–43. Elsevier B.V.

Liu, Y., Hu, Z.C., Li, M., and Gao, S. 2013. Applications of LA-ICP-MS in the elemental analyses of geological samples. Chinese Science Bulletin, **58**: 3863–3878.

McDonough, W.F., Horn, I., Lange, D.E., and Rudnick, R.L. 1999. Distribution of platinum group elements between phases in iron meteorites. 30th Lunar and Planetary Science Conference, **02138**: #2062.

McDonough, W.F., and Sun, S. s. 1995. The composition of the Earth. Chemical Geology, **120**: 223–253.

Meftah, N., Mostefaoui, S., Jambon, A., Guedda, E.H., and Pont, S. 2016. Minor and trace element concentrations in adjacent kamacite and taenite in the Krymka chondrite. Meteoritics and Planetary Science, **51**: 696–717.

Mullane, E., Alard, O., Gounelle, M., and Russell, S.S. 2004. Laser ablation ICP-MS study of IIIAB irons and pallasites: Constraints on the behaviour of highly siderophile elements during and after planetesimal core formation. Chemical Geology, **208**: 5–28.

Müller, W., Shelley, M., Miller, P., and Broude, S. 2009. Initial performance metrics of a new custom-designed ArF excimer LA-ICPMS system coupled to a two-volume laser-ablation cell. Journal of Analytical Atomic Spectrometry, **24**: 209–214.

NASA. 2018. OSIRIS-REx Overview. Available from https://www.nasa.gov/content/osiris-rex-overview [accessed 4 June 2018].

van Niekerk, D., Greenwood, R.C., Franchi, I.A., Scott, E.R.D., and Keil, K. 2007. Seymchan: a main group pallasite - not an iron meteorite. 70th Annual Meteoritical Society Meeting, **42**: 5196.

Paton, C., Hellstrom, J., Paul, B., Woodhead, J., and Hergt, J. 2011. Iolite: Freeware for the visualisation and processing of mass spectrometric data. Journal of Analytical Atomic Spectrometry, **26**: 2508–2518.

Pauling, L. 1970. General Chemistry. W. H. Freeman.

Petaev, M.I., and Jacobsen, S.B. 2004. Differentiation of metal-rich meteoritic parent bodies: I. Measurements of PGEs, Re, Mo, W, and Au in meteoritic Fe-Ni metal. Meteoritics & Planetary Science, **39**: 1685–1697.

Pettke, T., Oberli, F., Audétat, A., Guillong, M., Simon, A.C., Hanley, J.J., and Klemm, L.M. 2012. Recent developments in element concentration and isotope ratio analysis of individual fluid inclusions by laser ablation single and multiple collector ICP-MS. Ore Geology Reviews, **44**: 10–38. Elsevier B.V.

Righter, K., Campbell, A.J., Humayun, M., and Hervig, R.L. 2004. Partitioning of Ru, Rh, Pd, Re, Ir, and Au between Cr-bearing spinel, olivine, pyroxene and silicate melts. Geochimica et Cosmochimica Acta, **68**: 867–880.

Russo, R.E., Mao, X.L., Borisov, O. V., and Liu, H. 2000. Influence of wavelength on fractionation in laser ablation ICP-MS. Journal of Analytical Atomic Spectrometry, **15**: 1115–1120.

Ryan, D.E., Holzbecher, J., and Brooks, R.R. 1990. Rhodium and osmium in iron meteorites. Chemical Geology, **85**: 295–303.

Sanders, G.B., and Larson, W.E. 2015. Final review of analog field campaigns for in Situ Resource Utilization technology and capability maturation. Advances in Space Research, **55**: 2381–2404. COSPAR.

Scott, E.R.D. 1977. Geochemical relationships between some pallasites and iron meteorites. Mineralogical Magazine, **41**: 265–272.

Shannon, R.D. 1976. Revised effective ionic radii and systematic studies of interatomic distances in halides and chalcogenides. Acta Crystallographica Section A, **32**: 751–767.

Vander Voort, G.F. 2001. Metallography of iron meteorites. Advanced Materials and Processes, **159**: 37–41.

Walker, R.J., McDonough, W.F., Honesto, J., Chabot, N.L., McCoy, T.J., Ash, R.D., and Bellucci, J.J. 2008. Modeling fractional crystallization of group IVB iron meteorites. Geochimica et Cosmochimica Acta, **72**: 2198–2216.

Wasson, J.T., and Choi, B.-G. 2003. Main-group pallasites: Chemical composition, relationship to IIIAB irons, and origin. Geochimica et Cosmochimica Acta, **67**: 3079–3096.

Wasson, J.T., Choi, B.-G., Jerde, E.A., and Ulff-Møller, F. 1998. Chemical classification of iron meteorites: XII. New members of the magmatic groups. Geochimica et Cosmochimica Acta, **62**: 715–724.

Wasson, J.T., and Goldstein, J.I. 1968. The North Chilean hexahedrites: Variations in composition and structure. Geochimica et Cosmochimica Acta, **32**: 329-336,IN7-IN9,337-339.

Wasson, J.T., Ouyang, X., Wang, J., and Eric, J. 1989. Chemical classification of iron meteorites: XI. Multi-element studies of 38 new irons and the high abundance of ungrouped irons from Antarctica. Geochimica et Cosmochimica Acta, **53**: 735–744.

Watson, H.C., Watson, E.B., McDonough, W.F., and Ash, R.D. 2008. Low temperature siderophile element partition coefficients in iron meteorites. Lunar and Planetary Science XXXIX, **8520**.

Wood, J.A. 1964. The cooling rates and parent planets of several iron meteorites. Icarus, **3**: 429–459.

Yang, J., Goldstein, J.I., and Scott, E.R.D. 2010. Main-group pallasites: Thermal history,

relationship to IIIAB irons, and origin. Geochimica et Cosmochimica Acta, **74**: 4471–4492. Elsevier Ltd.

Zientek, M.L., and Loferski, P.J. 2014. Platinum-Group Elements — So Many Excellent Properties. *In* USGS Mineral Resources Program.

4 Discussion, Conclusions, and Future Work

This thesis began by introducing the concept of Space Resource Utilization (SRU), the general term for leveraging the naturally occurring resources of outer space to create useful products and services. It then examined the feasibility of NEAs as SRU targets through an in-depth literature review. The penultimate chapter characterised the concentration and subsolidus behaviour of a suite of elements, including the PGEs, in the PMG to evaluate pallasitic asteroids as potential targets for SRU.

Space resource utilization demonstrates tremendous potential, both in support of publicly funded space exploration missions and in the private sector. Potentially useful resources in space include water, solar wind implanted volatiles, base and precious metals, atmospheric gases, and solar energy (Sanders and Larson 2015). In the public sector, these materials can be leveraged to reduce the cost and risk and increase the scope and flexibility of space exploration missions. The private sector can utilize space resources to service the satellite industry and support space exploration. If economic activity in space can reach a critical mass of increasing demand, the abundance of space resources relatively near the Earth can support increasing economic activity long after the finite resources of Earth would be overdrawn.

The NEAs are particularly enticing potential targets for SRU. They contain base metals that can be used to build infrastructure, semiconductors to make electronics, volatiles for agricultural and life support applications, but most importantly, they contain two resources that could potentially be profitably produced in the current market conditions. These resources are water and the platinum group elements. Water is the most promising, as there is current demand in space. Water can be used to create propellant which can be used in turn to extend the lifespan of satellites, refuel spacecraft, and service the astronauts aboard the International Space Station. At a value of \$5,000 kg^{-1} (half the canonical cost of launching a kg of mass into LEO) a C-type asteroid with 16 wt% water and a diameter of only 12 m is worth over \$1 B. This study estimates that there are seven such asteroids among the catalogue of currently known NEAs that are accessible by a ΔV of less than 4.5 km s^{-1} and 62 within a ΔV of 5.5 km s^{-1}. Extrapolating to the entire estimated population

of NEAs there are expected to be ~13,000 water rich NEAs of 12 m diameter or greater that are within 4.5 km s^{-1} of LEO (Stokes et al. 2003). The advantages and disadvantages of concentrating water at the site of the asteroid prior to transport have been evaluated using transport costs developed by Brophy et al. (2012). The cost of delivering water from a NEA in a favourable orbit is \$2,927 kg^{-1} for a 90% pure concentrate and \$16,463 kg^{-1} for raw asteroid material at 16 wt% water. It becomes obvious that in situ processing is not only efficient, but necessary. In situ concentration of water from carbonaceous asteroids is expected to be relatively straightforward. Concentrated sunlight can be used to sublimate water ice and dehydrate phyllosilicates (TransAstra Corp. 2018). As the body devolatilizes it will fragment, continually exposing fresh surfaces. The liberated volatiles will condense in an enclosing bag and be can separated by fractional distillation.

Innovations in the commercial space launch sector promise to reduce launch costs to only \$1,411 kg^{-1} from Earth's surface to LEO, the advertised performance of SpaceX's Falcon Heavy (SpaceX 2017). If this, or similar technology can provide reliable and frequent service, similar degrees of innovation must also be made in the field of space propulsion if asteroid sourced water is to maintain a cost advantage.

It appears that the profitable production of PGEs from NEAs will require technology that does not yet exist. A metallic asteroid in the 50^{th} percentile of PGE enrichment needs to be 119 m in diameter to have a value of \$1 B. There are an estimated three asteroids in the known catalogue of NEAs that are expected to meet these criteria and have ΔV's of no more the 4.5 km s^{-1}, and 25 that are within 5.5 km s^{-1} of LEO. Considering the estimated abundance of the entire NEA swarm brings these totals to 49 and 403. Raw material from a 50^{th} percentile metallic asteroid is worth just \$0.28 kg^{-1} while 90^{th} percentile material is worth \$1.35 kg^{-1}. A 90% pure product is worth ~\$18,000 kg^{-1}. Clearly, a high degree of in situ concentration is required. The process by which this would be achieved is unclear. The orbits of NEAs bring them many light minutes away from Earth, requiring that operations be done autonomously. An extraction scenario would likely involve identifying regions of PGE enrichment, landing and securing to the asteroid, mechanically liberating material, and concentrating the desired elements via the Mond process or another similar technique. This is a complicated and nuanced system for which engineering an autonomous solution

would be certainly be a challenge. The details involved, and ultimately the feasibility based on the technological requirements, are beyond the scope of the current study.

The situation is further complicated by legal implications. The commercialization of extra-terrestrial material is not expressly prohibited by any well-endorsed piece of international legislation, but the Outer Space Treaty, a fundamental piece of space legislation to which all spacefaring nations are Parties, declares in Article II that "[o]uter space, including the Moon and other celestial bodies, is not subject to national appropriation by claim of sovereignty, by means of use or occupation, or by any other means (United Nations 1966)". Article VI goes on to make States responsible for the space activities of all governmental and non-governmental entities in their jurisdiction. This legislation forms the basis of the argument against the legality of the commercialization of space resources. Two nations, the United States and Luxembourg, have passed legislation explicitly permitting the acquisition and sale of space resources. The laws are similar and allow parties to own the material they extract from celestial bodies, but not lay claim to a body itself or a region therein. Whether these laws clarify or contradict the Outer Space Treaty remains up for debate.

At the time of writing, the private sector already contains companies working on some aspect of asteroid resource utilization, although mining itself has yet to occur. Key advancements that must be made include enhanced asteroid discovery and observation campaigns, with an emphasis on spectroscopy, the development of a cost-effective fleet of asteroid prospecting spacecraft, and advancements in autonomous extraction technology. At the most stringent accessibility cut off, there are only expected to be seven and three asteroids prospective for water and PGEs respectively in the known NEA catalogue. A more ambitious discovery campaign sensitive to smaller asteroids and capable of immediate follow up spectral observations will build a more robust collection of potentially desirable NEAs from which a short list of the most promising candidates can be made. Small scale and cost effective prospecting spacecraft, like those under development by Deep Space Industries and Planetary Resources (Deep Space Industries 2017, Planetary Resources 2018), are then required to rendezvous with, and study more closely, the bodies on the short list. Once the spacecraft has confirmed the presence of the desired resource in

an adequate quantity, a mining target can be selected. At this stage autonomous systems must be designed to carry out the harvesting, concentration, and transport of the desired resource.

In the third chapter of this thesis, we characterized the quantity, distribution, and low-temperature mobility of the HSEs in main-group pallasites to assess their potential as long-term targets for SRU. LA-ICP-MS was used to calculate the mean composition of kamacite and taenite in each sample. Measurements were also taken on taenite near the taenite-kamacite boundary to calculate taenite-kamacite subsolidus partition coefficients ($D_{T/K}$). Line scans were taken in strategical locations as to approximate the modal abundance of the metal phases in order to estimate bulk composition. Bulk composition was also estimated by combining the average taenite and kamacite concentrations from the spot analyses with modal abundance derived from BSE maps. In comparison with previous studies, the spot method seems to be more accurate. The HSE concentrations of the six samples vary modestly. Reported concentrations for Re, Os, and Ir are generally < 0.1 ppm (much lower for Re). Ruthenium, Rh and Pt are approximately 1 – 2 ppm while Pd and Au are ~2 ppm or greater. The taenite-kamacite partition coefficients are similar between samples and all the HSEs but Re prefer taenite on average. The partition coefficients are close to those reported by previous studies based on a variety of iron meteorite and pallasite chemical groups. It appears that $D_{T/K}$ is independent of parent body conditions.

A positive correlation was found between ionic radii and $D_{T/K}$ for most elements in the study. It remains unclear as to why the elements would behave as ions. While the elements are present in the metallic phases as atoms, no correlation is found between atomic radii and $D_{T/K}$. Invoking atomic configuration or preferred crystal orientation does not satisfactorily explain the behaviour either. Another intrinsic property of the elements must be at play to dictate which crystal structure the elements prefer.

The relatively low abundance of PGEs in the PMG when compared with iron meteorites makes the PMG parent body(ies) a non-ideal target for future PGE extraction through asteroid mining. The apparently constant nature of taenite-kamacite subsolidus partitioning

coefficients signifies that those obtained by this study are applicable to metallic asteroids in general.

4.1 References

Brophy, J.R., Friedman, L., and Culick, F. 2012. Asteroid retrieval feasibility. *In* IEEE Aerospace Conference Proceedings. pp. 1–51. doi:10.1109/AERO.2012.6187031.

Deep Space Industries. 2017. Prospector-1 | Deep Space Industries. Available from http://deepspaceindustries.com/prospector-1/ [accessed 8 December 2017].

Planetary Resources. 2018. Arkyd-301 | Planetary Resources. Available from https://www.planetaryresources.com/missions/arkyd-301/ [accessed 21 May 2018].

Sanders, G.B., and Larson, W.E. 2015. Final review of analog field campaigns for in Situ Resource Utilization technology and capability maturation. Advances in Space Research, **55**: 2381–2404. COSPAR. doi:10.1016/j.asr.2014.12.024.

SpaceX. 2017. Capabilities & Services | SpaceX. Available from http://www.spacex.com/about/capabilities [accessed 8 December 2017].

Stokes, G.H., Yeomans, D.K., Bottke, W.F., Jewitt, D., Chesley, S.R., Kelso, T.S., Evans, J.B., McMillan, R.S., Gold, R.E., Spahr, T.B., Harris, A.W., and Worden, S.P. 2003. Study to determine the feasibility of extending the search for near-Earth objects to smaller limiting diameters. *In* NASA Office of Space Science Solar System Exploration Division.

TransAstra Corp. 2018. TransAstra Corp. Home. Available from http://www.transastracorp.com/ [accessed 28 February 2018].

Appendices

Table 141. Taenite-kamacite subsolidus partition coefficients.

	Esquel		Fukang		Seymchan	
	$D_{T/K}$	±	$D_{T/K}$	±	$D_{T/K}$	±
Co	**0.46**	0.06	**0.45**	0.03	**0.52**	0.10
Ni	**3.47**	0.45	**3.40**	0.29	**3.18**	0.63
Cu	**6.85**	0.97	**6.46**	1.17	**6.35**	1.64
Zn	**3.82**	nd	**nd**	nd	**nd**	nd
Ga	**2.03**	0.26	**1.90**	0.45	**1.96**	0.80
Ge	**1.19**	0.14	**1.10**	0.16	**1.10**	0.25
As	**0.73**	0.18	**0.90**	0.24	**nd**	nd
Mo	**1.37**	0.29	**1.30**	0.18	**1.30**	0.23
Ru	**2.59**	0.54	**2.60**	0.54	**2.34**	0.61
Rh	**1.85**	0.16	**1.78**	0.16	**1.72**	0.16
Pd	**3.43**	0.48	**3.30**	0.42	**3.39**	0.87
W	**1.04**	0.45	**1.03**	0.48	**2.64**	3.48
Re	**nd**	nd	**0.86**	nd	**1.31**	0.36
Os	**1.60**	0.84	**1.05**	0.24	**1.13**	0.25
Ir	**0.78**	0.80	**1.07**	0.21	**1.14**	0.20
Pt	**1.19**	0.14	**1.40**	0.16	**1.20**	0.17
Au	**2.50**	0.27	**2.34**	0.41	**2.40**	0.76

Table A1. Cont.

	Brahin		Springwater		Brenham	
	$D_{T/K}$	±	$D_{T/K}$	±	$D_{T/K}$	±
Co	**0.56**	0.09	**0.55**	0.11	**0.59**	0.04
Ni	**2.70**	0.95	**3.15**	0.53	**2.79**	0.31
Cu	**6.02**	3.85	**6.51**	1.81	**5.24**	0.82
Zn	**nd**	nd	**4.26**	nd	**nd**	nd
Ga	**1.75**	1.27	**1.78**	0.49	**1.40**	0.24
Ge	**1.00**	0.40	**1.05**	0.21	**0.89**	0.11
As	**0.82**	nd	**0.78**	0.18	**0.75**	0.12
Mo	**1.31**	0.31	**1.30**	0.24	**1.34**	0.25
Ru	**1.82**	0.60	**1.85**	0.41	**2.08**	0.39
Rh	**1.58**	0.32	**1.60**	0.13	**1.72**	0.15
Pd	**2.88**	1.36	**3.18**	0.58	**2.81**	0.39
W	**0.90**	0.36	**1.21**	0.64	**0.86**	0.50
Re	**0.54**	0.18	**1.02**	0.41	**nd**	nd
Os	**1.71**	1.91	**0.99**	0.19	**1.10**	0.50
Ir	**1.19**	0.52	**1.21**	0.20	**1.03**	0.21
Pt	**1.08**	0.14	**1.14**	0.15	**1.16**	0.10
Au	**2.35**	1.48	**2.22**	0.45	**1.89**	0.24

Table A2. Mean taenite-kamacite partition coefficients.

	$D_{T/K}$	±		$D_{T/K}$	±
Co	**0.52**	0.06	**Rh**	**1.71**	0.10
Ni	**3.11**	0.31	**Pd**	**3.17**	0.26
Cu	**6.24**	0.56	**W**	**1.28**	0.68
Zn	**4.04**	0.31	**Re**	**0.93**	0.32
Ga	**1.80**	0.23	**Os**	**1.26**	0.31
Ge	**1.06**	0.10	**Ir**	**1.07**	0.16
As	**0.80**	0.07	**Pt**	**1.20**	0.11
Mo	**1.32**	0.03	**Au**	**2.28**	0.21
Ru	**2.22**	0.35			

Curriculum Vitae

Name:	Liam Innis
Post-secondary Education and Degrees:	University of Alberta Edmonton, Alberta, Canada 2010-2015 B.Sc. Spec. Geology The University of Western Ontario London, Ontario, Canada 2016-2018 M.Sc. Geology with Planetary Science
Honours and Awards:	Western Graduate Research Scholarship 2016-2017, 2017-2018 CPSX Travel Award 2017
Related Work Experience:	Teaching Assistant The University of Western Ontario 2016-2018

Publications:

Innis, L. R. J., Osinski, G. R. 2018. Subsolidus HSE partitioning in pallasites and application to asteroid resource prospecting (abstract #2070). *In* Resources for Future Generations Conference. Vancouver, BC, May 2018 (poster).

Osinski, G.R., Battler, M., Caudill, C.M., Francis, R., Haltigin, T., Hipkin, V.J., Kerrigan, M., Pilles, E., Pontefract, A., Tornabene, L.L., Allard, P., Bakambu, J.N., Balachandran, K., Beaty, D., Bednar, D., Bina, A., Bourassa, M., Cao, F., Christoffersen, P., Choe, B.-H., Cloutis, E., Cote, K., Cross, M., D'Aoust, B., Draz, O., Dudley, B., Duff, S., Dzamba, T., Fulford, P., Godin, E., Goordial, J., Grau, A., Haid, T., Harrington, E., Harrison, T., Hawkswell, J., Hickson, D., Hill, P., Innis, L., King, D., Kissi, J., Laughton, J., Li, Y., Lymer, B., Maggiori, C., Maloney, M., Marion, C.L., Maris, J., Mcfadden, S., McLennan, S.M., Mittelholz, A., Morse, Z., Newman, J., O'Callaghan, J., Pascual, A., Patel, P., Picard, M., Pritchard, I., Poitras, J., Ryan, C., Sapers, H., Silber, E.A., Simpson, S., Sopoco, R., Svensson, M., Tolometti, G., Uribe, D., Wilks, R., Williford, K., Xie, T., and Zylberman, W. 2018. The CanMars Mars Sample Return analogue mission. Planetary and Space Science,. doi:https://doi.org/10.1016/j.pss.2018.07.011.